# Claudins and tight junction-associated MARVEL proteins at the blood-brain barrier – contribution to paracellular barrier formation

Inaugural-Dissertation
to obtain the academic degree
Doctor rerum naturalium (Dr. rer. nat.)

submitted to the Department of
Biology, Chemistry and Pharmacy
of Freie Universität Berlin

by
PHILIPP BERNDT
from Rostock

2017

The dissertation was written from 16 September 2013 till 18 June 2017 under supervision of PD Dr. Ingolf E. Blasig at the Leibniz-Institut für Molekulare Pharmakologie (FMP).

1st Reviewer: PD Dr. Ingolf E. Blasig
Molecular cell physiology
Leibniz-Institut für Molekulare Pharmakologie (FMP)

2nd Reviewer: Prof. Dr. Petra Knaus
Institute of chemistry and biochemistry
Signal transduction
Freie Universität Berlin

Date of defence: 5 December 2017

I would like to thank PD Dr. Ingolf E. Blasig, leader of the research group Molecular Cell Physiology at the Leibniz-Institut für Molekulare Pharmakologie, who made this work possible. I thank Prof. Dr. Petra Knaus who kindly reviews this thesis. I would like to thank especially Dr. Lars Winkler for the scientific support. Special thanks go to all my colleagues, especially Başak Arslan, Dr. Christian Staat, Dr. Jimmi Cording, Nele Katinka Askerc and Valentina Rausch, who made this scientific experience very enjoyable. I would also like to thank my collaborators Prof. Dr. Hartwig Wolburg, Dr. Jingjing Zhang and PD Dr. André Rex for their contribution. Thanks go to all my beloved ones.

キッス

# Directory

# List of figures

## List of tables

## List of abbreviations

| | |
|---|---|
| °C | degree Celsius |
| µ | micro |
| ACTB | beta-actin |
| AJ | adherens junction |
| Amp | ampicillin |
| BBB | blood-brain barrier |
| BC | brain capillary |
| bEND | brain capillary endothelial cell |
| bEND.3 | mouse brain endothelial cell line |
| BSA | bovine serum albumin |
| $Ca^{2+}$ | calcium |
| Cdh5 | cadherin-5 |
| cDNA | complementary DNA |
| Cldn | claudin |
| Cldnd1 | claudin domain containing protein 1 |
| CNS | central nervous system |
| CS | coverslip |
| Ct | cycle threshold |
| Ctrl | control |
| Da | Dalton |
| DAPI | 4', 6'-diamidino-2-phenylindole |
| $ddH_2O$ | double distilled water |
| DMEM | dulbecco's modified eagle's medium |
| DMSO | dimethylsulfoxide |
| dNTP | deoxyribonucleotidetriphosphate |
| ECIS | electric cell-substrate impedance sensing |
| ECL | extracellular loop |
| *E.coli* | *Escherichia coli* |
| EDTA | ethylendiaminetetraacteic acid |
| EF | extracellular fracture-face |
| *et al.* | *et alii*, and others |
| f | femto |

| | |
|---|---|
| FCS | fetal calve serumalbumin |
| fw | forward |
| GFP | green fluorescence protein |
| GST | glutathione-S-transferase |
| h | hour |
| HBSS | hank's balanced salt solution |
| HEK-293 | human embryonic kidney cell line |
| HEK-293T | HEK-293 cells expressing the SV40 T-antigen |
| HRP | horse reddish peroxidase |
| IPTG | isopropyl-β-D-thiogalactopyranosid |
| IR | infrared |
| ISF | interstitial fluid |
| JAM | junctional adhesion molecule |
| k | kilo |
| Kan | kanamycin |
| KD | knockdown |
| $K_d$ | dissociation constant |
| LB | lysogeny broth |
| LSM | confocal laser scanning microscopy |
| m | milli |
| MBP | maltose binding protein |
| MDCK-II | canine cocker spaniel kidney 2 cell line |
| min | minute |
| MS | mass spectrometry |
| MST | microscale thermophoresis |
| NHS | N-hydroxysuccinimide |
| n | nano |
| Ocln | occludin |
| O.D. | optical density |
| PAGE | polyacrylamide gel electrophoresis |
| PBS | phosphate buffered saline |
| PCR | polymerase chain reaction |
| PDZ | PSD-95/discs-large/Zo |
| PEI | polyethylenimine |

| | |
|---|---|
| PF | protoplasmatic fracture-face |
| PLL | poly-L-lysine |
| P/S | penicillin-streptomycin |
| qRT-PCR | quantitative real time polymerase chain reaction |
| RCA1 | ricinus communis agglutinin-1 |
| rev | reverse |
| rpm | rounds per minute |
| RT | room temperature |
| SDS | sodium dodecyl sulfate |
| shRNA | short hairpin RNA |
| TBS-T | tris saline buffer and tween 20 |
| TER | transcellular electrical resistance |
| TEER | transendothelial electrical resistance |
| TEMED | tetramethylethylenediamine |
| TJ | tight junction |
| Tric | tricellulin |
| U | unit |
| V | volume |
| wt | wild type |
| YFP | yellow fluorescence protein |
| Zo | *zonula occludens* protein |

# 1 Introduction

## 1.1 The blood-brain barrier

Accurate function of the central nervous system (CNS) requires the maintenance of the sensitive brain microenvironment for neuronal signaling (Abbott, 2013). The blood-brain barrier (BBB), a diffusion barrier, separates components of the circulating blood from the brain interstitial fluid (ISF) (Ballabh et al., 2004). The existence of this barrier was suggested due to the absence of pharmacological actions in the CNS despite intravenous administration of bile acids or ferrocyanide (Lewandowsky, 1900). The BBB is organized as structured neurovascular units. Pericytes are embedded within the basement membrane and astrocyte end-feet enclose the microvessels lined by endothelial cells (Abbott et al., 2006) (Figure 1). Predominantly formed by tight junctions (TJs) between neighboring endothelial cells, the BBB prevents paracellular transport for most substances (Hawkins and Davis, 2005). Only lipophilic molecules < 400 Da with fewer than eight hydrogen bonds are able to diffuse freely through the plasma membrane of the brain endothelium (Pardridge, 2007). The transcellular passage of small hydrophilic molecules is realized through transport systems on the luminal and abluminal membranes. Large hydrophilic molecules such as peptides and proteins can be taken up selectively by receptor- or adsorptive-mediated transcytosis (Pardridge, 2003). The composition of the ISF differs from the blood plasma in its much lower protein content, reduced $K^+$ and $Ca^{2+}$ levels and a higher $Mg^{2+}$ concentration. The restriction of ion flux and fluid movements protects the brain from fluctuations in the ionic composition, which would disturb synaptic and axonal signaling (Cserr and Bundgaard, 1984).

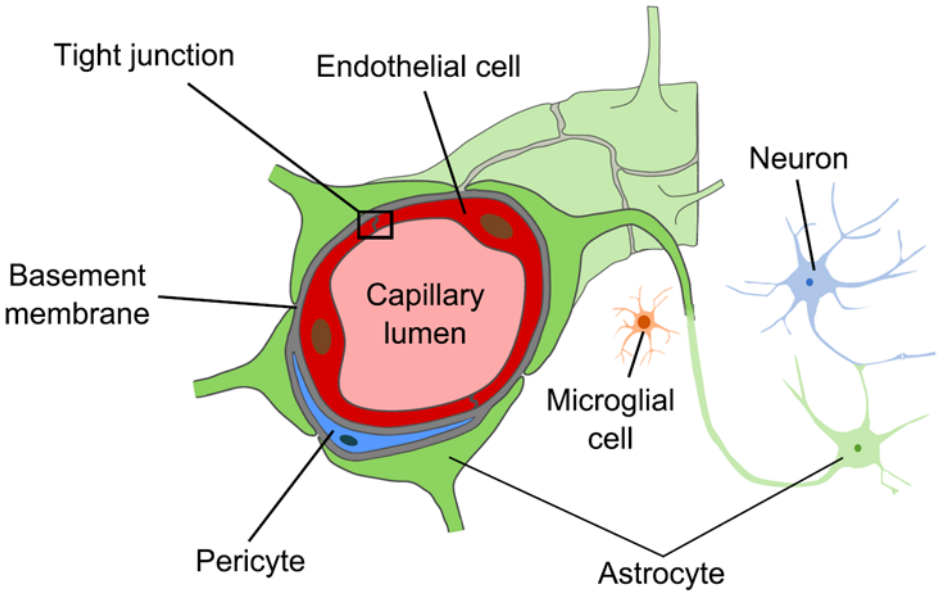


**Figure 1 Cellular constituents of the neurovascular unit.** The transverse section illustrates the blood-brain barrier, mainly formed by TJs between neighboring endothelial cells that are separated from pericytes through the basement membrane. The cellular interaction with neurons is established via astrocytes. (Heye et al., 2014)

## 1.2 Molecular composition of brain endothelial tight junctions

The brain endothelium differs from that of peripheral tissues in absence of fenestrations, lower degree of transcytosis and particularly very impermeable TJs (Ballabh et al., 2004). TJs of the BBB inhibit even the passage of small ions such as $Na^+$ and $Cl^-$, resulting in a higher transendothelial electrical resistance (TEER) of > 1000 ohm · $cm^2$ compared to values of 2 - 20 ohm · $cm^2$ in peripheral tissues (Butt et al., 1990). Ultrastructurally, TJs appear as merging plasma membranes of neighbouring endothelial cells. At those cell-cell contacts, freeze-fracture electron micrographs reveal an intramembranous network of strands of particles (~10 nm in diameter) and complementary grooves (Staehelin, 1974) (Figure 2).

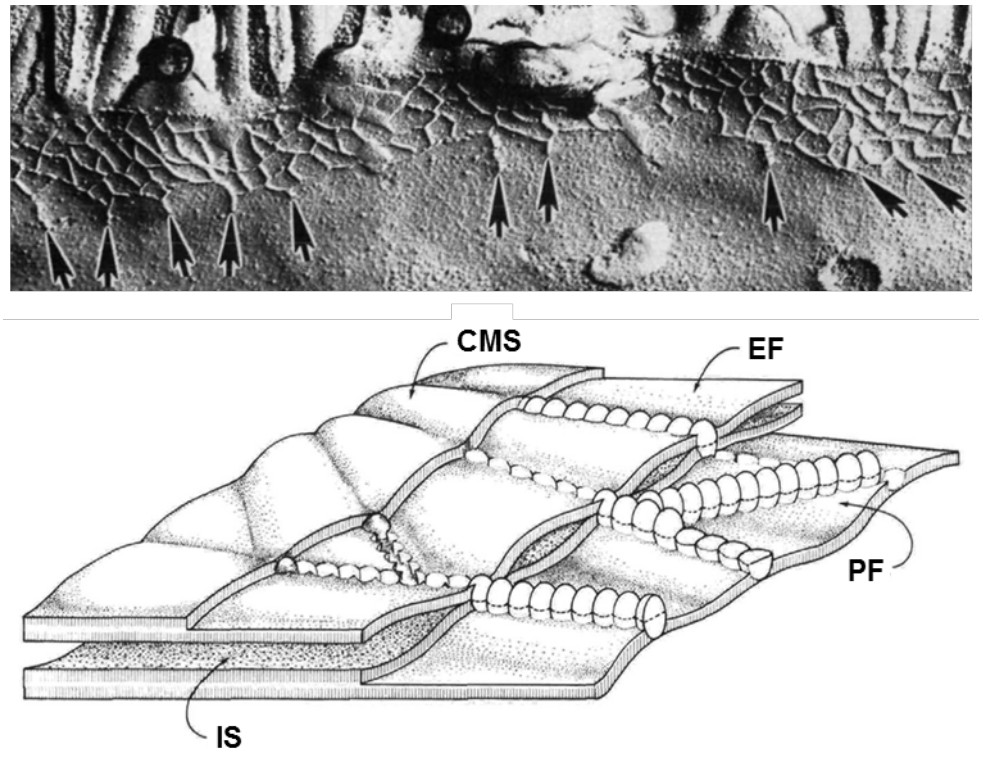


**Figure 2 View of tight junctions upon freeze-fracture electron microscopy (FFEM).** Top: FFEM image of the rat jejunum. TJs are visible as a network of interconnected strands. Bottom: Scheme of the intramembranous particle strands seen upon FFEM. Rows of particles are visible on the protoplasmatic fracture-face (PF) and complementary grooves on the extracellular fracture-face (EF). IS, intercellular space; CMS, cytoplasmic membrane surface. (modified according to Van Itallie and Anderson, 2014)

Various transmembrane proteins are involved in the formation of TJs, whereby three protein families can be distinguished. Among those are the claudins (Cldns) (Morita et al., 1999a) that comprise of 27 family members in mammals (Mineta et al., 2011). These tetraspan proteins with varying barrier properties (Table 1) mainly determine the paracellular impermeability (Krause et al., 2008). Another family are the tight junction-associated MARVEL proteins (TAMPs), occludin (Ocln) (Furuse et al., 1993), tricellulin (Tric) (Ikenouchi et al., 2005) and marveld3 (Raleigh et al., 2010). Ocln (Furuse et al., 1993) as well as Tric (Iwamoto et al., 2014; Mariano et al., 2013) are known to localize in brain endothelial TJs whereas a contribution of marveld3 is yet unknown. Ocln mediates intercellular adhesion and contributes to barrier function (Balda et al., 1996; McCarthy et al., 1996; Yu et al., 2005). In tricellullar TJs, Tric forms a barrier for macromolecules but not for ions (Krug et al., 2009). Distinct but overlapping functions of TAMPs are reported, whereby marveld3 partially compensates a loss of Ocln or Tric (Raleigh et al.,

2010). Also the junctional adhesion molecules JAM-A, JAM-B and JAM-C are involved in the formation and maintenance of TJs (Mandell et al., 2004) (Figure 3). TJ proteins are typically associated with *zonula occludens* proteins (Zo1, Zo2 and Zo3), scaffold proteins that stabilize TJs via interaction with the cytoskeleton (Ebnet et al., 2000; Itoh et al., 1999; Mitic et al., 2000). Endothelial TJs are typically found intermingled with adherens junctions (AJs). Within the AJs, the endothelial-specific integral membrane protein VE-cadherin (Cdh5) is bound to the cytoskeleton via catenins (Bazzoni and Dejana, 2004). Beyond its stabilizing function, Cdh5 mediated adhesion is found to be involved in direct control of Cldn expression (Gavard and Gutkind, 2008).

In addition to the function in restricting paracellular permeability, TJs also segregate the apical and basal domains of the plasma membrane. Based on these polarized properties, carriers including Glut1, the glucose transporter and Lat1, the large neutral amino acid transporter are localized in the plasma membrane to regulate the supply of nutrients to the brain (Begley and Brightman, 2003).

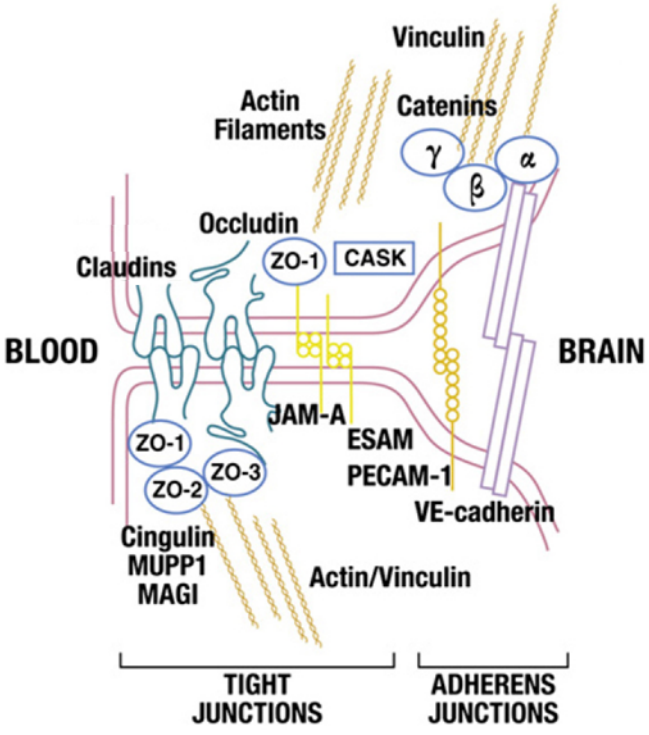


**Figure 3 Molecular composition of tight junctions at the BBB.** Claudins, occludin and junctional adhesion molecules (JAMs) are transmembrane proteins localized at the TJs of the BBB. Within the cytoplasm various first-order adaptor proteins including *zonula occludens* proteins (Zo)-1-3 connect TJ proteins with the actin cytoskeleton. (modified according to Zlokovic, 2008)

## 1.3 Structure and function of claudins

Cldn1 and -2 were discovered as integral membrane proteins exclusively localized in TJs (Furuse et al., 1998a). The Cldn family consists of 27 members currently identified in human and mice. The molecular masses range from 20 to 29 kDa (Mineta et al., 2011). In addition to the tightening potential of Cldns demonstrated for Cldn1, -3, -4, -5, -6, -9, -11, -14, -18 and -19, formation of paracellular ion pores is reported for Cldn2, -7, -8, -10, -15, -16, -17 and -21 (Table 1). Only little is known about the function of Cldn12, -13, -20, -22, -23, -24, -25, -26 and -27. Phylogenetic analysis reveals a high sequence similarity between Cldn1 to -10, -14, -15, -17 and -19. This group is defined as classic Cldns, whereas all remaining family members are namely non-classic Cldns (Krause et al., 2009).
Similar to Ocln and Tric, Cldns exhibit four $\alpha$-helical transmembrane domains connected via two extracellular (ECL) and one intracellular loop (ICL) (Morita et al., 1999a). Most Cldns consist intracellularly of ~7 $NH_2$-terminal, ~12 loop and 25-55 COOH-terminal amino acids. A PDZ-binding motif is localized at the COOH-terminal positions (Zhang et al., 2006). ~50 amino acids with two conserved cysteins form typically the ECL1, whereas the ECL2 has less than ~25 amino acids (Wen et al., 2004) (Figure 4). Residues in the ECL1 are involved in the formation of paracellular ion pores and the determination of their charge selectivity. The ECL2 is thought to associate with itself to possess holding function and to narrow the paracellular cleft (Krause et al., 2008).

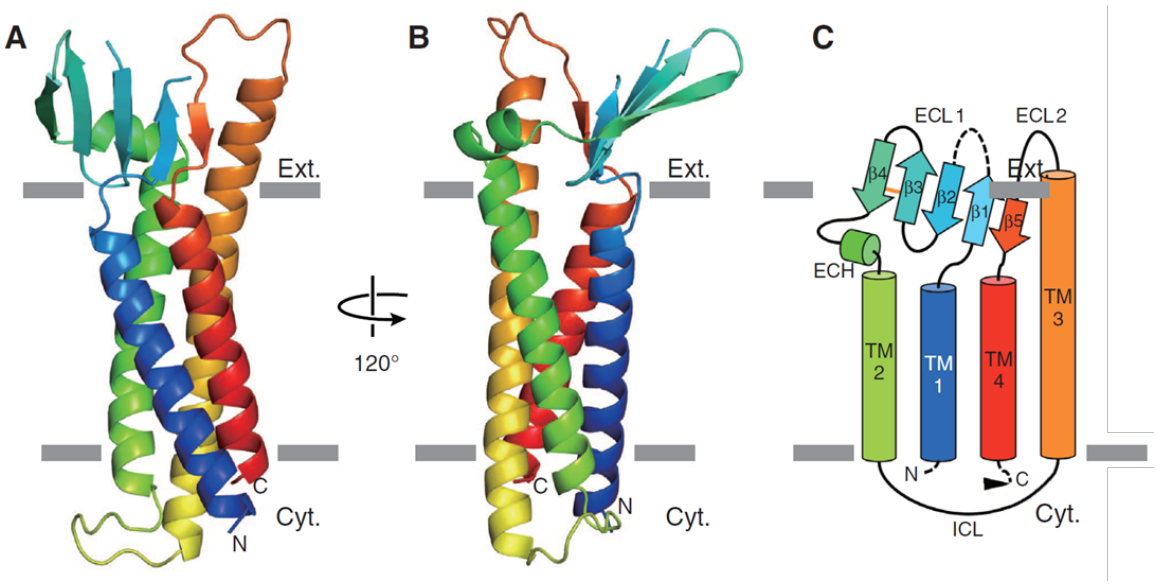

**Figure 4 Crystal structure of a claudin.** All claudins (Cldns) consist of four transmembrane domains (TM), two extracellular loops (ECL) as well as one intracellular loop (ICL), COOH- and $NH_2$-terminus. (A, B) The structure of mouse Cldn15 is shown in ribbon representation. The color changes gradually from $NH_2$-terminus (blue) to COOH-terminus (red). Gray bars indicate the plasma membrane. (C) Secondary structure of mouse Cldn15. A disulfide bond in the ECL1 is shown as orange line. (modified according to Suzuki et al., 2014)

## 1.4 Interaction between claudins

The paracellular barrier formation, the main function of Cldns is realized through interactions of their ECLs. Homophilic interaction of identical Cldns is described as well as heterophilic association between different Cldn subtypes (Furuse et al., 1999). In addition to *trans*-interaction of Cldns of opposing cells, *cis*-interaction occurs within the plasma membrane of the same cell and induces Cldn polymerization visible as TJ strands (Piontek et al., 2008) (Figure 5).

The ECL2 with its aromatic (F147, Y148, Y158) and hydrophilic (Q156, E159) residues is specified in its contribution to *trans*-interaction. A strong binding core formed by aromatic residues of two loops from opposing cells, constricts the paracellular space (Piontek et al., 2008). Overexpression of different Cldn subtypes in HEK-293 cells, which do not exhibit endogenous TJs, results in assembly of TJ strands visualized by freeze fracture electron microscopy (Piontek et al., 2008). Unlike the classic Cldn1, -3, and -5, Cldn12 does not show homophilic *trans*-interaction. Heterophilic *trans*-interaction of Cldn3 and -5 is less pronounced than between Cldn3 and -1, Cldn5 and -1 and all described homophilic interactions (Piontek et al., 2011).

Depending on interacting Cldn subtypes, *cis*-interactions are differentially pronounced in the order: Cldn5/ Cldn5 > Cldn5/ Cldn1 > Cldn3/ Cldn3 > Cldn3/ Cldn5. Therefore steric variation is suggested for different Cldn-*cis*-homooligomers including a higher number of molecules for Cldn5 in comparison with Cldn3 (Piontek et al., 2011).

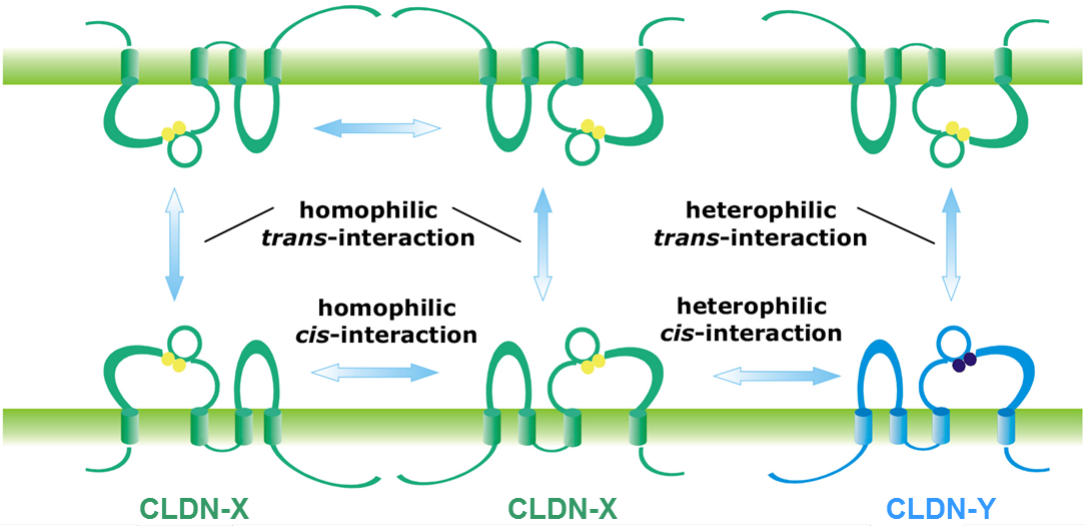


**Figure 5 Interaction possibilities between claudins.** *Trans*-interaction between claudins (Cldns) of two neighboring endothelial cells is crucial for the formation of a paracellular barrier. *Cis*-interaction describes polymerization of Cldns within the same plasma membrane, visible as tight junction strands. Both interactions can be homophilic between Cldns of the same subtype (X-X) or heterophilic between different Cldns (X-Y). (modified according to Krause et al., 2008)

## 1.5 Claudin subtypes at the blood-brain barrier

Cldn subtypes that differ in their barrier properties (Table 1) are expressed in a tissue specific pattern (Krause et al., 2008). A certain combination of Cldns, predominantly tightening or paracellular ion pore forming, within the TJ-strands determines the paracellular tightness (Gunzel and Yu, 2013). In mouse brain endothelial cells, the transcript of *Cldn5* is found most abundant among Cldn1-24 (Ohtsuki et al., 2008). Cldn5 knockout mice exhibit an increased BBB permeability for molecules < 800 Da, but no change in the appearance of TJs in electron micrographs. Also the expression of Cldn12 is considered as a certainty, but its function is unknown (Nitta et al., 2003). Cldn12 is not forming TJ-strands and its incorporation in existing strands is questionable since neither homo- nor heterophilic interactions are found (Piontek et al., 2011). Other tightening Cldns such as Cldn1 or -3 are relatively low expressed compared to Cldn5 (Daneman et al., 2010; Kooij et al., 2014; Ohtsuki et al., 2008). Although, a central role of Cldn3 in determining the integrity of TJs is suggested due to its loss from brain microvessels surrounded by leucocytes associated with inflammation. This observation is accompanied by irregular formation of TJ strands and leakage

through the inflamed vessel walls (Wolburg et al., 2003). The expression of further Cldns is reported only on mRNA level and mainly *in vitro* (Table 1). Hence a contribution of these Cldns to the BBB remains still unclear.

**Table 1 Function of claudin subtypes and the reported expression in the brain endothelium.** Synonyms: Cldn21, putative Cldn25; Cldn25, Cldnd1; Cldn26, Tmem114; Cldn27, Tmem235. -, limited functional knowledge/ no expression in the brain endothelium reported.

| Cldn | Function: paracellular sealing or ion pore-forming | Expression among species and subcellular localization |
|---|---|---|
| **1** | Increases the TER and reduces the paracellular flux of molecules between 4 and 40 kDa in the canine kidney epithelium (Inai et al., 1999) | mRNA in human brain capillaries (Kooij et al., 2014) as well as rat brain endothelial cells (Bocsik et al., 2016)/ mainly cytoplasmic localization in human brain capillaries (Wolburg et al., 2003) |
| **2** | Cation selective channel in canine kidney epithelial cells (Amasheh et al., 2002) | mRNA in rat brain endothelial cells (Bocsik et al., 2016) |
| **3** | Seals for ions of charged and uncharged solutes (Milatz et al., 2010) | mRNA in human brain capillaries (Kooij et al., 2014) as well as rat brain endothelial cells (Bocsik et al., 2016)/ localizes at TJs in human brain capillaries (Wolburg et al., 2003) |
| **4** | Decreases the sodium permeability in canine kidney epithelial cells (Van Itallie et al., 2001) | mRNA in rat brain capillaries (Kratzer et al., 2012) as well as rat brain endothelial cells (Bocsik et al., 2016) |
| **5** | Seals the mouse BBB against molecules < 800 Da (Nitta et al., 2003) | mRNA in human (Kooij et al., 2014) and rat (Kratzer et al., 2012) brain capillaries as well as rat (Bocsik et al., 2016; Ohtsuki et al., 2007) and mouse brain endothelial cells (Brown et al., 2007; Daneman et al., 2010; Ohtsuki et al., 2008; Urich et al., 2012)/ localizes at TJs in human (Wolburg et al., 2003) and mouse (Nitta et al., 2003) brain capillaries as well as in mouse brain endothelial cells (Watanabe et al., 2013) |
| **6** | Increases the TER and reduces the chloride permeability in canine kidney epithelial cells (Sas et al., 2008) | - |
| **7** | Increases the chloride permeability in canine kidney epithelial cells (Hou et al., 2006) | - |
| **8** | Supports the paracellular chloride conductance in mouse collecting duct cells (Hou et al., 2010) | mRNA in mouse brain endothelial cells (Ohtsuki et al., 2008) |
| **9** | Increases the TER and reduces the chloride permeability in canine kidney epithelial cells (Sas et al., 2008) | mRNA in rat brain endothelial cells (Bocsik et al., 2016) |

| | | |
|---|---|---|
| **10** | Cldn10a increases the permeability of anions and Cldn10b of cations in canine kidney epithelial cells (Van Itallie et al., 2006) | mRNA in mouse brain endothelial cells (Ohtsuki et al., 2008) |
| **11** | Absence of TJ strands upon loss of Cldn11 in the CNS myelin and between Sertoli cells (Gow et al., 1999) increases the TER in Sertoli cells (McCabe et al., 2016) | mRNA in rat brain endothelial cells (Bocsik et al., 2016) |
| **12** | - | mRNA in rat (Ohtsuki et al., 2007) and mouse brain endothelial cells (Daneman et al., 2010)/ localizes at TJs in mouse brain capillaries (Nitta et al., 2003) |
| **13** | - | - |
| **14** | Increases the TER and decreases the paracellular permeability for cations in canine kidney epithelial cells (Ben-Yosef et al., 2003) | - |
| **15** | Increases the paracellular cation permeability (Colegio et al., 2002) | mRNA in rat (Bocsik et al., 2016) and mouse brain endothelial cells (Ohtsuki et al., 2008) |
| **16** | Increases the paracellular permeability of magnesium in canine kidney epithelial cells (Gunzel et al., 2009) | mRNA in rat brain capillaries (Kratzer et al., 2012) |
| **17** | Increases the paracellular anion permeability (Krug et al., 2012) | mRNA in mouse brain endothelial cells (Ohtsuki et al., 2008) |
| **18** | Increases the TER and reduces the paracellular permeability of sodium and protons in canine kidney epithelial cells (Jovov et al., 2007) | - |
| **19** | Reduces the permeability of chloride in pig kidney epithelial cells (Hou et al., 2008) | mRNA in rat (Bocsik et al., 2016) and mouse brain endothelial cells (Ohtsuki et al., 2008) |
| **20** | Contrastingly, reduces the TER and the paracellular permeability in human breast cancer cells (Martin et al., 2013) | mRNA in mouse brain endothelial cells (Ohtsuki et al., 2008) |
| **21** | Paracellular channel for small cations and larger solutes (Tanaka et al., 2016) | - |
| **22** | - | mRNA in mouse brain endothelial cells (Ohtsuki et al., 2008) |
| **23** | - | mRNA in mouse brain endothelial cells (Ohtsuki et al., 2008) |
| **24** | - | - |
| **25** | - | mRNA in mouse brain endothelial cells (Daneman et al., 2010) |
| **26** | - | - |
| **27** | - | - |

## 1.6 Post-translational modification of claudins

Post-translational modifications are crucial for proper Cldn function e.g. oligomerization, trafficking, interaction with binding partners, subcellular localization and Cldn homeostasis. These modifications include phosphorylation, palmitoylation, ubiquitination and glycosylation (Liu et al., 2016). Phosphorylation is the most frequent post-translational modification of Cldns. The majority of predicted phosphorylation sites is located in the COOH-terminus. Phosphorylation of tyrosine in the highly conserved COOH-terminal PDZ binding motif disturbs the association of Cldn4 with Zo1 and reduces its localization at TJs (Tanaka et al., 2005). Palmitoylation of cysteine residues in the ICL as well as the COOH-terminus are reported to be essential for TJ assembly (Van Itallie et al., 2005). Polyubiquitination of Cldn5 is found to induce proteasomal degradation resulting in the disassembly of TJs (Mandel et al., 2012). The impact of glycosylation on Cldn function is not clear yet.

### 1.6.1 Glycosylation of claudins

Glycosylation can result in changes of protein folding or half-life and influences various cellular functions, e.g. mediation of cell signaling, immune surveillance, hormone action and carcinogenesis (Moremen et al., 2012). However, an impact on Cldn function is not yet reported. Over 200 gene-encoded glycosyltransferases are responsible for specific glycosylation of membrane proteins (Cummings and Pierce, 2014). The most common glycosylation type is the amide-linked glycosylation of an asparagine (N) side chain (*N*-glycosylation), followed by oxygen (O)-linked glycosylation (*O*-glycosylation) of a serine or threonine side chain (Spiro, 2002). The attachment of certain classes of glycans occurs site specific and varies in pathology (Hanisch and Breloy, 2009) (Figure 6). *N*-glycosylation occurs at the N-X-S/T consensus tripeptide, whereby X can be any amino acid except proline (Kaplan et al., 1987; Marshall, 1972). Characteristic gylcan features of membrane proteins that are unique to cancer cells were previously identified (Anugraham et al., 2014). *N*-glycosylation of the ECL1 of voltage-dependent calcium channel gamma subunits, members of the PMP-22/EMP/MP20/Cldn family is reported to be crucial for proper membrane localization (Price et al., 2005). Via mass-spectrometry two *N*-glycosylation sites

are identified in the first extracellular loop of Cldn25 (Wollscheid et al., 2009). Additionally, *N*-glycosylation of the ECL1 of Cldn1 and -12 were predicted, but experimental evidence is still missing (Price et al., 2005).

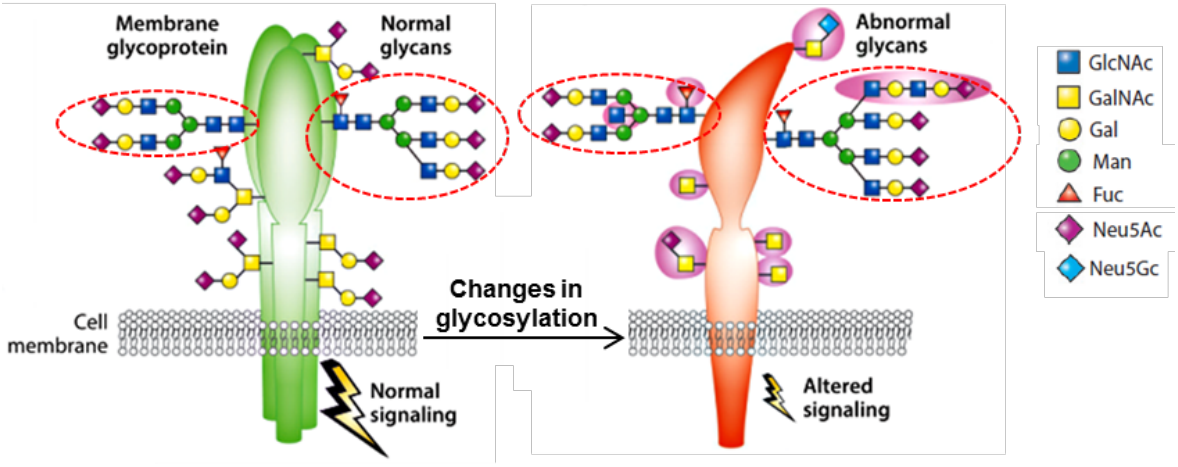


**Figure 6 Cellular transformation e.g. in carcinogenesis is accompanied with the alteration of protein glycan features.** Frequently studied glycans are *N*- (red encircled) and *O*-glycans. The modification of glycan features can result in changes of the protein conformation, oligomerization or turnover and is associated with the alteration of cell signaling pathways. Abbreviations: Fuc, fucose; Gal, galactose; GalNAc, N-acetylgalactosamine; GlcNAc, N-acetylglucosamine; Man, mannose; Neu5Ac, 5-N-acetylneuraminic acid; Neu5Gc, 5-N-glycolylneuraminic acid. (modified according to Stowell et al., 2015)

## 1.7 *Zonula occludens* – a scaffolding protein family

The proper localization and arrangement of Cldns and TAMPs within the plasma membrane is crucial for the formation and maintenance of TJs. Zo proteins bind to the COOH-terminus of Cldns (Itoh et al., 1999) as well as Ocln (Fanning et al., 1998; Furuse et al., 1994; Haskins et al., 1998) and thereby associate with the TJ complex. Association of the TJ complex with the cytoskeleton is supported by interaction of Zo proteins with actin (Haskins et al., 1998). Ocln is known to directly interact with F-actin (Wittchen et al., 1999), whereas Cldns require these scaffolding proteins to associate with the cytoskeleton. In epithelial cells that do not form TJs due to the loss of Zo1 and -2, exogenously expressed Zo1 and -2 are recruited to the junctional area and induce Cldn polymerization (Umeda et al., 2006). Furthermore, a role of Zo1 and -2 in regulating the organization and functional activity of the apical cytoskeleton is reported (Fanning et al., 2012). The embryonic lethality of Zo1 deficient mice associated with defects in vascular

development emphasizes the importance of this TJ associated protein (Katsuno et al., 2008).

### 1.7.1 Association of claudins and TAMPs with *zonula occludens* protein 1

All three Zo proteins exhibit three different domains that alter in their function, three PDZ domains, the SRC homology 3 domain (SH3) and a guanylate kinase-like (GK) domain (Figure 7). PDZ domains are crucial for the anchoring and clustering of transmembrane proteins (Kim et al., 1995). The PDZ1 domain is reported to bind COOH-terminally of Cldns (Itoh et al., 1999). The binding sequences of Zo1-PDZ1 are characterized by valine, isoleucine or leucine at position$^{0}$; tryptophan or tyrosine at position$^{-1}$; threonine or serine at position$^{-2}$ and arginine, lysine, serine or threonine at position$^{-3}$. Strong preferences for hydrophobic residues at position$^{-4}$ and aromatic residues at position$^{-6}$, but no clear preferences at position$^{-5}$ are reported (Zhang et al., 2006). A mutation in the PDZ1 binding motif is reported to lead to intracellular retention and lysosomal mistargeting of Cldn16 (Kausalya et al., 2006; Muller et al., 2003). Zo1 associates with Zo2 and -3 through heterophilic interaction of their PDZ2 domains (Fanning and Anderson, 1996). Furthermore, PDZ2 and -3 are binding sites for JAMs (Ebnet et al., 2000). Ocln interacts with the GK domain of Zo1 (Mitic et al., 2000) as well as with Zo2 and 3 (Fanning et al., 1998; Furuse et al., 1994; Haskins et al., 1998). The ELL domain in the COOH-terminus of Ocln is identified as interaction site (Li et al., 2005). The COOH-terminal domain of Zo1 directly binds to actin and thereby associates with the cytoskeleton (Fanning et al., 1998). Importantly, this interaction is demonstrated to be vital for the stabilization of the TJ complex (Van Itallie et al., 2009).

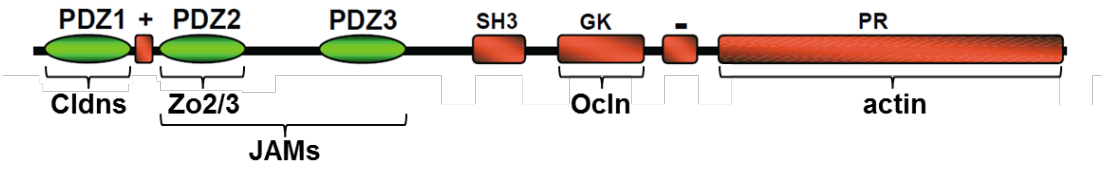


**Figure 7 Structure of *zonula occludens* protein (Zo)-1. The** PDZ domains are indicated in green. Association with TJ proteins, Zo proteins or actin is written below. Cldn, claudin; JAM, junctional adhesion molecule; Ocln, occludin. (modified according to Gonzalez-Mariscal et al., 2003)

## 1.8 Pathologies associated with disruption of brain endothelial tight junctions

In various cerebral pathologies, BBB tightness is affected and the expression of TJ proteins changed (Daneman and Prat, 2015). Disruption of TJs can involve an opening to ions and molecules as well as infiltration of immune cells. In short term, this process can enable protective immunoreactions in the CNS. Extended BBB disruption leads to vasogenic edema, characterized by an increase of the brain volume due to enhanced movement of water and plasma proteins into the brain (Daneman, 2012). A breakdown of the BBB often arises as a consequence of a primary event such as in traumatic brain injury or stroke. Concerning CNS disorders like multiple sclerosis, epilepsy and Alzheimer's disease, it is still under investigation whether BBB dysfunction plays a role in the onset of the disease (Correale and Villa, 2007; Huang et al., 2006; Oby and Janigro, 2006).

### 1.8.1 Ischemic stroke increases blood-brain barrier permeability

Edema subsequent to stroke is the second leading cause of death and disability in developed countries (Yu et al., 2011). Two periods of ischemic stroke can be distinguished, ischemia and reperfusion, which differ in their pathological impact (Figure 8).

The initial ischemic phase is characterized by the loss of cerebral blood-flow due to mechanical plugging of a blood vessel by thrombi or emboli. As a result, the supply of oxygen and nutrients to the surrounding tissue is disturbed. The endothelium of brain capillaries in the core ischemic zone is reported to be associated with dysregulation and disassembly of TJs resulting in an increase of the paracellular permeability (Sandoval and Witt, 2008). Within the first hours of ischemic onset, Cldn5, Ocln and Cdh5 are degraded at protein level (Teng et al., 2013; Yang et al., 2007). Restriction of oxygen supply for 24 h is reported to alter the location of Cldn5 in the plasma membrane of brain endothelial cells accompanied with a decrease in protein level (Koto et al., 2007). A degradation of Cldn5 and Ocln by matrix metalloproteinases (MMPs) that are activated under hypoxic conditions is reported (Yang and Rosenberg, 2011). Hyperoxia treatment (95% $O_2$) of isolated brain capillaries inhibited MMP-9 mediated Ocln degradation

(Liu et al., 2009). Furthermore, Cldn1 in mouse brain endothelial cells (Brown et al., 2003) as well as Cldn3 and -5 in the rat brain (Li et al., 2015) are indicated to respond to oxidative stress. Ocln plays a key role in the response of cellular barriers to redox changes and is a redox sensor at TJs (Bellmann et al., 2014; Cording et al., 2015). Various events are associated with ischemia e.g. decrease of ATP, acidosis, increased intracellular calcium, oxidative stress and activation of inflammatory processes (Sandoval and Witt, 2008).

Following ischemia, the reperfusion period is characterized by a re-establishment of the cerebral blood-flow. Despite being crucial for tissue survival, reperfusion can lead to brain hemorrhage due to rupture of weakened brain capillaries. Initial hypoperfusion is followed by permeability changes in a biphasic manner (Figure 8). The first phase, ~3 - 8 h post ischemic reperfusion is characterized by increased inflammatory and oxidative stress at the BBB (Heo et al., 2005; Wang and Shuaib, 2007). The second phase, ~18 - 96 h after reperfusion is associated with angiogenesis and increased vasogenic edema (Kuroiwa et al., 1985). Assembly and disassembly of TJs resulting in changes of the paracellular permeability are reported (Sandoval and Witt, 2008). The regulatory mechanisms supporting the assembly of TJs after ischemic reperfusion are still unclear.

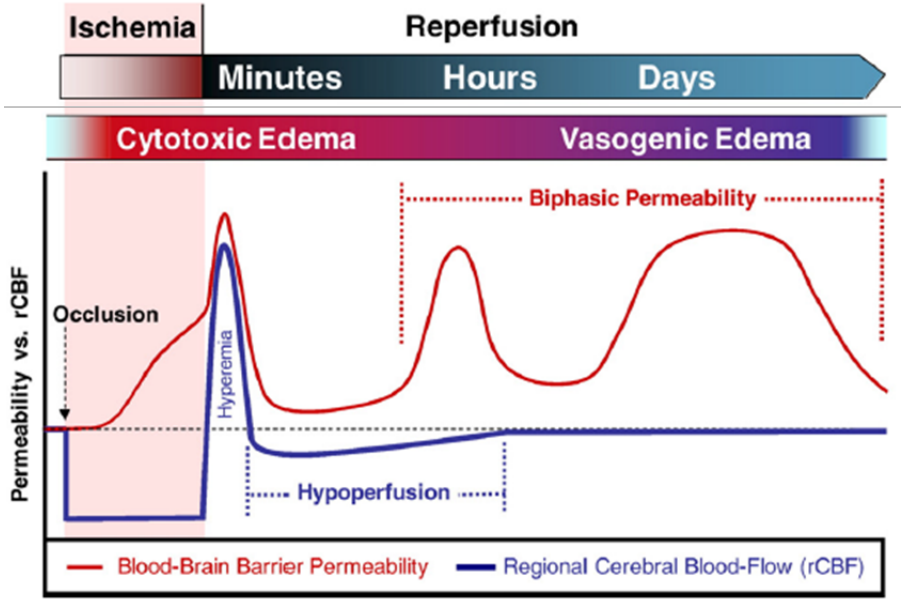


**Figure 8 Impact of cerebral ischemia on blood-brain barrier permeability.** The course of changes in permeability as well as regional cerebral blood-flow is indicated depending on reperfusion time. Variability might occur with respect to distance from ischemic core or duration of ischemic insult. (modified according to Sandoval and Witt, 2008)

# 2 Objectives

Cldn5 is thought to dominate the TJs of the BBB. However, the loss of Cldn5 in mice does not alter the appearance of those TJs in electron micrographs. A major goal of this work is to systematically analyze the expression of all TJ proteins in the human and mouse brain endothelium. Differences in expression between the species are especially of importance to evaluate scientific data originating from the mouse model, which is widely used in BBB research. Furthermore, the impact of translational regulation on the expression of TJ proteins is not yet investigated and of great necessity to interpret differences in mRNA levels. Furthermore, *in vitro* BBB models are investigated in their complexity of TJ protein expression with respect to the brain endothelium *ex vivo*. Novel BBB-Cldns need to be characterized with respect to subcellular localization within the brain endothelium as well as their function as paracellular barrier. The TEER upon knockdown of Cldns is analyzed to investigate their barrier properties. It is of particular importance to elucidate the potential of novel BBB-Cldns to interact with Zo1, known to stabilize the TJ complex at cell-cell contacts. A deeper analyzes of the impact of the loss of Cldn5 at the BBB is intended. This includes the TJ strand morphology visualized by freeze-fracture electron microscopy as well as the expression of other TJ proteins. Additionally, it is of interest if changes in BBB permeability during post ischemic reperfusion are associated with the transcriptional regulation of TJ proteins. In summary, the aim of this work is to elucidate the contribution of Cldns and TAMPs to the BBB, and to reveal differences in function and response to pathology.

# 3 Material and methods

## 3.1 Material

### 3.1.1 Devices

All devices, the version and the supplier are listed in Table 2.

**Table 2 Devices**

| Device | Version | Supplier |
|---|---|---|
| Agarose gel chamber | Agagel Mini | Biometra GmbH, Göttingen, Germany |
| Blotting device | Trans-Blot®-SD (semi dry) | Bio-Rad Laboratories GmbH, Munich, Germany |
| Centrifuge | 5810R | Eppendorf, Hamburg, Germany |
| Centrifuge | 5415C | Eppendorf, Hamburg, Germany |
| Dounce tissue grinder set | | Sigma-Aldrich Chemie GmbH, Steinheim, Germany |
| Clean bench | S-1200 | BDK Luft- und Raumtechnik, Sonnenbühl-Genkingen, Germany |
| Cover slip holder | - | Custom build by the FMP, Berlin, Germany |
| Coverslip staining tray | - | Custom build by the FMP, Berlin, Germany |
| Cryocontainer | - | Nalgene Labware, Rochester, NY, USA |
| Cryostat | Cryostat CM 3000 | Leica, Wetzlar, Germany |
| Electric cell-substrate impedance sensing (ECIS) instrument | ECIS 1600R + 16 well array station | Applied Biophysics Inc, Troy, NY, USA |
| Electrophoresis power supply (SDS-PAGE) | 3000Xi | Bio-Rad Laboratories GmbH, Munich, Germany |
| Electrophoresis power supply (agarose gel) | Consort E835 | Sigma-Aldrich Chemie GmbH, Steinheim, Germany |
| Electroporation cuvette | - | Peqlab, Biotechnologie GmbH, Erlangen Germany |
| Electroporation device | EasyjecT prima | Equibio/Thermo Electron, Milford, MA, USA |
| Emulsifier | EmulsiFlex-C3 | Avestin Europe GmbH, Mannheim, Germany |
| Fluorescence-microscope | BH-2 | OLYMPUS Europa GmbH, Hamburg, Germany |
| Gel documentation device | FLA-5000 | Fujifilm Europe GmbH, Düsseldorf, Germany |
| Glass plates (SDS-PAGE) | Hoefer® vertical slab gels | Hoefer, Pharmacia Biotech Inc. San Francisco, California, USA |

| | | |
|---|---|---|
| Heating block | Thermomixer 5436 | Eppendorf, Hamburg, Germany |
| Hemocytometer | - | Carl Roth GmbH, Karlsruhe, Germany |
| Homogenizer | LM10 Microfluidizer® | Microfluidics, Westwood, MA, USA |
| Incubator for bacteria | CB210 | Binder GmbH, Tuftlingen, Germany |
| Incubator for cell culture | CB210 | Binder GmbH, Tuftlingen, Germany |
| Laser capture microdissection microscope | PALM MicroBeam; AxioCam MRm, 355 nm cut laser (0.5 mW, 90 µJ, 2 ns); Fluar 10x/ NA = 0.5 (WD = 1.9 mm) (420140-9900); LD Plan-Neofluar 20x/ NA = 0.4 (WD = 7.9 mm) (421350-9970) | Carl Zeiss Jena GmbH, Jena, Germany |
| Laser scanning microscope | LSM 780 & META-UV | Carl Zeiss Jena GmbH, Jena, Germany |
| Light microscope | IMT-2 | Olympus Europa GmbH, Hamburg, Germany |
| Magnetic stirrer | IKAMA®RCT | IKA®-Labortechnik, Staufen, Germany |
| Microscale thermophoresis device | Monolith NT.115 | NanoTemper Technologies GmbH, Munich, Germany |
| Monochromator-based microplate detection system | Safire | Tecan Group Ltd, Männedorf, Switzerland |
| PCR-thermocycler | DNA Engine | Bio-Rad Laboratories GmbH, Munich, Germany |
| pH-meter | CG 840 | Schott AG, Mainz, Germany |
| Power supply (blotting device) | 200/2.0 | Bio-Rad Laboratories GmbH, Munich, Germany |
| Real Time PCR system | StepOne TM Real-Time PCR system, 48/96 well | Life Technologies GmbH, Darmstadt, Germany |
| Scale | MC1 LC 2200S | Sartorious AG, Göttingen, Germany |
| SDS-PAGE gel chamber | Small II (SE250/260) | Might Hoefer, Pharmacia Biotech Inc. San Francisco, California, USA |
| Shaker | TH 15 | Edmund Bühler GmbH, Hechingen, Germany |
| Spectral photometer | DU 640 | Beckman Coulter GmbH, Krefeld, Germany |
| Spectral photometer | NanoDrop2000c | Thermo Fisher SCIENTIFIC GmbH, Bremen, Germany |
| Speed Vac | Sarvant DNA Speed Vac®, DNA 110 | Thermo Fisher SCIENTIFIC GmbH, Bremen, Germany |
| Transilluminator | Lumi-Imager F1T | Boehringer-Mannheim GmbH, Mannheim, Germany |

| | | |
|---|---|---|
| Tube rotator | SB1 | Stuart, Staffordshire, UK |
| Vaccum pump | Vacusafe | Integra Biosciences GmbH, Biebertal, Germany |
| Vortex device | VF-2 | IKA®-Labortechnik, Staufen, Germany |
| Waterbath | 1002 | GFL, Burgwedel, Germany |

### 3.1.2 Consumable supplies

Consumable supplies are listed in Table 3.

**Table 3 Consumable supplies**

| Consumable supplies | Supplier |
|---|---|
| 12-well-tissue culture plate (4 $cm^2$ per well) | TPP Techno Plastic Products AG, Trasadingen, Germany |
| 24-well-tissue culture plate (2 $cm^2$ per well) | TPP Techno Plastic Products AG, Trasadingen, Germany |
| 25 $cm^2$-tissue culture flask | Corning Incorporated, NY, USA |
| 3 mm Whatman-paper | Biostep GmbH, Jahnsdorf, Germany |
| 6-well-tissue culture plate (10 $cm^2$ per well) | TPP Techno Plastic Products AG, Trasadingen, Germany |
| 75 $cm^2$-tissue culture flask | Corning Incorporated, NY, USA |
| 96-well plate | TPP Techno Plastic Products AG, Trasadingen, Germany |
| Adhesive Caps 500 opaque | Carl Zeiss Jena GmbH, Jena, Germany |
| Amicon® Ultra-15 Centrifugal Filter Device (30K, 100K) | Merck Millipore, MA, USA |
| BD Falcon (polystyrene Round-Bottom) | BD, Dickinson and Company, Franklin Lakes, NJ |
| Biosphere®Filter Tip (0.1 – 1000 µl) | Sarstedt AG & Co., Numbrecht, Germany |
| Cannula | B.Braun AG, Melsungen, Germany |
| Capillaries (standard treated) | NanoTemper Technologies GmbH, Munich, Germany |
| tissue culture flask CellBIND Surface | Corning Incorporated, NY, USA |
| Cell scraper | TPP, Trasadingen, Switzerland |
| Coverslips (diameter 12 mm) | Menzel GmbH, 15 Braunschweig, Germany |
| Coverslips (diameter 30 mm) | Menzel GmbH, 15 Braunschweig, Germany |
| Cryotubes | Corning Incorporated, NY, USA |
| ECIS® chip 8W10E+ | Ibidi GmbH, Planegg / Martinsried, Germany |
| Electroporation-cuvette | Peqlab, Biotechnologie GmbH, Erlangen, |
| Emersion oil for microscopy | VWR International GmbH, Darmstadt, Germany |
| Histo PAP pen | Abcam plc, Cambridge, UK |
| Membrane Slides 1.0 PEN | Carl Zeiss Jena GmbH, Jena, Germany |
| MicroAmp® Fast Optical 96-Well Reaction Plate | Life Technologies GmbH, Darmstadt, |

| | |
|---|---|
| MicroAmp® Fast Optical 48-Well Reaction Plate | Life Technologies GmbH, Darmstadt, Germany |
| MicroAmp® Optical Adhesive Film | Life Technologies GmbH, Darmstadt, Germany |
| Mr. Frosty™ Freezing Container | ThermoFisher Scientific, Waltham, MA, USA |
| Nitrocellulose membrane (Amersham Hybond) | GE Healthcare, Buckinghamshire, UK |
| Object slide | Menzel GmbH, 15 Braunschweig, Germany |
| Parafilm | Carl Roth GmbH, Karlsruhe, Germany |
| Protein columns (20 ml) | Bio-Rad Laboratories GmbH, Munich, Germany |
| Tissue-Tek | VWR International GmbH, Darmstadt, Germany |

### 3.1.3 Chemicals and kits

Chemicals are listed in Table 4.

**Table 4 Chemicals and kits**

| Chemicals | Supplier |
|---|---|
| 1 kb DNA Ladder (GeneRuler™) | Fermentas Life Science, St. Leon-Rot, Germany |
| 1,4-Dithiothreitol (DTT) | Carl Roth GmbH, Karlsruhe, Germany |
| 100 bp Plus DNA Ladder (GeneRuler™) | Fermentas Life Science, St. Leon-Rot, Germany |
| 2-Methylbutane | Sigma-Aldrich Chemie GmbH, München, Germany |
| 4', 6-diamidino-2-phenylindole (DAPI) | Sigma-Aldrich Chemie GmbH, München, Germany |
| 6x DNA loading dye | Fermentas Life Science, St. Leon-Rot, Germany |
| Acetone | Carl Roth GmbH, Karlsruhe, Germany |
| Acetonitrile | Sigma-Aldrich Chemie GmbH, München, Germany |
| Acrylamide | Carl Roth GmbH, Karlsruhe, Germany |
| Agarose | Serva Electrophoresis GmbH, Heidelberg, Germany |
| Ammonium bicarbonate | Sigma-Aldrich Chemie GmbH, München, Germany |
| Ammoniumperoxidsulfate (APS) | Bio-Rad Laboratories GmbH, Munich, Germany |
| Ampicillin | Carl Roth GmbH, Karlsruhe, Germany |
| Amylose Resin | New England Biolabs, Ipswich, MA, US |
| Blotting grade blocker non-fat dry milk | Bio-Rad Laboratories GmbH, Munich, Germany |
| Bovine serum albumin (BSA) | Serva Electrophoresis GmbH, Heidelberg, Germany |
| Bradford Reagent | Sigma-Aldrich Chemie GmbH, München, Germany |

| | |
|---|---|
| Collagen | Carl Roth GmbH, Karlsruhe, Germany |
| Coomassie brilliant blue G-250 | Carl Roth GmbH, Karlsruhe, Germany |
| Dimethyl sulfoxide (DMSO) | Sigma-Aldrich Chemie GmbH, Steinheim, Germany |
| DMSO (cell culture quality) | Biochrom AG, Berlin, Germany |
| DNA Clean and Concentrator-5 kit | Zymo Research, Irvine, CA, USA |
| dNTPs (10 mM) | Fermentas Life Science, St. Leon-Rot, Germany |
| Dulbecco's PBS with $Mg^{2+}$ and $Ca^{2+}$ | Invitrogen GmbH, Darmstadt, Germany |
| Dylight® 594 labeled ricinus communis agglutinin I (RCA1) | Vector Laboratories, Burlingame, CA, USA |
| E.Z.N.A Plasmid DNA Midi Kit I | VWR International GmbH, Darmstadt, Germany |
| E.Z.N.A Plasmid DNA Mini Kit I | VWR International GmbH, Darmstadt, Germany |
| Ethanol | J.T. Baker, Deventer, Netherlands |
| Ethylenediaminetetraacetic acid (EDTA) | Sigma-Aldrich Chemie GmbH, München, Germany |
| Fluorescein labeled ricinus communis agglutinin I (RCA1) | Vector Laboratories, Burlingame, CA, USA |
| GeneMatrix Universal RNA purification kit | Roboklon GmbH, Berlin, Germany |
| Geneticin (G418) | Carl Roth GmbH, Karlsruhe, Germany |
| GFP-Trap®_A | Chromotek, Planegg-Martinsried, Germany |
| Glycerol | Carl Roth GmbH, Karlsruhe, Germany |
| Glycin | Carl Roth GmbH, Karlsruhe, Germany |
| Hank's Balanced Salt Solution (HBSS++) | ThermoFisher Scientific, Waltham, MA, USA |
| Immomount | Thermo Fisher Scientific Inc., Waltham, MA, USA |
| Isopropyl alcohol | Carl Roth GmbH, Karlsruhe, Germany |
| Isopropyl β-D-1-thiogalactopyranoside (IPTG) | Carl Roth GmbH, Karlsruhe, Germany |
| Kanamycin | Carl Roth GmbH, Karlsruhe, Germany |
| LB (Lysogeny broth) | Carl Roth GmbH, Karlsruhe, Germany |
| LB agar | Carl Roth GmbH, Karlsruhe, Germany |
| L-cysteine | Carl Roth GmbH, Karlsruhe, Germany |
| Lumi-Light Western Blotting Substrate | Roche Diagnostics GmbH, Mannheim, Germany |
| Luminaris Color HiGreen qPCR Master Mix, high ROX qPCR Master Mix | ThermoFisher Scientific, Waltham, MA, USA |
| Magnesium chloride | ThermoFisher Scientific, Waltham, MA, USA |
| Maltose | Carl Roth GmbH, Karlsruhe, Germany |
| Maxima First Strand cDNA Synthesis Kit for RT-qPCR | Thermo Fisher Scientific Inc., Waltham, MA, USA |
| Methanol | Carl Roth GmbH, Karlsruhe, Germany |
| Monolith NTTM Protein Labeling Kit RED-NHS | NanoTemper Technologies GmbH, Munich, Germany |
| NP-40 Alternative | Merck Millipore, MA, USA |
| PageRuler Plus Prestained Protein Ladder | Thermo Fisher Scientific Inc., Waltham, MA, USA |
| Penicillin/ streptomycin (P/S) | Carl Roth GmbH, Karlsruhe, Germany |
| Perchloric acid | Carl Roth GmbH, Karlsruhe, Germany |
| Phosphate buffered saline (PBS) | Biochrom AG, Berlin, Germany |
| Pierce Glycoprotein Staining Kit | Thermo Fisher Scientific Inc., Waltham, MA, |

| | |
|---|---|
| | USA |
| Pierce Protease Inhibitor mini tablets | ROCHE, Basel, Switzerland |
| Polyacrylamide mix (30%) | Carl Roth GmbH, Karlsruhe, Germany |
| Polyethylenimine (PEI) | Polysciences, Warrington, PA, USA |
| Poly-L-lysine (PLL) | Sigma-Aldrich Chemie GmbH, Steinheim, Germany |
| Puromycin | Sigma-Aldrich Chemie GmbH, Steinheim, Germany |
| Rat tail collagen | ROCHE, Basel, Switzerland |
| Roti-Mount FlourCare DAPI (mounting medium) | Carl Roth GmbH, Karlsruhe, Germany |
| Sodium azide | Carl Roth GmbH, Karlsruhe, Germany |
| Sodium-Dodecyl sulfate (SDS) | Sigma-Aldrich Chemie GmbH, München, Germany |
| SuperSignal® West Femto Maximum Sensitivity Substrate (super ECL) | ThermoFisher Scientific, Waltham, MA, USA |
| SYBR®Safe DNA gel staining solution (10000x concentrated in DMSO) | Invitrogen GmbH, Darmstadt, Germany |
| Tetramethylethylenediamine (TEMED) | Carl Roth GmbH, Karlsruhe, Germany |
| Tris Base | Carl Roth GmbH, Karlsruhe, Germany |
| Triton X-100 | Sigma-Aldrich Chemie GmbH, Steinheim, Germany |
| Trypan blue | Merck Bioscience Ltd, Darmstadt, Germany |
| Trypsin/ EDTA (0.05% or 0.25%/ 0.02%), in PBS without $Ca^{2+}$/ $Mg^{2+}$ | Biochrom AG, Berlin, Germany |
| Tween®20 (polysorbate) | Merck Schuchardt, Hohenbrunn, Germany |
| ZR Plasmid Miniprep™-Classic | Zymo Research Corp, Irvine, CA, USA |
| Zymoclean™ Gel DNA Recovery Kit | Zymo Research Corp, Irvine, CA, USA |
| β-mercaptoethanol | Sigma-Aldrich Chemie GmbH, Steinheim, Germany |

### 3.1.4 Cultivation media

Table 5 comprises the cultivation media for procaryotic and eukaryotic cells, as well as their composition.

**Table 5 Cultivation media**

| Cultivation medium | Composition | Supplier |
|---|---|---|
| *For bacteria* | | |
| LB agar | LB medium with 2% (w/v) agar | Carl Roth GmbH, Karlsruhe, Germany |
| LB medium | 1% (w/v) NaCl, 0.5% (w/v) yeast extract, 1% (w/v) peptone | Carl Roth GmbH, Karlsruhe, Germany |
| *For cell culture* | | |
| BC medium | DMEM high glucose, 20% (v/v) FCS, 1% (v/v) penicillin (100 U/ml)/ streptomycin (100 µg/ml) | - |
| bEND.3/ HEK-293T medium | DMEM high glucose, 10% (v/v) FCS, 1% (v/v) penicillin (100 U/ml)/ streptomycin (100 µg/ml) | - |

| | | |
|---|---|---|
| Caco-2 medium | DMEM, 20% (v/v) FCS, 1% (v/v) penicillin (100 U/ml)/ streptomycin (100 µg/ml), 1% non-essential amino acids | - |
| DMEM | 4 mM L-glutamine, 1 g/l glucose, 1 mM Na-Pyruvat, phenol red | Invitrogen GmbH, Darmstadt, Germany |
| DMEM high glucose | 4 mM L-glutamine, 4.5 g/l glucose, 1 mM Na-Pyruvat, phenol red | Invitrogen GmbH, Darmstadt, Germany |
| Fetal calve serum (FCS) | | Biochrom AG, Berlin, Germany |
| HEK-293/ MDCKII medium | DMEM, 10% (v/v) FCS, 1% (v/v) penicillin (100 U/ml)/ streptomycin (100 µg/ml) | - |
| Opti-MEM | L-glutamine, 2.4 g/l sodium bicarbonate, phenol red | Invitrogen GmbH, Darmstadt, Germany |
| Primary bEND medium | DMEM high glucose, 20% (v/v) FCS, 1% (v/v) penicillin (100 U/ml)/ streptomycin (100 µg/ml), 0.5% (v/v) mouse serum, 0.33% (v/v) endothelial cell growth factor (ECGF) | - |
| Transfection medium | DMEM, 5% (v/v) FCS | - |

### 3.1.5 Buffers and solutions

All buffers and solutions as well as the composition are listed in Table 6.

**Table 6 Buffers and solutions**

| Buffers and solutions | Composition |
|---|---|
| *Agarose gel electrophoresis* | |
| TAE buffer | 400 mM Tris (pH 8.5), 10 mM EDTA, 200 mM perchloric acid |
| *Immunofluorescence labeling* | |
| Blocking buffer | PBS (pH 7.4), 1% BSA, 0.05% Tween 20, 0.02% sodium azide |
| *Protein purification* | |
| Benzonase mix | 50 mM Tris (pH 8.8), 2 mM $MgCl_2$, 100 U/ml benzonase |
| Cell lysis extraction buffer | PBS (pH 7.4), 1% Triton X-100, protease inhibitor (1 tablet per 10 ml) |
| Cell lysis solubilisation buffer (pH 8.8) | 50 mM Tris (pH 8.8), 5 mM EDTA, 1% SDS |
| MBP elution buffer | PBS (pH 7.4), 1 mM EDTA, 10 mM Maltose |
| MBP lysis buffer | PBS (pH 7.4), protease inhibitor (1 tablet per 10 ml), 100 U/ml benzonase |
| MBP wash buffer | PBS (pH 7.4), 1 mM EDTA |
| *SDS-PAGE* | |
| SDS running buffer | 25 mM Tris (pH 8.3), 192 mM glycine, 0.1% (w/v) SDS |
| 4x SDS loading buffer | 200 mM Tris/HCl (pH 6.8), 8% (w/v) SDS; 40% (v/v) glycerol, 0.4 M DTT; 0.04% (w/v) bromophenol blue |
| Coomassie dye | 0.04% Coomassie G250, 3.5% ethanol, 3.4% perchloric acid |
| Ponceau dye | 0.2% (w/v) Ponceau S, 1% acetic acid |

| | |
|---|---|
| Separation gel (12%) | 1.5 M Tris (pH 8.8), 12% acrylamide mix, 10% SDS, 10% ammonium persulfate, 1% TEMED |
| Stacking gel | 1 M Tris (pH 6.8), 4% acrylamide mix, 10% SDS, 10% ammonium persulfate, 1% TEMED |
| *Western blotting* | |
| TBST buffer | 10 mM Tris (pH 7.4), 150 mM NaCl, 0.05% (v/v) Tween 20 |
| Transfer buffer | 25 mM Tris (pH 8.3), 192 mM glycine, 10% (v/v) methanol |

### 3.1.6 Enzymes

Table 7 registers enzymes and the associated buffers.

**Table 7 Enzymes**

| **Enzyme** | **Concentration/ activity** | **Supplier** |
|---|---|---|
| AccuPOL DNA Polymerase | 2.5 U/µl; 1 U/ 20 ng template DNA, 1-2 min/kb template DNA, 72 ºC | VWR International GmbH, Darmstadt, Germany |
| Benzonase | 25 U/µl; 1 U/ 37 µg DNA, 30 min, 37 ºC | Merck Biosciences Ltd, Darmstadt, Germany |
| Collagenase | 125 U/mg solid; 1 U/ 1 nmol Leu equivalent, collagen, 1 min, 37°C, pH 7.2 | Merck Biosciences Ltd, Darmstadt, Germany |
| Dispase | 10 U/mg solid, 1 U/ Folin-positive amino acids and peptides (corresponding to 1 µmol tyrosine), 1 min, 37 °C, pH 7.5 | Merck Biosciences Ltd, Darmstadt, Germany |
| Fast Digest *Bam*HI | 1 U/µl; 1 U/ 1 µg plasmid DNA, 5 min, 37 ºC; 1 U/ 0.2 µg PCR product, 5 min, 37 ºC | Fermentas Life Science, St. Leon-Rot, Germany |
| Fast Digest *Dpn*I | 1 U/µl; 1 U/ 1 µg plasmid DNA, 5 min, 37 ºC | Fermentas Life Science, St. Leon-Rot, Germany |
| Fast Digest *Hind*III | 1 U/µl; 1 U/ 1 µg plasmid DNA, 15 min, 37 ºC; 1 U/ 0.2 µg PCR product, 20 min, 37 ºC | Fermentas Life Science, St. Leon-Rot, Germany |
| Fast Digest *Sal*I | 1 U/µl; 1 U/ 1 µg plasmid DNA, 15 min, 37 ºC; 1 U/ 0.2 µg PCR product, 60 min, 37 ºC | Fermentas Life Science, St. Leon-Rot, Germany |
| T4-DNA-ligase | 400 U/µl; 1 U/ 50% ligation of *Hind*III fragments of λ DNA (0.12 µM), 30 min, 16°C | Promega, Madison, WI, USA |
| Trypsin | 10000 U/mg; 1 U/ $\Delta A_{253}$ of 0.001, Na-benzoyl-L-arginine ethyl ester as substrate, 1 min, 30°C | Promega, Madison, WI, USA |
| **Buffer** | **Composition** | **Supplier** |
| Fast Digest buffer (10X) | (confidential) | Fermentas Life Science, St. Leon-Rot, Germany |
| T4-ligase buffer (10X) | 300 mM Tris HCl (pH 7.8), 100 mM $MgCl_2$, 100 mM DTT, 10 mM ATP | Promega, Madison, WI, USA |
| AccuPOL Key Buffer (10X) | Tris-HCl (pH 8.5), $(NH4)_2SO_4$ (concentration confidential), 15 mM $MgCl_2$, 1% Tween 20 | VWR International GmbH, Darmstadt, Germany |

### 3.1.7 Plasmids

Plasmid constructs (m, mouse), the originating vector, restrictions sites of the insert and the resistance for bacterial selection as well as the corresponding references are listed in Table 8.

**Table 8 Plasmids**

| Construct | Vector | Restriction site | Resistance* | Supplier/ reference |
|---|---|---|---|---|
| - | pMal-c2x | - | Amp | New England Biolabs, Boston, MA, USA |
| MBP-mCldn1$_{188-211}$ | pMal-c2x | BamHI/ SalI | Amp | This work |
| MBP-mCldn4$_{186-210}$ | pMal-c2x | BamHI/ SalI | Amp | This work |
| MBP-mCldn5$_{141-161}$ | pMal-c2x | - | Amp | (Blasig et al., 2006) |
| MBP-mCldn5$_{184-218}$ | pMal-c2x | BamHI/ SalI | Amp | This work |
| MBP-mCldn11$_{179-207}$ | pMal-c2x | BamHI/ SalI | Amp | This work |
| MBP-mCldn12$_{200-244}$ | pMal-c2x | BamHI/ SalI | Amp | This work |
| MBP-mCldn25$_{26-140}$ | pMal-c2x | BamHI/ SalI | Amp | This work |
| MBP-mCldn25$_{196-215}$ | pMal-c2x | BamHI/ SalI | Amp | This work |
| MBP-mCldn25$_{237-253}$ | pMal-c2x | BamHI/ SalI | Amp | This work |
| MBP-mCldn25$_{237-252}$ | pMal-c2x | BamHI/ SalI | Amp | This work |
| MBP-mCldn25$_{237-251}$ | pMal-c2x | BamHI/ SalI | Amp | This work |
| MBP-mCldn25$_{237-250}$ | pMal-c2x | BamHI/ SalI | Amp | This work |
| MBP-mCldn25$_{237-249}$ | pMal-c2x | BamHI/ SalI | Amp | This work |
| MBP-mCldn25$_{237-247}$ | pMal-c2x | BamHI/ SalI | Amp | This work |
| MBP-mOcln$_{406-521}$ | pMal-c2x | - | Amp | (Muller et al., 2005) |
| MBP-mZO1$_{23-110}$ | pMal-c2x | BamHI/ SalI | Amp | This work |
| MBP(-stop) | pMal-c2x | - | Amp | (Dabrowski et al., 2015) |
| psPAX2 virus packaging | psPAX2 | - | Amp | Sigma-Aldrich, St. Louis, USA |
| pMD2.G virus envelope | pMD2.G | - | Amp | Sigma-Aldrich, St. Louis, USA |
| shRNA mCldn5 | pLKO.1-puro | - | Amp | Sigma-Aldrich, St. Louis, USA |
| shRNA mCldn25 | pLKO.1-puro | - | Amp | Sigma-Aldrich, St. Louis, USA |
| shRNA non-mammalian Ctrl | pLKO.1-puro | - | Amp | Sigma-Aldrich, St. Louis, USA |
| YFP-mCldn5$_{1-218}$ | pEYFP-C1 | - | Kan | Gehne, FMP, Berlin, Germany |
| YFP-mCldn25$_{1-253}$ | pEYFP-C1 | HindIII/ SalI | Kan | Winkler, FMP, Berlin, Germany |
| YFP-mCldn25$_{1-249}$ | pEYFP-C1 | HindIII/ SalI | Kan | This work |
| YFP-mCldn25$_{1-247}$ | pEYFP-C1 | HindIII/ SalI | Kan | This work |
| YFP-mCldn25$_{N42Q}$ | pEYFP-C1 | HindIII/ SalI | Kan | This work |
| YFP-mCldn25$_{N72Q}$ | pEYFP-C1 | HindIII/ SalI | Kan | This work |
| YFP-mCldn25$_{N4272Q}$ | pEYFP-C1 | HindIII/ SalI | Kan | This work |
| YFP(-stop) | pEYFP-C1 | - | Kan | (Dabrowski et al., 2015) |

* for bacterial selection

### 3.1.8 Primers

All primers (oligodeoxynucleotides) used for molecular cloning (Chapter 3.3.3, Table 9), site directed mutagenesis (Chapter 3.3.7, Table 10) as well as for quantitative real time polymerase chain reaction (qRT-PCR) (Chapter 3.3.1, Table 11) are presented below (m, mouse; h, human; fw, forward; rev, reverse). The primers were supplied by BioTEZ Berlin-Buch GmbH.

**Table 9 Primers used for amplification**

| Amplicon | Primer sequence (5'→3') | |
|---|---|---|
| | fw | rev |
| mCldn1$_{188-211}$ | GATCGGATCCCGGAAAACAACCTCTTACCCAACAC | GATCGTCGACTCACACATAGTCTTTCCCACTAGAAGG |
| mCldn4$_{186-210}$ | GATCGGATCCCCACCTCGTAGCAACG | GATCGTCGACTTACACATAGTTGCTGGCG |
| mCldn5$_{184-218}$ | GATCGGATCCGGCGCCTGGGTC | GATCGTCGACTTAGACATAGTTCTTCTTGTCG |
| mCldn11$_{179-207}$ | GATCGGATCCTCCGGGGATGCACAG | GATCGTCGACTTAGACATGGGCACTCTTGG |
| mCldn12$_{200-244}$ | GATCGGATCCAAGTCTTTGTCCTCTCCTTTCTGGC | GATCGTCGACTTAAGTGCTGTGTGAGACTACTGGAATG |
| mCldn25$_{26-140}$ | GATCGGATCCTCCATAGGCACGGACTTCTG | GATCGTCGACTCACTGGCAGCGCCACAG |
| mCldn25$_{196-215}$ | GATCGGATCCGAACTCTTACATCAGAAAGTAGAGCTG | GATCGTCGACTCAGGACCATCCAAATTCTCCAG |
| mCldn25$_{237-253}$ | GATCGGATCCGCCCACACCAACCGG | GATCGTCGACTCATGCCACACGATAAGCC |
| mZo1$_{23-110}$ | GATCGGATCCACAGTGACGCTTCACAGGG | GATCGTCGACTTACTTCTTCCTTCGGATAGTAATTTTTG |

**Table 10 Primers used for site-directed mutagenesis**

| Amplicon | Primer sequence (5'→3') | |
|---|---|---|
| | *fw* | *rev* |
| MBP-mCldn25$_{237-252}$ | CCTTAATGAAGGCTTATCGTGTGTGATGAGTCGACCTGCAGG | CCTGCAGGTCGACTCATCACACACGATAAGCCTTCATTAAGG |
| MBP-mCldn25$_{237-251}$ | CCTTAATGAAGGCTTATTGAGTGGCATGAGTCGACCTGCAGG | CCTGCAGGTCGACTCATGCCACTCAATAAGCCTTCATTAAGG |
| MBP-mCldn25$_{237-250}$ | CCTTAATGAAGGCTTATCGTTAGGCATGAGTCGACCTGCAGG | CCTGCAGGTCGACTCATGCCTAACGATAAGCCTTCATTAAGG |
| MBP-mCldn25$_{237-249}$ | CCTTAATGAAGGCTTAACGTGTGGCATGAGTCGACCTGCAGG | CCTGCAGGTCGACTCATGCCACACGTTAAGCCTTCATTAAGG |
| MBP-mCldn25$_{237-247}$ | CCTTAATGTAGGCTTATCGTGTGGCATGAGTCGACCTGCAGG | CCTGCAGGTCGACTCATGCCACACGATAAGCCTACATTAAGG |
| YFP-mCldn25$_{1-249}$ | CCTTAATGAAGGCTTAACGTGTGGCATGAGTCGACGGTACC | GGTACCGTCGACTCATGCCACACGTTAAGCCTTCATTAAGG |

| | | |
|---|---|---|
| YFP-mCldn25$_{1-247}$ | CCTTAATGTAGGCTTATCGTGTG<br>GCATGAGTCGACGGTACCG | CGGTACCGTCGACTCATGCCACA<br>CGATAAGCCTACATTAAGG |
| YFP-mCldn25$_{N42Q}$ | CGAAGTCCCATTCAAGAGCAATC<br>AAGTGACTCGAATAAAATCGCC | GGCGATTTTATTCGAGTCACTTG<br>ATTGCTCTTGAATGGGACTTCG |
| YFP-mCldn25$_{N72Q}$ | CGATGTTCTGTTCCGATACCAAG<br>GCAGCTTGGGGCTGTGG | CCACAGCCCCAAGCTGCCTTGG<br>TATCGGAACAGAACATCG |
| YFP-mCldn25$_{N4272Q}$ | CGAAGTCCCATTCAAGAGCAATC<br>AAGTGACTCGAATAAAATCGCC/<br>CGATGTTCTGTTCCGATACCAAG<br>GCAGCTTGGGGCTGTGG | GGCGATTTTATTCGAGTCACTTG<br>ATTGCTCTTGAATGGGACTTCG/<br>CCACAGCCCCAAGCTGCCTTGG<br>TATCGGAACAGAACATCG |

Primers listed in Table 11 were designed with an optimal length of 20 bases and a melting temperature of around 60 °C. Synonyms: Cldn21, putative Cldn25; Cldn25, Cldnd1; Cldn26, Tmem114; Cldn27, Tmem235.

The sequence of m*Cldn21* is listed neither by UniProtKB/ Swiss-Prot nor by the National Center for Biotechnology Information (NCBI) (Rockville Pike, MD, USA), commonly used as databases for protein and nucleotide sequences. However, *Cldn21* was recently described in mice (Tanaka et al., 2016). The respective sequence (NCBI Reference Sequence: NG_020884.1) was only referred to as "pseudogene (Cldn25-ps) on chromosome 9". Sequence alignment with h*Cldn21* (NCBI Reference Sequence: NM_001101389.1) using Blast® (NCBI, Rockville Pike, MD, USA) unveils a relatively low sequence identity of 82%. Therefore m*Cldn21* was not included.

**Table 11 Primers used for qRT-PCR**

| **Amplicon** | **Primer sequence (5'→3')** | |
|---|---|---|
| | *fw* | *rev* |
| h*Actb* | GGACTTCGAGCAAGAGATGG | AGCACTGTGTTGGCGTACAG |
| h*Cdh5* | CCTACCAGCCCAAAGTGTGT | GACTTGGCATCCCATTGTCT |
| h*Cldn1* | CGATGCTTTCTGTGGCTAAAC | GAGGGCATCACTGAACAGATAG |
| h*Cldn2* | GGGCTACATCCTAGGCCTTC | GATGTCACACTGGGTGATGC |
| h*Cldn3* | CCACGCGAGAAGAAGTACAC | TTAGACGTAGTCCTTGCGGT |
| h*Cldn4* | TCCACCCTCCTCTGGATATT | AGATCCCAAAGTCAGGGTTAAG |
| h*Cldn5* | GAGGCGTGCTCTACCTGTTT | GTACTTCACGGGGAAGCTGA |
| h*Cldn6* | GATGCAGTGCAAGGTGTACG | GCCTTGGAATCCTTCTCCTC |
| h*Cldn7* | GGATGATGAGCTGCAAAATG | ATGGCTATACGGGCCTTCTT |
| h*Cldn8* | GGCTGTTTCTTGGTGGTGTT | GATTTTGCACTGCATCCTGA |
| h*Cldn9* | CTTCGACCGGCTTAGAACTG | CGTACACCTTGCACTGCATC |
| h*Cldn10* | TCATACTGTCAGGGCTGTGC | GGCCCCGTTGTATGTGTATC |
| h*Cldn11* | TGGTGTTTTGCTCATTCTGC | CATGAGTCGGGGAGCTAGAG |
| h*Cldn12* | CTCCCCATCTATCTGGGTCA | GGTGGATGGGAGTACAATGG |
| h*Cldn14* | GTCATCTCCTGCCTGCTCTC | CCTGGCCAATCTCAAACTTC |
| h*Cldn15* | GGCTTCTTCATGGCAACTGT | GGGAACTCCCAGCAGTTGTA |

| | | |
|---|---|---|
| h*Cldn16* | CCAGGAATCATTGGCTCTGT | GAACAGCTCCAGCCAAAAAG |
| h*Cldn17* | CCCTGCTTATTGGCATCTGT | GGATGGCTGGGTTGTAGAAA |
| h*Cldn18* | GGTATCCATCTTTGCCCTGA | GGTCTGAACAGTCTGCACCA |
| h*Cldn19* | GCCACAGTGGAAGCAGTCTT | TTCATGCCAACTACGCTGAG |
| h*Cldn20* | TTCATCCTGGCCTTATCTGG | TCCCAGTGCTGTACCACGTA |
| h*Cldn21* | CTATTGGGGCTTTTGCTCTG | CTCCCACCGAGGTATGATGT |
| h*Cldn22* | CTGCTGAACTCAGGGTCTCC | CAGAATTCCTCCCAGGATCA |
| h*Cldn23* | GTCAGCTACAGCCTGGTCCT | GGCCGTCGCTGTAGTACTTG |
| h*Cldn24* | GGAGTTCTGGGATGAGAACG | GCTGTCCCATCTTCCAGGTA |
| h*Cldn25* | CCGAAGCTTATATCCCACCA | AGCCCAGATGAAGAGAGCAG |
| h*Cldn26* | AGGCTGGAGAACGTGACAGT | TGGCTCCAAAGAGGAAGAGA |
| h*Cldn27* | GGGGGTCAGCATCTACATCA | GGGGACTCAGATGACCACAG |
| h*Marveld3* | GGACCCGGAGAGAGACCAG | CTCCGAAGGGGGTTCACT |
| h*Ocln* | TCCAATGGCAAAGTGAATGA | GCAGGTGCTCTTTTTGAAGG |
| h*Tric* | AGGCAGCTCGGAGACATAGA | TCACAGGGTATTTTGCCACA |
| h*Zo1* | GAACGAGGCATCATCCCTAA | CCAGCTTCTCGAAGAACCAC |
| m*Actb* | TTTGAGACCTTCAACACCCC | ATAGCTCTTCTCCAGGGAGG |
| m*Cdh5* | ATTGAGACAGACCCCAAACG | TTCTGGTTTTCTGGCAGCTT |
| m*Cldn1* | GATGTGGATGGCTGTCATTG | CGTGGTGTTGGGTAAGAGGT |
| m*Cldn2* | ATGGTGACGTCCAGTGCAAT | GGCGAGTAGAAGTCCCGAAG |
| m*Cldn3* | GAGATGGGAGCTGGGTTGTA | GTAGTCCTTGCGGTCGTAGG |
| m*Cldn4* | CCCGAGCCCTTATGGTCATC | GAGTAGGGCTTGTCGTTGCT |
| m*Cldn5* | CTGGACCACAACATCGTGAC | GCCGGTCCAGGTAACAAAGA |
| m*Cldn6* | GAGCCAAGTGCACTACCTGT | TGGTGGGATATTCGGAGGGT |
| m*Cldn7* | GCGACAACATCATCACAGCC | TACCAAGGCAGCAAGACCTG |
| m*Cldn8* | TTGCTGACAGCCGGAATCAT | TCGGAGATCTCTTTTCGGCG |
| m*Cldn9* | CCAAGGCCCGTATCGTACTC | GGACACGTACAGCAGAGGAG |
| m*Cldn10* | GCTAAAATTGCTTGCTTGGC | TCCGTTGTATGTGTAGCCCA |
| m*Cldn11* | TAGCCACTTGCCTTCAGGTG | GAGCAGCAGACGATGACACA |
| m*Cldn12* | AACTGGCCAAGTGTCTGGTC | AGACCCCCTGAGCTAGCAAT |
| m*Cldn13* | CCCTGTCCTGGGTAACACAC | GGCTCCTGAAGGTCTAGCAC |
| m*Cldn14* | GCACAGGCATCTACCAGTGT | TGAGGAGATGAAGCCCAGGT |
| m*Cldn15* | TGTCTACGGTCCATGGCAAC | CCACGAGATAGCCACCATCC |
| m*Cldn16* | CCTGCGATGAGTACGACTCC | CTCCTGCCAAAAAGCAACCC |
| m*Cldn17* | TCTCCCTCCGGTACTGGAAG | GCTCCTCCAAGTTCTCGCTT |
| m*Cldn18* | GTGTCCATCTTCGCCCTGAA | GGTGTACCTGGTCTGAACGG |
| m*Cldn19* | TTCTTCAACCCCAGCACTCC | GCGGGCAACTTAACAACAGG |
| m*Cldn20* | CTTTCATCCTGGCCGTGTCT | GGCTTTCCGGAATGGTCAGA |
| m*Cldn22* | GGGCTTAGTCTTCCGAACG | CTTCAAGTGCGGCAAGTAGT |
| m*Cldn23* | GGACATATGTCGCGAGCAGA | CGAAAAACACCACGCCAGAG |
| m*Cldn24* | CTGTCATTGCTGGGATGGGT | TGCACAGGGACATCAAGACC |
| m*Cldn25* | CTACATGGCGGCCTCCATAG | CGATGCCGCTATTGTGGTTG |
| m*Cldn26* | TGACCGGGTTCTTGAGCTTC | CAGAGACCAGCCAAAGCGTA |
| m*Cldn27* | GCCTGGAAGTTTCTCCCTCC | ATGTAGATGCTGAGCCCTGC |
| m*Glut-1* | GCTGTGCTTATGGGCTTCTC | AGAGGCCACAAGTCTGCATT |
| m*Hbegf* | CCACCTCACTCCCTTTGTGT | GTCAACTCCAAAGCTCCCTG |
| m*Marveld3* | TGGAGAAGTCCCGTCAAAGC | AGCCACTATAAGCCCCTCCA |
| m*Ocln* | ACTCCTCCAATGGCAAAGTG | CCCCACCTGTCGTGTAGTCT |
| m*Rn28s* | CCCGACGTACGCAGTTTTAT | CCTTTTCTGGGGTCTGATGA |
| m*Tric* | GAGAATCCTGGGTGTGGTGG | TTTCGATGACAACGACGGGT |
| m*Zo1* | CCCACCCCCATCTCAGAGTA | GGGACAGCTTTAGGCATGGT |

### 3.1.9 Antibodies

Antibodies used for immunostaining or immunoblotting are listed with catalogue number (Cat. No.) and supplier in Table 12. Additionally, the required dilution factors with regard to application are denoted.

**Table 12 Antibodies**

| **Antibody (host)** | **Dilution for immuno-staining** (in blocking buffer) | **Dilution for immuno-blotting** (in TBST buffer) | **Cat. No.** | **Supplier** |
|---|---|---|---|---|
| *Primary antibody* | | | | |
| Actb (mouse) | | 1:100 - 1:1000 | CP01 | Merck Millipore, MA, USA |
| Cldn1 (rabbit) | 1:50 | 1:250 | 51-9000 | ThermoFisher Scientific, Waltham, MA, USA |
| Cldn3 (rabbit) | 1:50 | - | 341700 | ThermoFisher Scientific, Waltham, MA, USA |
| Cldn4 (rabbit) | 1:25 | 1:250 | 364800 | ThermoFisher Scientific, Waltham, MA, USA |
| Cldn5 (mouse) | 1:100 | 1:300 - 1:5000 | 1548773A | ThermoFisher Scientific, Waltham, MA, USA |
| Cldn5 (rabbit) | 1:100 | 1:500 | QE215213 | ThermoFisher Scientific, Waltham, MA, USA |
| Cldn10 (rabbit) | 1:50 | - | - | Manufactured and kindly provided by D. Günzel |
| Cldn11 (rabbit) | 1:50 | 1:250 | 36-4500 | ThermoFisher Scientific, Waltham, MA, USA |
| Cldn12 (rabbit) | 1:50 | 1:250 | JP18801 | IBL International, Hamburg, Germany |
| Cldn15 (rabbit) | - | 1:200 | 389200 | ThermoFisher Scientific, Waltham, MA, USA |
| Cldn20 (rabbit) | 1:50 | - | 117678-1-Ab | Proteintech Group, Inc., Rosemont, IL, USA |
| Cldn25 (rabbit) | - | 1:500 | AP52015PU-N | OriGene Technologies, Inc., Rockville, MD, USA |
| Cldn25 (rabbit) | 1:50 | - | PA-25733 | ThermoFisher Scientific, Waltham, MA, USA |
| GFP (mouse) | - | 1:50 | 3E6 | ThermoFisher Scientific, Waltham, MA, USA |
| MBP (mouse) | - | 1:5000 | E8032S | New England BioLabs, Ipswich, MA, USA |
| NeuF (mouse) | 1:50 | - | ab24574 | Abcam, Cambridge, UK |
| Ocln (mouse) | 1:100 | | 33-1500 | ThermoFisher Scientific, Waltham, MA, USA |
| ZO-1 (rat) | 1:75 - 1:100 | | LSC124822 | Biozol Diagnostica Vertrieb GmbH, Eching, Germany |

| *Secondary antibody* | | | | |
|---|---|---|---|---|
| Mouse_IgG-Cy3® (goat) | 1:250 | - | A10520 | ThermoFisher Scientific, Waltham, MA, USA |
| Mouse_IgG-Alexa Flour® 647 (goat) | 1:250 | - | A21236 | ThermoFisher Scientific, Waltham, MA, USA |
| Mouse_IgG-HRP (goat) | - | 1:2000 - 1:100000 | 62-6520 | Merck Millipore, MA, USA |
| Rabbit_IgG-Alexa Flour® 555 (goat) | 1:250 | - | A21431 | ThermoFisher Scientific, Waltham, MA, USA |
| Rabbit_IgG-Alexa Flour® 647 (goat) | 1:250 | - | A21244 | ThermoFisher Scientific, Waltham, MA, USA |
| Rat_IgG-555 (goat) | 1:250 | - | A211434 | ThermoFisher Scientific, Waltham, MA, USA |
| Rabbit_IgG-HRP (goat) | - | 1:2000 - 1:100000 | 117711717 | Merck Millipore, MA, USA |

### 3.1.10 Cell lines

Table 13 outlines cell lines and the originating species, tissue and cell type.

**Table 13 Cell lines**

| Cell line | Species/tissue/cell type | Reference/ supplier |
|---|---|---|
| bEND.3 | Mouse/ cerebral cortex/ endothelium | (Ni et al., 2014) |
| Caco-2 | Human/ colon/ epithelium | (Staat et al., 2015) |
| HEK-293 | Human/ kidney/ epithelium | (Piontek et al., 2008) |
| HEK-293T | Human/ kidney/ epithelium | (Kaempf et al., 2015) |
| MDCK-II | Dog/ kidney/ epithelium | (Piehl et al., 2010) |

### 3.1.11 Bacteria

All bacterial strains and the supplier are listed in Table 14.

**Table 14 Bacteria**

| Bacteria strain | Reference/ supplier |
|---|---|
| *E.coli* DH5α | (Hanahan, 1985) |
| *E.coli* BL21 | (Studier et al., 1990) |

### 3.1.12 Mice

C57BL/6N mice, wild type (wt) or Cldn3-knockout (*Cldn3* KO) (Kooij et al., 2014) were housed under standard conditions with 12 h light-dark cycle and free access to food and water. All experiments were approved by the "Landesamt für

Gesundheit und Soziales Berlin" (LAGeSo). The animal experiment numbers according to LAGeSo: To sacrifice mice for the removal of organs, T0457/09, of 16/11/2009; for the removal of organs of living mice (tail tips for genotyping), O0369/11, of 14/02/2011 as well as the animal experiment approval, G0030/13, of 07/01/2013.

### 3.1.13 Model of Cerebral Ischemia

Filamentous middle cerebral artery occlusion (MCAO) was performed in collaboration with PD Dr. André Rex (Charité, Center Neurology, Berlin, Germany) as described (Engel et al., 2011). In brief, male mice between 11 and 37 weeks of age were anesthetized with 1% isofluorane in 70% $N_2O$ and 30% $O_2$ using a Vapor 2000 Vaporizer (Dräger Medical, Lübeck, Germany). The left MCAO was induced with a 7-0 nylon monofilament coated with a silicone resin/ hardener mixture (Doccol, Redlands, USA). The filaments were removed after 30 or 60 min of ischemia to allow reperfusion for 48 or 3 h, respectively. At those time points an increase of BBB permeability is reported (Figure 8). Therefore those time points were chosen for the investigation of the expression of TJ proteins. Magnetic resonance tomography (MRT) was performed in collaboration with Susanne Müller (Charité, CSB, Berlin, Germany) to determine the infarct localization and size (Table 15). At 3 h of reperfusion the imaging was realized by diffusion-weighted magnetic resonance imaging (DWI). T2-weighted magnetic resonance imaging (T2WI) was performed at 48 h of reperfusion. Additionally brain sections (Chapter 3.2.1) were stained with hematoxylin in collaboration with Dr. Rosel Blasig (FMP, Berlin, Germany) to validate the MRT data (Table 15). The behavior of mice after MCAO was monitored in collaboration with Dr. Rosel Blasig (FMP, Berlin, Germany). No significant differences with respect to neuroscore, postural reflex, forelimb placing, vertical screen and side placement were found between mice that did not undergo surgery and MCAO control group (MCAO surgery, but no occlusion of the middle cerebral artery).

**Table 15 MCAO animals**

| MCAO no. | Genotype | Age [weeks] | Ischemia [min] | Reper-fusion [h] | Infarct localization | Infarct size [% per hemisphere] | | |
|---|---|---|---|---|---|---|---|---|
| | | | | | | MRT 3 h DWI | MRT 48 h T2WI | Hema-toxylin |
| 1005 | wt | 21 | 60 | 3 | striatum/ cortex | - | - | 8.74 |
| 1010 | wt | 19 | 60 | 3 | striatum | - | - | 4.27 |
| 1205 | *Cldn3* KO | 25 | 60 | 3 | striatum/ cortex | - | - | 11.93 |
| 1206 | *Cldn3* KO | 12 | 60 | 3 | striatum | - | - | 10.64 |
| 1208 | *Cldn3* KO | 25 | 30 | 48 | striatum/ cortex | - | - | 16.62 |
| 1210 | wt | 33 | 30 | 48 | striatum | - | - | 14.60 |
| 13k2 | wt | 15 | 60 | 3 | striatum | 5.0 | - | - |
| 13k4 | wt | 15 | 60 | 3 | striatum | 5.0 | - | - |
| 1503 | wt | 37 | 30 | 48 | striatum | - | 3.04 | 4.10 |
| 1504 | wt | 18 | 30 | 48 | striatum/ cortex | - | -0.01 | 7.74 |
| 1604 | wt | 15 | 30 | 48 | striatum | 7.74 | 1.75 | 3.21 |
| 1804 | wt | 11 | 30 | 48 | striatum/ cortex | 4.85 | 8.73 | 21.58 |
| 1806 | wt | 12 | 30 | 48 | striatum | 4.89 | -0.45 | 4.59 |
| 1906 | *Cldn3* KO | 11 | 30 | 48 | striatum | 4.25 | 1.52 | 17.04 |
| 1907 | *Cldn3* KO | 22 | 30 | 48 | striatum | 1.05 | 1.72 | 8.87 |
| 1908 | *Cldn3* KO | 22 | 30 | 48 | cortex | 29.99 | 14.87 | 33.71 |
| 2001 | *Cldn3* KO | 11 | 60 | 3 | striatum/ cortex | 1.70 | - | 2.01 |
| 2003 | *Cldn3* KO | 11 | 60 | 3 | cortex/ hippocampus | 6.28 | - | 14.55 |
| 2005 | *Cldn3* KO | 11 | 60 | 3 | striatum | 7.36 | - | - |
| 2007 | wt | 13 | 60 | 3 | striatum/ cortex | 10.41 | - | 6.85 |
| 2009 | wt | 13 | 60 | 3 | striatum | 5.57 | - | 1.07 |

### 3.1.14 Human cortex

The human cortex samples of two male (age of 46 and 54) and two female (age of 31 and 54) Caucasians were provided by AMS Biotechnology (Abingdon, United Kingdom) and ethically approved by the Western Institutional Review Board (Puyallup, USA; Protocol #CU-M-01142014-C). The causes of death were car accidents. The tissue of the cerebral cortices was obtained and frozen 1 - 3 h post mortem during autopsy.

### 3.1.15 Software

Microsoft® Office 2010, GraphPad Prism® 5.04, ImageJ 1.48v, Zeiss ZEN 2009

## 3.2 Histological Methods

### 3.2.1 Cryosections

C57BL/6N mice between 8 and 20 weeks of age were sacrificed by Dr. Winkler (FMP, Berlin, Germany). The brains were removed and immediately frozen on dry ice in 2-methylbutane for 10 min. The brains were stored at -80 °C or embedded on a disc in Tissue-Tek for direct preparation of cryosections. 8 µm sections were cut using a microtome blade at -18 °C. The sections were mounted to glass slides for immunohistochemistry or membrane slides for laser capture microdissection. Attachment was realized by brief increase of the slide temperature. The slides were stored at -80 °C.
The preparation of human cortical cryosections was followed the same procedure as described for mouse brains. The human cortex samples embedded in Tissue-Tek were provided by AMS Biotechnology (Abingdon, United Kingdom).

### 3.2.2 Immunohistochemistry and confocal microscopy of brain sections

The cryosections were mounted to glass slides (Chapter 3.2.1) and fixed with methanol for 10 min at -20 °C, washed thrice for 10 min and blocked with PBS containing 2% bovine serum albumin for 30 min. The slides were washed again for 10 min with PBS containing 0.5% bovine serum albumin. The tissue was incubated with the primary antibody in PBS containing 0.5% bovine serum albumin for 18 h at 4°C. After washing thrice for 10 min, the tissue was incubated with the secondary antibody for one hour in darkness. When washed thrice for 10 min, the sections were optionally incubated with fluorescein-labeled RCA1 (1:20 in dd$H_2O$) for 2 min, followed by three washing steps with $H_2O$ for 10 min. The tissue was mounted with Roti-Mount FlourCare DAPI. The microscopy was performed using the Zeiss LSM 780 with a 64x/1.40 oil objective.

### 3.2.3 Purification of brain capillaries

C57BL/6N mice between 8 and 20 weeks were sacrificed by Dr. Winkler (FMP, Berlin, Germany). The brains were removed and the cerebral cortices separated. The cortices were homogenized with a Dounce tissue grinder set in DMEM high glucose. Myelin was removed by adding of 16% (w/v) dextran (60 - 70 kDa) and centrifugation at 4500 x g and 4 °C for 15 min. The brain capillaries were resuspended in 3 ml DMEM high glucose per brain and centrifuged to remove the remaining dextran for 10 min at 1500 x g and 4 °C. The pellet containing the brain capillaries was resuspended and filtered through a nylon mesh with a pore size of 40 µm. The pure capillaries that remained on the filter were collected by rinsing the membrane with 1 ml BC medium (Table 5). For immediate RNA or protein purification, the capillaries were centrifuged at 1500 x g and 4 °C for 10 min to add the respective buffer (Chapter 3.3.1.1 or 3.5.1).

### 3.2.4 Laser capture microdissection of brain capillaries

8 µm frozen brain sections were mounted to membrane slides (Chapter 3.2.1). After 10 min of fixation with methanol at -20°C, the slides were washed once with $ddH_2O$. The brain sections were stained for 2 min with Ricinus communis agglutinin (RCA) 1 DyLight 594 diluted 1:20 in $ddH_2O$ to visualize brain capillaries (Mojsilovic-Petrovic et al., 2004). Additional washing thrice in $ddH_2O$ was followed by consecutive dehydration steps (1 min 70%, 1 min 90%, 3 min 96%, 5 min 100% ethanol). Brain capillaries were dissected using the Zeiss PALM MicroBeam. Applying the cut laser function “LineAutoLPC” the tissue was catapulted contact-free via a series of laser pressure catapulting (LPC) shots along the vessels into a Zeiss opaque Adhesive Cap 500. To selectively mark brain capillaries a 10x/0.1 dry objective was used. A LD 20x/0.2 dry objective was used for cutting and catapulting. The cutting precision of this objective is around 2.5 µm (resulting defocused LPC shot around 3 - 4 µm). The PALM Microbeam is using a frequency-tripled solid-state laser with a wavelength of 355 nm. 500 - 1000 capillaries were dissected from each brain sample. 400 µl lysis buffer of the GeneMatrix Universal RNA Purification Kit were immediately added to the dissected brain capillaries for storage at -20 °C or direct RNA purification (Chapter 3.3.1.1).

## 3.3 Molecular biological methods

### 3.3.1 Quantitative real time polymerase chain reaction (qRT-PCR)

#### 3.3.1.1 RNA purification and cDNA synthesis

RNA was extracted from laser-dissected or purified brain capillaries as well as 2 $cm^2$ cultured cells at full confluency following the cell culture protocol of the GeneMatrix Universal RNA Purification Kit. Starting from whole organ, the material was frozen under liquid nitrogen and grinded with mortar and pestle to fine tissue powder before following the animal tissue protocol of the GeneMatrix Universal RNA Purification Kit. The RNA concentration was photometrically determined by absorbance at 260 nm as well as the degree of purity characterized by a ratio of absorbance at 260 nm and 280 nm using the NanoDrop 2000c. The reverse transcription of complementary DNA (cDNA) from isolated RNA was performed using the Maxima First Strand cDNA Synthesis Kit for RT-qPCR following the supplier's instructions. To examine contamination with genomic DNA reverse transcription was additionally performed without adding the reverse transcriptase.

#### 3.3.1.2 qRT-PCR

qRT-PCR was carried out in the StepOne™ Real-Time PCR System according to the cycling protocol in Table 16 using the Luminaris Color HiGreen high ROX qPCR Master Mix. The Master Mix contained a *Taq* polymerase that had been modified to be inactive at room temperature and a fluorescent intercalating dye that emits a fluorescent signal upon binding to the double stranded cDNA. During qRT-PCR the detected fluorescence increases proportionally to the DNA accumulation. The species-specific primers (Table 11) were designed for an amplicon length of approximately 200 bp with Primer3Plus (Free Software Foundation, Boston, MA, USA, http://primer3plus.com/) and tested for its binding specificity using Blast® (NCBI, Rockville Pike, MD, USA). 20 µl of the reaction mix were pipetted according to Table 16 in each well of a MicroAmp® Fast Optical 48- or 96-Well reaction plate. For data analyses and export the StepOne Software v2.2.1 was used. In order to calculate the relative expression of the examined genes, the cycle threshold (Ct) was set to 0.4, within the linear phase of the

logarithmic amplification plot for all tested primers. The Ct values were normalized to *Actb* or *Rn28s* ($\Delta Ct = Ct_{target} - Ct_{Actb\ or\ Rn28s}$). To compare the expression between two groups, ΔΔCt ($\Delta\Delta Ct = \Delta Ct_B - \Delta Ct_A$) was calculated. cDNA amplification during the PCR is exponential. A reduction of the Ct value by 1 describes the doubling of the template concentration. Hence, the relative expression values were determined as $2^{\Delta(\Delta)Ct}$. The values, $8.06 \cdot 10^{-5}$, $2.02 \cdot 10^{-5}$, $5.75 \cdot 10^{-7}$, $8.83 \cdot 10^{-7}$ were the experimental detection limits in laser-dissected brain capillaries, purified mouse brain capillaries, primary mouse brain capillary endothelial cells and bEND.3 cells, respectively. Unspecific products were identified by melt-curve analyses (gradual increase of temperature by 0.3 °C from 60 to 95 °C). A single peak at the calculated temperature indicates specific amplification of cDNA. Primer efficiencies were selectively analyzed (Actb, Cldn3, -5 and -12) by plotting the Ct values against a 5-fold serial dilution of the cDNA template (Figure S 1). The efficiencies were optimal for all tested primers. Further primer sets were evaluated with respect to parallelism of their amplification curves to Actb, Cldn3, -5 and -12 using the StepOne Real-Time PCR system software (Real-time monitoring of amplification growth curves) to ensure comparable cDNA amplification.

**Table 16 qRT-PCR**

| **Component** | **Concentration** | **Cycling protocol** | | | |
|---|---|---|---|---|---|
| Luminaris Color HiGreen qPCR Master Mix (2X) | 1X | **Step** | **Temperature [°C]** | **Time** | **Number of cycles** |
| Primer fw | 0.3 μM | Uracil-DNA glycosylase pre-treatment | 50 | 2 min | 1 |
| Primer rev | 0.3 μM | Initial denaturation | 95 | 10 min | 1 |
| cDNA | ≤ 0.5 ng/μl | Denaturation | 95 | 15 s | 40 |
| | | Annealing/ extension | 60 | 60 s | |

### 3.3.2 RNA sequencing

RNA sequencing was performed in collaboration with Dr. Jingjing Zhang (Affiliated Hospital of Guangdong Medical College, Zhanjiang, Guangdong, China).

Therefore, brain capillaries were prepared (Chapter 3.2.3). RNA was extracted following the cell culture protocol of the GeneMatrix Universal RNA Purification Kit. The following steps were performed by BGI-Tech (Shenzhen, China; composition of buffers is confidential). The RNA samples were treated with DNase I to degrade any possible DNA contamination. mRNA was enriched by use oligo(dT) magnetic beads and fragmented into 200 bp fragments by use of fragmentation buffer. The first cDNA strand was synthesized using random hexamers. The second strand was synthesized by adding of dNTPs, RNase H and DNA polymerase I. The double stranded cDNA was purified with magnetic beads. End preparation as well as 3'-end single adenine addition were performed to ligate sequencing adaptors to the fragments. The fragments were enriched by PCR amplification. The Agilent 2100 Bioanalyzer and the ABI StepOnePlus Real-Time PCR System were used for qualitative and quantitative analyses of the sample library. The sequencing of the library products was performed by use of the Illumina HiSeq$^{TM}$ 2000 sequencer. Therefore, the library was loaded into a flow cell (glass slide coated with adapter-complementary oligonucleotides), where the fragments were captured. Each fragment was amplified into distinct, clonal clusters. Fluorescently labeled nucleotides were added and detected as they were incorporated into the cDNA template strands. The emission from each cluster was recorded. The emission wavelengths and intensities were used to identify the base. Reads (data strings of A, T, C, and G bases corresponding to the sample cDNA) were aligned to a reference sequence. The mRNA expression levels were calculated using the RPKM (Reads Per Kilobase of transcript per Million mapped reads) method (equation below; C, number of reads that uniquely aligned to the gene of interest; N, total number of reads that uniquely aligned to all genes; L, number of bases of the gene of interest).

$$RPKM = \frac{10^3 \cdot C}{N \cdot L}$$

This method eliminates the influence of distinct mRNA length and sequencing discrepancy on the determination of the mRNA expression level. RPKM values can be directly used to compare mRNA expression among samples.

### 3.3.3 Molecular cloning

#### 3.3.3.1 Polymerase chain reaction

The amplification of target DNA from mouse brain cDNA (Chapter 3.3.1.1) using primers (Table 9) was performed in a thermocycler. The set-up as well as the thermal cycling conditions for a PCR volume of 100 µl are shown in Table 17. The PCR product was purified using the DNA Clean and Concentrator-5 kit according to the supplier's manual. The concentration was photometrically determined using the NanoDrop 2000c.

**Table 17 Polymerase chain reaction**

| **Component** | **Concentration** | **Cycling protocol** | | | |
|---|---|---|---|---|---|
| AccuPol buffer (10X) | 1X | **Step** | **Temperature [°C]** | **Time** | **Number of cycles** |
| dNTP Mix | 0.2 mM | Initial denaturation | 95 | 2 min | 1 |
| Template DNA | 0.5 ng/µl | Denaturation | 95 | 30 s | 35 |
| Primer (fw) | 0.5 µM | Annealing | 55 | 30 s | |
| Primer (rev) | 0.5 µM | Elongation | 72 | 90 s | |
| AccuPol DNA polymerase | 0.025 U/µl | Final elongation | 72 | 5 min | 1 |

#### 3.3.3.2 Restriction of DNA

Directed ligation of the amplified DNA with the pMAL-c2x or pEYFP-C1 expression vector required the digestion with fast digest restriction enzymes. The restriction sites of each construct are indicated in Table 8. The generation of sticky ends by these enzymes ensures the right orientation of the incorporated fragment. The restriction was performed in a volume of 30 µl for the PCR product or 20 µl for the plasmid DNA (Table 18) at 37 °C. The incubation varied from 30 min for the vector DNA to 1.5 h for the insert. Heating at 80 °C for 5 min inactivated the enzymes.

**Table 18 Restriction of DNA**

| Restriction of the PCR product | | Restriction of plasmid DNA | |
|---|---|---|---|
| **Component** | **Concentration** | **Component** | **Concentration** |
| PCR product | 6.7 ng/µl | Plasmid DNA | 50 ng/µl |
| Fast Digest buffer (10X) | 1X | 10x Fast Digest buffer (10X) | 1X |
| Fast Digest enzyme A | 0.025 U/µl | Fast Digest enzyme A | 0.036 U/µl |
| Fast Digest enzyme B | 0.025 U/µl | Fast Digest enzyme B | 0.036 U/µl |

### 3.3.3.3 Recovery of DNA from agarose gels

After restriction, the PCR product as well as the plasmid DNA were separated by agarose gel electrophoresis. Therefore 1.2% (w/v) agarose was melted in 1x TAE buffer by boiling in a microwave and cooling down in a gel chamber. After adding of 6x DNA loading dye, the DNA sample was loaded together with the DNA ladder to the agarose gel. The electrophoresis was performed at 120 V in a gel chamber containing 1x TAE buffer. Afterwards, the gel was stained for 30 min in 50 ml 1x TAE buffer with SYBR®-Safe DNA gel staining solution at RT and visualized using the FLA-5000. According to the fluorescent bands with the respective size, agarose gel fragments were cut out. The DNA was extracted using the Zymoclean™ Gel DNA Recovery Kit according to the product information. The concentration and the degree of purity of the purified DNA were determined by photometric measurement of the absorption at 260 and 280 nm using the NanoDrop 2000c.

### 3.3.3.4 Ligation

The ligation of the PCR product and the linearized plasmid DNA was executed in 20 µl of reaction mix (Table 19) for 14 h at 16 °C. The enzyme was inactivated by heating at 65 °C for 10 min.

**Table 19 Ligation**

| Component | Concentration |
|---|---|
| Ligase buffer (10X) | 1X |
| Plasmid DNA | 5 ng/µl |
| PCR product | molar ratio of 5:1 plasmid DNA |
| T4 DNA ligase | 20 units/µl |

### 3.3.4 Preparation of electrocompetent bacteria

The *Escherichia coli* (*E. coli*) strains DH5α and BL21 were used for transformation of plasmid DNA. DH5α allows optimized replication of the plasmid DNA (Hanahan, 1985) whereas BL21 is primarily used as enhanced protein expression host (Studier et al., 1990). The following procedure promotes uptake of plasmid DNA upon electroporation. The bacteria were cultured overnight in 5 ml salt-free LB medium at 37 °C. The next day, a 1:300 dilution of 500 ml was cultured in an Erlenmeyer flask under the same culture conditions until reaching an O.D. between 0.4 and 0.6 at 600 nm, measured with the spectral photometer DU 640. After 10 min of incubation on ice, the bacteria were centrifuged at 4000 rpm and 4 °C for 15 min. The bacteria pellets were washed by resuspension in 100 ml ice-cold, sterile dd$H_2O$. The cells were harvested in the same way as in the previous centrifugation step. The described washing step was repeated twice followed by a final washing step with 50 ml ice-cold 10 % (v/v) glycerol. The cells were resuspended in 3 ml of ice-cold 10 % (v/v) glycerol. For a single transformation aliquots of 50 µl were frozen in liquid $N_2$ and stored at -80 °C.

### 3.3.5 Transformation of electrocompetent bacteria

An aliquot of 50 µl of electrocompetent bacteria was thawed on ice and transferred into an electroporation cuvette together with either 2 µl of the ligation product or 20 ng of the plasmid DNA. The bacteria were exposed to 1.8 kV, allowing the cells to take up the plasmid. Immediately the transformed bacteria were incubated with 500 µl LB medium at 37 °C. Selective growth was realized by plating of the bacteria on agar plates containing either ampicillin (50 µg/ml) or kanamycin (100 µg/ml). The agar plates were incubated overnight at 37 °C before picking of positive clones from single colonies. The plasmid-encoded resistance for bacterial selection is indicated in Table 8.

### 3.3.6 Purification of plasmid DNA

Single colonies of transformed *E. coli* DH5α were picked and shaken at 230 rpm in 5 ml ampicillin (50 µg/ml) or kanamycin (100 µg/ml) containing LB medium

(according to the plasmid encoded resistance in Table 8) overnight at 37 °C . The bacteria were centrifuged for 15 min at 4000 rpm and 4 °C. The extraction of plasmid DNA from pelletized bacteria was processed with the ZR Plasmid Miniprep$^{TM}$-Classic according to the supplier's manual.

### 3.3.7 Site directed mutagenesis

Via site directed mutagenesis, codons were specifically altered by point mutation to code for either glutamine instead of asparagine (Chapter 4.4.2) or to insert a stop codon (Chapter 4.5.2. and 4.5.3). Primers that carry the modified codon were designed as listed in Table 10. The PCR mix with a volume of 15 µl (Table 20) contained an AccuPOL DNA Polymerase with high proofreading capacity for replication of the plasmid DNA. Only one strand of the plasmid DNA was initially replicated by separate incubation with either forward or reverse primer in a thermocycler (Table 21, A). Subsequently, both reactions were mixed to amplify the DNA containing the point mutation (Table 21, B). The PCR product was purified using the DNA Clean and Concentrator-5 kit following the supplier's instructions. The plasmid was eluted with 10 µl of nuclease free water and the concentration spectrophotometrically determined at a wavelength of 260 nm. The FastDigest enzyme DpnI, specific for methylated DNA, removed the methylated template plasmid DNA. The unmethylated plasmid DNA amplified by PCR remained undigested. Therefore, 30 µl of a digestion mix (Table 22) were incubated for 7 - 9 h at 37 °C. The enzyme was inactivated at 80 °C for 5 min. The plasmid DNA was purified using the DNA Clean and Concentrator-5 Kit according to the supplier's manual.

**Table 20 Mutagenesis polymerase chain reaction mix**

| Component | Concentration |
|---|---|
| AccuPol buffer (10X) | 1X |
| AccuPol DNA polymerase | 0.08 U/µl |
| dNTP mix | 0.2 mM |
| Forward or reverse primer | 0.5 µM |
| Template plasmid DNA | 0.1 ng/µl |

**Table 21 Mutagenesis polymerase chain reaction cycle protocol**

| | A | | B | |
|---|---|---|---|---|
| | Temperature [°C] | Time | Temperature [°C] | Time |
| **1** Initial denaturation | 95 | 2 min | 95 | 30 sec |
| **2** denaturation | 95 | 30 sec | 95 | 30 sec |
| **3** annealing | 65 | 45 sec | 65 | 1 min |
| **4** elongation | 72 | 6 min | 72 | 6 min |
| Repeat step **2-4** | 4 times | | 16 times | |
| **5** Final elongation | | | 72 | 20 min |

**Table 22 Digestion of methylated template DNA**

| Component | Concentration |
|---|---|
| Fast Digest buffer (10X) | 1X |
| Plasmid DNA | 50 ng/µl |
| Fast Digest *Dpn*I | 0.1 U/µl |

### 3.3.8 Sequencing

Purified plasmid DNA was sequenced by Source BioScience (Berlin, Germany) and analyzed using FinchTV (Geospiza Inc, Seattle, Washington).

### 3.3.9 Preparation of glycerol stocks

750 µl of an overnight culture were gently mixed with 250 µl glycerol (100%) and frozen in a cryotube in liquid $N_2$ for storage at -80 °C.

## 3.4 Cell biological methods

### 3.4.1 Cell culture

All cell culture steps were carried out under sterile conditions in a clean bench (S-120). The cells were exposed to 5% or 10% $CO_2$ and 95% air humidity at 37 °C in an incubator (CB210) to simulate constant physiological conditions.

#### 3.4.1.1 Culturing of HEK-293 cells

HEK-293 cells were cultured in 75 $cm^2$ tissue culture flasks that contained 9 ml culture medium (DMEM, 10% (v/v) FCS, 1% (v/v) penicillin (100 U)/ streptomycin

(100 g/l); Table 5) at 10% $CO_2$. For passaging, cells grown to a confluency of 95% were washed with PBS (without $Ca^{2+}$/ $Mg^{2+}$) and detached by incubation with 500 µl 0.05% trypsin/ 0.02% EDTA at 37 °C for 5 min. After resuspension in culture medium, $1 \cdot 10^5$ cells/$cm^2$ were seeded into culture plates.

#### 3.4.1.2 Culturing of MDCK-II cells

The cells were cultured as described for HEK-293 cells (Chapter 3.4.1.1), but 0.25% trypsin/ 0.02% EDTA was used for detachment and passaging.

#### 3.4.1.3 Culturing of Caco-2 cells

The cells were cultured as described for HEK-293 cells (Chapter 3.4.1.1), but CellBIND Surface tissue culture flasks at 5% $CO_2$ were used. The cultivation medium (Table 5) contained 20% FCS and 1% non-essential amino acids. For passaging, the cells were detached with 0.25% trypsin/ 0.02% EDTA.

#### 3.4.1.4 Culturing of HEK-293T cells

The cells were cultured as described for HEK-293 cells (Chapter 3.4.1.1), but cultivation medium containing DMEM high glucose (4.5 g/l glucose, Table 5) was used at 5% $CO_2$.

#### 3.4.1.5 Culturing of bEND.3 cells

bEND.3 cells were cultured in 6-well-tissue culture plates containing 3 ml bEND.3 medium (Table 5). The cells were passaged at a confluency of 95 % every 3 - 5 days. Therefore, bEND.3 cells were washed and incubated for 3 min with PBS (without $Ca^{2+}$/ $Mg^{2+}$) to weaken $Ca^{2+}$ depended adhesion. Incubation for 5 min with 100 µl 0.25% trypsin/ 0.02% EDTA at 37 °C detached the cells from the flask. After resuspending in 3 ml medium to minimize the effect of trypsin/ EDTA, the cells were centrifuged for 5 min at 250 x g and resuspended in bEND.3 medium. $2 \cdot 10^4$ cells/$cm^2$ were seeded into culture plates.

#### 3.4.1.6 Culturing of primary bEND cells

Brain capillaries of mice were purified (Chapter 3.2.3) and digested for 1 h at 37 °C by adding of dispase (1.1 g/l) and collagenase (0.5 g/l) in 1 ml cultivation medium (DMEM 4.5 g/l glucose; 20% (v/v) FCS; 1% (v/v) penicillin (100 U)/ streptomycin (100 g/l); 0.5% (v/v) mouse serum; 0.33% (v/v) endothelial cell growth factor). After centrifugation at 1000 x g to remove enzymes and resuspension in cultivation medium, the cells were seeded into collagen coated 24-well tissue culture plates to promote attachment of the outgrowing cells. The cells were cultured at 37 °C and 5% $CO_2$ until harvest at a confluency of 100%.

### 3.4.2 Cryoconservation and thawing of cells

For conservation in liquid nitrogen, the cells were resuspended in 90% FCS with 10% DMSO, aliquoted in cryotubes and transferred into a freezing container filled with 100% isopropanol. The cells were slowly frozen at -80 °C before being transferred into liquid nitrogen.
For cultivation, the cell suspension was thawed in a water bath at 37 °C and transferred into the respective culture medium. After centrifugation at 150 x g for 5 min, the cells were resuspended in medium for seeding into tissue culture plates.

### 3.4.3 Transfection of cells

Transient transfection of MDCK-II, HEK-293 or HEK-293T cells with plasmid DNA was realized using polyethylenimine (PEI). PEI complexes DNA to cationic particles that are taken up by the cell via endocytosis after attachment to negatively charged cell surface residues (Boussif et al., 1995). $1 \cdot 10^5$ cells/cm$^2$ were seeded into 6-well tissue culture plates. The following day plasmid DNA (16 ng/µl Opti-MEM) as well as PEI (0.04 µl/µl Opti-MEM) were separately incubated for 5 min before mixing (1:2). After additional 20 min incubation, the mix (167 µl/ml transfection medium, Table 5) was added to the culture plates (3 ml transfection medium/6-well). After 48 h the transfection success was verified by microscopic analysis of the fluorescently tagged proteins (Chapter 3.4.7).

### 3.4.4 Lentiviral transduction of bEND.3 cells

The following steps were performed under biosafety level 2. For lentiviral production HEK-293T cells ($1 \cdot 10^5$ cells/cm$^2$) were transfected with three plasmids, psPAX2 (virus packaging, 3 ng/µl Opti-MEM), pMD2.G (virus envelope, 1.5 ng/µl Opti-MEM) and pLKO.1-puro (shRNA and puromycin resistance, 3 ng/µl Opti-MEM) as described in chapter 3.4.3. During the following 96 h of culture at 37 °C and 5% $CO_2$, the HEK-293T cells produced the virus particles for transduction of bEND.3 cells. The transfection medium containing the virus particles was harvested, centrifuged at 600 x g and the supernatant filtered (10 ml transfection medium/ Steriflip® filter unit, 50 ml, 0.45 µm, Merck Millipore). The filtrate was concentrated (Amicon® Ultra-15 Centrifugal Filter Device 100K, Merck Millipore) for 60 min at 3000 x g before adding to the culture medium of $1.5 \cdot 10^4$ bEND.3 cells/cm$^2$ (60 µl/ml culture medium, Table 5). After 48 h the positive transduced bEND.3 cells were selected using puromycin (1 µg/ml, Table 4). This puromycin concentration was tested as cytotoxic for untransduced bEND.3 cells (no survival of cells after 48 h).

### 3.4.5 Determination of cell number

A hemocytometer was used to determine the number of cells in suspension. The counted cells present in an area of 1 mm$^2$ represent the cell number in 0.1 µl of the analyzed suspension.

### 3.4.6 Determination of transendothelial electrical resistance

The transendothelial electrical resistance (TEER) was determined using electric cell-substrate impedance sensing (ECIS). Recording the TEER over time at different frequencies allows examining of the endothelial proliferation (40000 Hz) in addition to paracellular tightness (4000 Hz). At low frequencies, the passage of the electric current is restricted to the intercellular space while at high frequencies transcellular passage is possible (Szulcek et al., 2014). The ECIS arrays (ECIS chip 8W10E+, Ibidi GmbH) were initially stabilized and cleaned to prevent electrode drift, to improve well-to-well reproducibility and the signal-to-noise ratio.

Therefore, the arrays were pretreated with 10 mM L-cysteine (200 µl/well) for 10 min. After washing twice with $ddH_2O$, culture medium (Table 5) was added to the arrays (200 µl/well). A high current (3 mA), high frequency (64 kHz) pulse was applied to clean the electrodes. $4.8 \cdot 10^4$ cells resuspended in 200 µl culture medium were seeded into each 0.8 $cm^2$ well of the ECIS arrays. The configuration "Multiple frequencies/ time" allowed the measurement at multiple frequencies (4000 and 40000 Hz). 1 h was selected as interval between the measurements. The cells were cultured for 70 - 100 h at 37 °C and 5% $CO_2$ while the electrical resistance was recorded.

### 3.4.7 Life cell imaging

Life cell imaging was performed to investigate subcellular localization of fluorescently labeled proteins. In advance, cells were transfected on 10 $cm^2$ PLL coated glass coverslips (Menzel, Braunschweig, Germany) (Chapter 3.4.3). The cells were grown as confluent monolayers and imaged in HBSS. Placed in a coverslip holder, trypane blue was added to stain the plasma membrane. Imaging was performed using a LSM 510 META UV system, by use of an Axiovert 135 microscope equipped with a PlanNeofluar 1006/1.3 NA oil immersion objective (Carl Zeiss, Jena, Germany). Zeiss ZEN 2009 was used to quantify the localization at the plasma membrane by means of the weighted colocalization coefficient. As expressed in the formula below the coefficient describes the sum of intensities (i) of YFP pixels colocalizing with trypan blue compared to the overall sum of YFP pixel intensities (0, no colocalization; 1, all pixels colocalize).

$$\text{Weighted colocalization coefficent} = \frac{\sum_i YFP_{coloc}}{\sum_i YFP_{total}}$$

### 3.4.8 Immunofluorescence labeling and microscopy

The coverslips were placed in a 24-well-tissue culture plate and coated with rat tail collagen. bEND.3 cells were seeded and grown to full confluency. Before fixation, cells were washed twice with ice-cold PBS. The coverslips were transferred to a

staining tray with ice-cold acetone for 5 min and ice-cold ethanol for 1 min. After washing for 2 min with ice-cold PBS, unspecific binding was prevented by 1 h blocking with 5% milk powder in PBS containing 0.05% tween20. Cells were incubated overnight with a primary antibody diluted in 0.25% milk powder in PBS (Table 12) at 4 °C. After washing five times with 0.25% milk powder in PBS, the cells were incubated with a fluorophore coupled secondary antibody, diluted in 0.25% milk powder in PBS for 1 h at RT in the dark (Table 12). The cells were washed thrice with 0.25% milk powder in PBS and mounted with Roti-Mount FlourCare DAPI. The microscopy was performed using the Zeiss LSM 780 with a 64x/1.40 oil objective.

### 3.4.9 Freeze fracture electron microscopy

At a confluency of 100%, bEND.3 cells were washed with PBS (containing $Ca^{2+}$/ $Mg^{2+}$) and fixed with 2.5% glutaraldehyde for 2 h. After washing twice with PBS (containing $Ca^{2+}$/ $Mg^{2+}$), the cells were stored at 4 °C. The following steps of the sample preparation as well as the freeze fracture electron microscopy were performed in collaboration with Prof. Dr. Hartwig Wolburg (University of Tübingen, Germany). Small rectangles of the bottom of the culture flasks were cut out, the attached cells were cryoprotected in 30% glycerol for 30 min, placed between two gold specimen holders and shock frozen in nitrogen slush (-210 °C). The samples were fractured using the freeze-fracture device BAF 400 D (BAL-TEC, Balzers, Liechtenstein) at -150 °C and $5 \cdot 10^{-6}$ mbar. The fracture faces were immediately shadowed with platinum/ carbon (2.5 nm, 45 °C) for contrast and carbon (25 nm, 90 °C) for replica stabilization. The replicas were cleaned with 12% sodium hypochlorite, washed several times in $ddH_2O$ and mounted on Pioloform-coated copper grids (Wacker Chemie, München, Germany). The Zeiss EM10 electron microscope was used to examine the replicas.

## 3.5 Biochemical methods

### 3.5.1 Purification of total proteins from lysates

For western blotting, brain capillaries were purified (Chapter 33). To analyze cultured cells, the harvest was carried out by use of a cell scraper after a washing step with ice-cold PBS. The cells were pelleted at 450 x g and 4 °C for 5 min. The supernatant was discarded. The following protocol allows the separation of the Triton X-100 soluble and insoluble fraction. The soluble fraction contains mainly cytoplasmic proteins whereas membrane-bound proteins enrich in the insoluble fraction (Patton et al., 1989). Both purified brain capillaries as well as cell cultures were resuspended in cell lysis extraction buffer (30 µl/1 · $10^6$ cells or brain capillary preparations of 2 mice, Table 6) and incubated for 20 min on ice. The lysate was centrifuged for 1 min at 13000 x g. The supernatant, the Triton X-100 soluble fraction was mixed with the cell lysis solubilisation buffer (3.3 µl/1 · $10^6$ cells or brain capillary preparations of 2 mice, Table 6). The remaining pellet was resuspended in the benzonase mix (5 µl/1 · $10^6$ cells or brain capillary preparations of 2 mice, Table 6) and incubated for 10 min at 37 °C. After homogenizing via pipetting, the solubilisation buffer (16.6 µl/1 · $10^6$ cells or brain capillary preparations of 2 mice) was added. The benzonase was inactivated by heating at 95 °C for 3 min. Extraction buffer (11.7 µl/1 · $10^6$ cells or brain capillary preparations of 2 mice) was added to the Triton X-100 insoluble fraction to adjust the volume.

### 3.5.2 Expression and purification of MBP tagged protein domains

Transformation of *E. coli* BL21 was performed as described in chapter 3.3.5. Single colonies were picked from agar plates and incubated overnight in 5 ml LB medium at 37 °C and 230 rpm. The medium contained antibiotics for selection according to Table 8. The bacteria were diluted 1:300 in 500 ml LB medium with 2 g/l glucose and selection antibiotics and further cultured in an Erlenmeyer flask under the same culture conditions until reaching an O.D. between 0.6 and 0.8 at 600 nm. The expression of the plasmid encoded MBP-fusion protein was induced by adding of 1 mM IPTG and further cultured for 3 h at 37 °C and 230 rpm. The

bacteria were centrifuged at 3220 x g and 4 °C for 15 min. To break down the bacterial cell walls, the pellet was resuspended in 15 ml MBP lyses buffer and homogenized via EmulsiFlex-C3. The lysate was centrifuged at 20000 x g and 4 °C for 15 min. Afterwards, the supernatant was centrifuged at 60000 x g and 4 °C for 1 h. The supernatant was diluted 1:3 in 1 mM EDTA containing PBS and loaded to a column that contained 5 ml equilibrated Amylose Resin. The column bound MBP-fusion proteins were washed four times with MBP wash buffer (Table 6) before elution of ten fractions of 1 ml in MBP elution buffer (Table 6). The purified proteins were concentrated in Amicon® ultra 30K tubes at 3220 x g and 4 °C for 1 h.

### 3.5.3 Purification of YFP tagged proteins

HEK-293 cells were transfected as described in chapter 3.4.3. In contrast to prokaryotic expression systems, eukaryotically expressed YFP tagged proteins exhibit post-translational modifications like *N*-glycosylation. 48 h after transfection, the cells were washed twice with ice-cold PBS and harvested by use of a cell scraper. For purification, the GFP-Trap® A was used following the manufacturer's instructions.

### 3.5.4 Determination of the protein concentration

The concentrations of purified MBP tagged protein domains were determined using the calculated mass extinction coefficient for a 10 mg/ml (1%) solution of the respective protein (Table 23, ProtParam tool, www.expasy.org) and the absorbance at an excitation wavelength of 280 nm measured via NanoDrop 2000c (Protein A280, E 1%).

**Table 23 Mass extinction coefficients of MBP tagged protein domains**

| MBP tagged protein domain | Mass extinction coefficient [L $gm^{-1}cm^{-1}$] |
|---|---|
| MBP-mCldn1$_{188-211}$ | 15.02 |
| MBP-mCldn4$_{186-210}$ | 15.02 |
| MBP-mCldn5$_{141-161}$ | 14.79 |
| MBP-mCldn5$_{184-218}$ | 15.77 |
| MBP-mCldn11$_{179-207}$ | 14.60 |
| MBP-mCldn12$_{200-244}$ | 14.69 |

| | |
|---|---|
| MBP-mCldn25$_{26-140}$ | 17.97 |
| MBP-mCldn25$_{196-215}$ | 15.38 |
| MBP-mCldn25$_{237-253}$ | 14.91 |
| MBP-mCldn25$_{237-252}$ | 14.94 |
| MBP-mCldn25$_{237-251}$ | 14.97 |
| MBP-mCldn25$_{237-250}$ | 15.02 |
| MBP-mCldn25$_{237-249}$ | 14.75 |
| MBP-mCldn25$_{237-247}$ | 14.81 |
| MBP-mOcln$_{406-521}$ | 14.62 |
| MBP-mZO1$_{23-110}$ | 12.32 |
| MBP(-stop) | 14.93 |

The total protein concentration of lysates was determined using the Pierce BCA Protein Assay Kit according to the supplier's manual. Photometric measurements were carried out at an excitation wavelength of 562 nm using the Safire, a monochromator-based microplate detection system.

### 3.5.5 SDS-PAGE

Proteins were separated according to their electrophoretic mobility by one-dimensional sodium dodecyl sulfate polyacrylamide gel electrophoresis (SDS-PAGE). SDS, an anionic detergent, linearizes the polypeptide and imparts an even distribution of negative charge per mass unit that allows a fractioning by approximate size via electrophoresis. The composition of the stacking as well as the separation gel is listed in Table 6. The protein probes were incubated with 4x SDS loading buffer (Table 6) for 10 min at 60 °C and loaded to the SDS-polyacrylamid gel. The separation was performed for 15 min at 80 V followed by 40 min at 120 V in a SDS-PAGE chamber containing 1x SDS running buffer.

### 3.5.6 Coomassie R250 staining

After SDS-PAGE, gels were incubated for 10 min in Coomassie staining solution (Table 6). Decolourization of the background was achieved by overnight incubation in tap water.

### 3.5.7 Glycoprotein staining

SDS-PAGE was performed as described in chapter 3.5.5 and glycans stained by use of the Pierce™ Glycoprotein Staining Kit according to the supplier's

instructions. Final washing was carried out for 30 min in 3% acetic acid followed by 30 min in dd$H_2O$.

### 3.5.8 Western blotting

The specific detection of proteins via western blotting requires the transfer from SDS-polyacrylamid gel onto a nitrocellulose membrane. Therefore, the gel as well as a nitrocellulose membrane was equilibrated in 1x transfer buffer (Table 6) for 10 min. The transfer was performed using a wet blotting system at 100 V for 1 h. The transfer was verified by water removable staining of proteins with Ponceau dye. Afterwards the membrane was shaken for 1 h in TBST buffer containing 5% (w/v) milk powder to block unspecific antibody binding sites. After three washing steps of 10 min in TBST, the membrane was incubated with a primary antibody (Table 12) in TBST containing 1 % (w/v) milk powder overnight at 4 °C. Next day the membrane was washed thrice for 10 min in TBST and incubated with a secondary antibody, coupled to horse reddish peroxidase (HRP) (Table 12) in TBST for 1 h at RT. Following three final washing steps the membrane was incubated 5 min with the super ECL solution. Protein bands were detected by use of the Lumi-Imager F1T transilluminator and further quantified with ImageJ (NIH).

### 3.5.9 Epitope dilution assay

To quantify the molalities of endogenous TJ proteins, the MBP tagged epitopes were recombinantly expressed and purified (Chapter 3.5.2). The degree of purity was determined by densitometric analyses of the Coomassie R250 stained SDS-PAGE (Figure S 8) by use of ImageJ 1.48v. The protein concentration was determined with the NanoDrop 2000c using the calculated mass extinction coefficient (ProtParam tool, www.expasy.org). A dilution series of the MBP tagged epitope was blotted (Chapter 3.5.8) together with the lysate of purified brain capillaries (Chapter 3.5.1, Figure 15). The Lumi-Imager F1T was used to determine the biochemical light units (BLU) of each protein band of the dilution series of the MBP tagged epitope as well as the endogenous TJ protein in the Triton X-100 soluble and insoluble lysate fraction (Table S 2). A calibration curve of epitope mass and BLU was generated (m, slope; Figure S 3) to calculate the

mass of the blotted endogenous TJ protein under consideration of the degree of purity of the MBP tagged epitope ($s_{MBP\text{-}epitope}$) (equation 1, below; Table S 2). The mass concentration of the TJ protein in the lysate was calculated knowing the volume of the lysate (equation 2, below; Table S 2). The molar concentration was determined considering the conversion factor (conversion ng to kDa, $6.022 \cdot 10^{11}$) and the mass of the MBP tagged epitopes (Table S 2) by use of the Avogadro constant ($6.022 \cdot 10^{23}$ $mol^{-1}$) (equation 3, below; Table S 2). The protein concentration of the lysate was included to calculate the molality (equation 4, below; Table S 2).

$$(1)\quad x_1\ ng = \frac{[BLU] \cdot s_{MBP\text{-}epitope}}{m} \qquad (2)\quad x_2 \frac{ng}{\mu l} = \frac{x_1\ ng}{\mu l_{lysate}}$$

$$(3)\quad x_3 \frac{mol}{\mu l} = \frac{x_2\ ng \cdot 6.022 \cdot 10^{11} \cdot mol}{\mu l \cdot [kDa]_{MBP\text{-}epitope} \cdot 6.022 \cdot 10^{23}} \qquad (4)\quad x_4 \frac{fmol}{\mu g} = \frac{x_3\ mol \cdot 10^{15} \cdot \mu l_{lysate}}{\mu l \cdot \mu g_{lysate}}$$

## 3.6 Biophysical methods

### 3.6.1 Microscale thermophoresis

Microscale thermophoresis was performed to determine the binding affinities between purified MBP tagged protein domains. Thermophoresis is directed at the motion of molecules in microscopic temperature gradients, depending on the size, hydration shell and conformation of molecules. Binding events influence at least one of these factors and thereby define thermophoretical particle movement (Seidel et al., 2013). The principle of MST is shown in Figure 9. Infrared (IR) laser and excitation light are coupled and directed to a glass capillary. 15 capillaries contain a fluorescently labeled as well as an unlabelled binding partner in increasing concentration. The IR radiation creates a temperature gradient which influences thermophoretic movement of bound and unbound particles differently. Unbound particles diverge more rapidly from the area of fluorescence recording, resulting in a deep slope of the fluorescence signal over time. Bound particles remain longer in focus resulting in a stronger fluorescence signal (Jerabek-Willemsen et al., 2014).

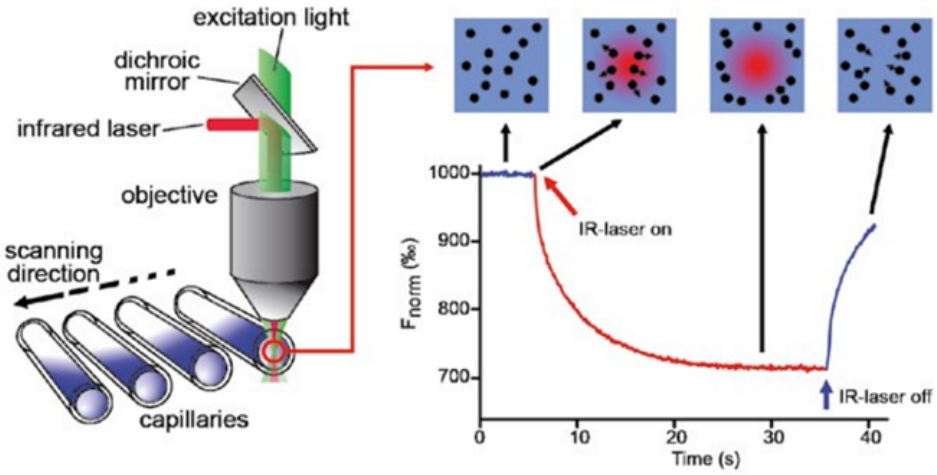


**Figure 9 Principle of microscale thermophoresis.** Normalized fluorescence intensity ($F_{norm}$), defined as difference of the mean fluorescence in the initial state and the steady state, is recorded time-dependently. Fluorescence of the initial state is high due to evenly distributed fluorescent molecules (dots). Signal intensity decreases when the IR-laser is turned on and levels out when the molecules move across the temperature gradient (dots with arrows in the red circle). This is followed by the steady state, were thermophoresis is counterbalanced by mass diffusion. Turning off of the IR-laser leads to an inverse temperature jump and backdiffusion. (modified according to Jerabek-Willemsen et al., 2014)

#### 3.6.1.1 Labeling of MPB tagged proteins domains

To monitor protein-protein interactions, one of the binding partners was coupled with a fluorescent dye using the Monolith NT Protein Labeling Kit RED-NHS according to the supplier's manual. The fluorescent dye is linked to a crosslinker reactive group (e.g. N-hydroxysuccinimide), which in turn randomly binds primary amines of lysine chains, the $NH_2$-terminus of proteins or arginine's guanidino group. Random labeling minimizes possible local effects of a label on the binding behavior (Seidel et al., 2013). Labeled proteins were analyzed by SDS-PAGE for dye residues. Therefore, the gels were excited at 635 nm and imaged with the FLA-5000 (Fujifilm, Tokyo, Japan) (Figure S 9). Afterwards, the concentration of the labeled binding partner was adjusted to achieve optimal fluorescence between 400 and 1000 units.

#### 3.6.1.2 Experimental set up and procedure

In order to measure binding events, the unlabeled protein domain was titrated against a fixed concentration of the labeled binding partner. Therefore, 15 dilutions (1:2) in PBS were prepared. Incubation was allowed for 1 h in darkness. Subsequently, samples were transferred into standard treated capillaries and measured using the Monolith NT.115. The IR-laser was set to 50% of power for 35 s, while the excitation light was adjusted to an optimal fluorescence of 400 - 1000 units. For plotting, fluorescence values were normalized by subtracting the baseline and dividing the amplitude of both plateaus. The dissociation constant ($K_d$) was calculated using the MO.Affinity Analysis software (Seidel et al., 2013).

## 3.7 Statistics

Data analysis and generation of graphs were achieved by employing GraphPad Prism® 5.04 and Microsoft Excel 2010. Mean ± standard deviation were blotted, unless stated otherwise. The standard deviation was calculated for $n \geq 3$. The Mann-Whitney U-test was used to determine significant differences between two groups. The Kruskal-Wallis test followed by the Dunns test was employed to determine significant differences between more than two groups. P-values $< 0.05$ were considered statistically significant (* $p < 0.05$, ** $p < 0.01$, *** $p < 0.001$).

# 4 Results

## 4.1 Quantification of claudins and TAMPs in the brain endothelium

The paracellular barrier tightness of epithelia and endothelia highly depends on transcellular interactions of extracellular Cldn loops. These interactions can be found between Cldns of the same or different subtypes (Krause et al., 2008). In the brain endothelium it is still unclear which Cldns are expressed and interact to form TJs. Those TJs are thought to be formed mainly by Cldn5 but appear ultrastructurally normal even after knockout of Cldn5 (Nitta et al., 2003). Cldn12 is not forming TJ-strands due to the lack of homo- or heterophilic Cldn interactions (Piontek et al., 2011). The tightening Cldn1 and -3 are compared to Cldn5 relatively low expressed (Daneman et al., 2010; Kooij et al., 2014; Ohtsuki et al., 2008). Therefore, the involvement of further Cldns and TAMPs can be hypothesized.

### 4.1.1 mRNA expression of claudins and TAMPs in laser-dissected human and mouse brain capillaries

To investigate the Cldn and TAMP mRNA expression pattern in the brain endothelium, mRNA expression of human brain capillaries was screened *ex vivo.* Laser capture microdissection was performed to isolate brain capillaries from cryosections of the human cerebral cortex. The endothelium specific lectin, RCA1 (Mojsilovic-Petrovic et al., 2004), fluorescently labeled was used to stain capillaries for dissection. RNA was isolated and cDNA synthesized according to chapter 3.3.1.1. The mRNA expression levels were determined by quantitative RT-PCR. The primers were designed with Primer3Plus (S. Rozen and Skaletsky, 2000) and the sequences checked for specificity using the NCBI Basic Local Alignment Search Tool (Geer et al., 2010). The primer efficiencies were selectively determined to ensure optimal and comparable cDNA amplification (Figure S 1). mRNA levels were additionally determined in brain capillaries of mice following the same experimental procedure. It was investigated if the mouse model, mostly used in BBB research, reflects the human phenotype. mRNA expression was analyzed for *Ocln*, a TJ marker, *Zo1,* a TJ associated protein and *Cdh5,* the major adherens junction protein (Figure 10). All expression levels were normalized to β-

actin (*Actb*), encoding a ubiquitous cytoskeleton protein and being expressed at moderately abundant levels in most cell types (Bustin, 2000). All markers were expressed in the same order of magnitude referring to the same species. mRNA expression of the markers was generally lower in human compared to mouse, significantly for *Ocln* (-6.6-fold, Figure 10). Hence, the expression values were ranked by order of magnitude with regard to the expression of the TJ marker *Ocln* in the same species (Table S 1). In human, six TJ proteins were expressed above the mRNA level of *Ocln* (*Cldn1* (1.8-fold), *-5* (12.5-fold), *-11* (9.9-fold), *-12* (6.9-fold), *-25* (38.8-fold) and *-27* (4.7-fold); Table 24; Figure 11, 13) whereby *Cldn-5* and *-25* were even more than one order of magnitude higher expressed. In mouse, only four TJ proteins were expressed above the level of the TJ marker (*Cldn5* (6.7-fold), *-11* (5.3-fold), *-12* (1.5-fold), and *-25* (1.6-fold); Table 24; Figure 11, 13). Expressed less than one order of magnitude below *Ocln* were nine TJ proteins in human (*Cldn3, -4*, *-6*, *-9*, *-15*, *-17*, *-20*, *-22* and *Tric;* Table 24; Figure 11 - 13) and six in mouse (*Cldn1*, *-14*, *-20*, *-22*, *-24* and *-26*; Table 24; Figure 11, 13). Among these TJ proteins the majority contributes to paracellular sealing (Cldn1, -3, -4, -5, -6, -9, -11, -14 and Tric) and only Cldn15 and -17 are known to enhance paracellular ion flux (Table 1). The functions of seven further Cldns (Cldn12, -20, -22, -24, -25, -26 and -27) remain still unclear.

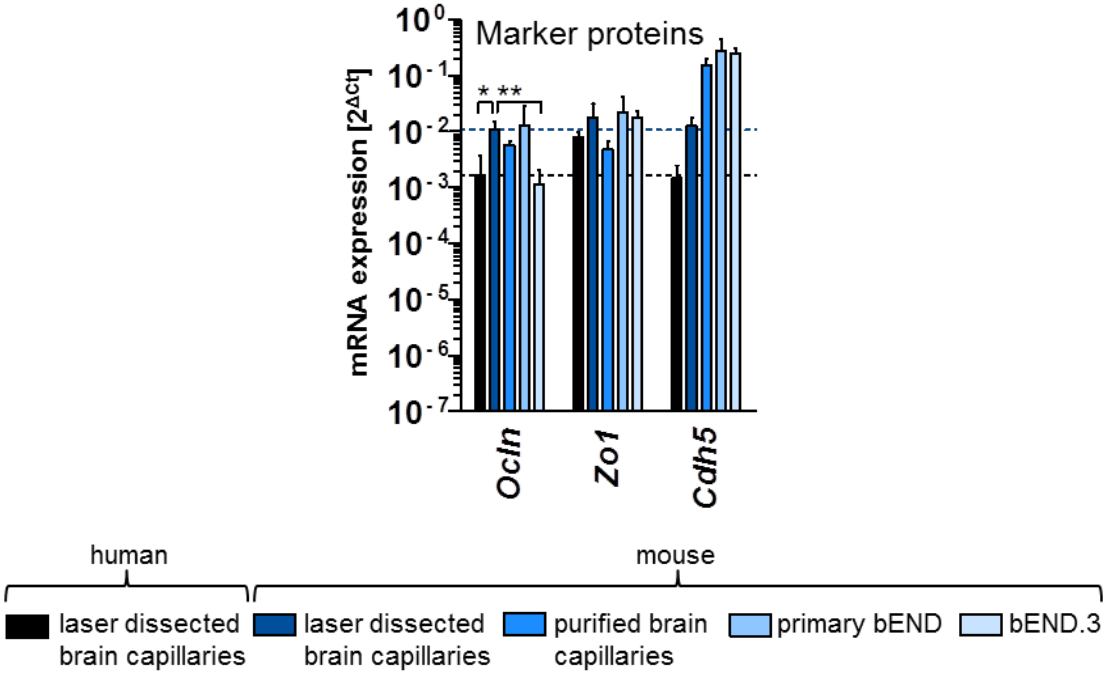

**Figure 10 mRNA expression levels of occludin as tight junction marker, *zonula occludens* protein 1, a tight junction associated protein and cadherin-5, the major adherens junction protein.** Expression in laser-dissected human and mouse brain capillaries compared with purified mouse brain capillaries, primary mouse brain capillary endothelial cells (primary bEND) and bEND.3, an endothelial cell line of the mouse cerebral cortex. mRNA normalized to β-actin (*Actb*) (ΔCt = $Ct_{target}$ - $Ct_{Actb}$). Dashed line, *Ocln* expression of laser-dissected human (black) or mouse (blue) brain capillaries; „-“, not detectable. Kruskal–Wallis test; mean ± SD; n ≥ 4; *, p < 0.05; **, p < 0.01. *Ocln*, occludin; *Zo1*, *zonula occludens* protein 1; *Cdh5*, cadherin-5 (VE-cadherin).

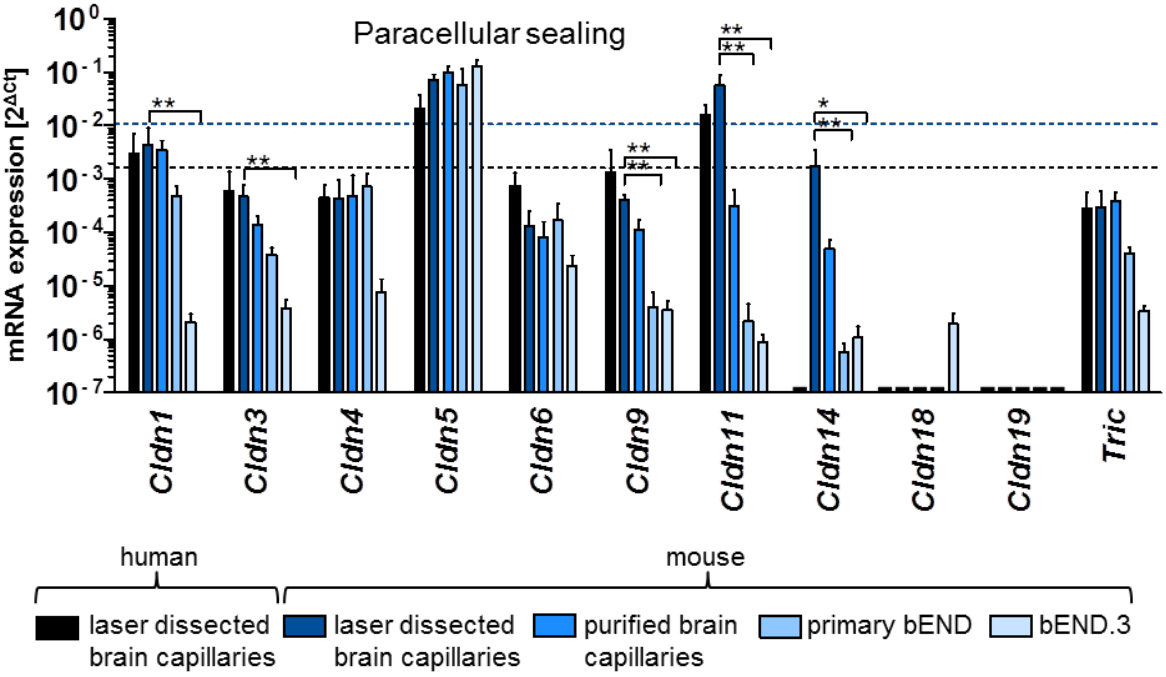


**Figure 11 mRNA expression levels of tight junction proteins with proven paracellular sealing function.** Expression in laser-dissected human and mouse brain capillaries compared with purified mouse brain capillaries, primary mouse brain capillary endothelial cells (primary bEND) and bEND.3, an endothelial cell line of the mouse cerebral cortex. mRNA normalized to β-actin (*Actb*) (ΔCt = $Ct_{target}$ - $Ct_{Actb}$). Dashed line, *Ocln* expression of laser-dissected human (black) or mouse (blue) brain capillaries; „-“, not detectable. Kruskal–Wallis test; mean ± SD; n ≥ 4; *, p < 0.05; **, p < 0.01. *Cldn*, claudin; *Tric*, tricellulin.

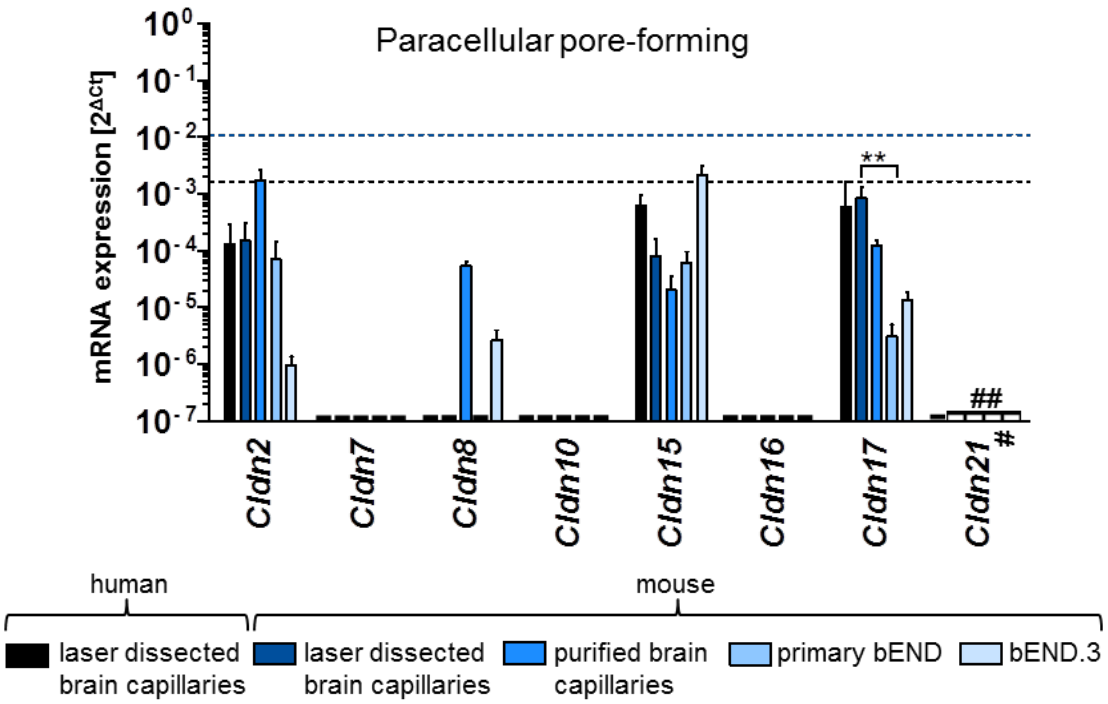


**Figure 12 mRNA expression levels of claudins with paracellular ion pore-forming function.** Expression in laser-dissected human and mouse brain capillaries compared with purified mouse brain capillaries, primary mouse brain capillary endothelial cells (primary bEND) and bEND.3, an endothelial cell line of the mouse cerebral cortex. mRNA normalized to β-actin (*Actb*) (ΔCt = $Ct_{target}$ - $Ct_{Actb}$). Dashed line, *Ocln* expression of laser-dissected human (black) or mouse (blue) brain capillaries; „-“, not detectable. Kruskal–Wallis test; mean ± SD; n ≥ 4; *, p<0.05; **, p < 0.01. *Cldn*, claudin. # synonyms: *Cldn21*, putative *Cldn25*; ## no primer for mCldn21 (Table 11).

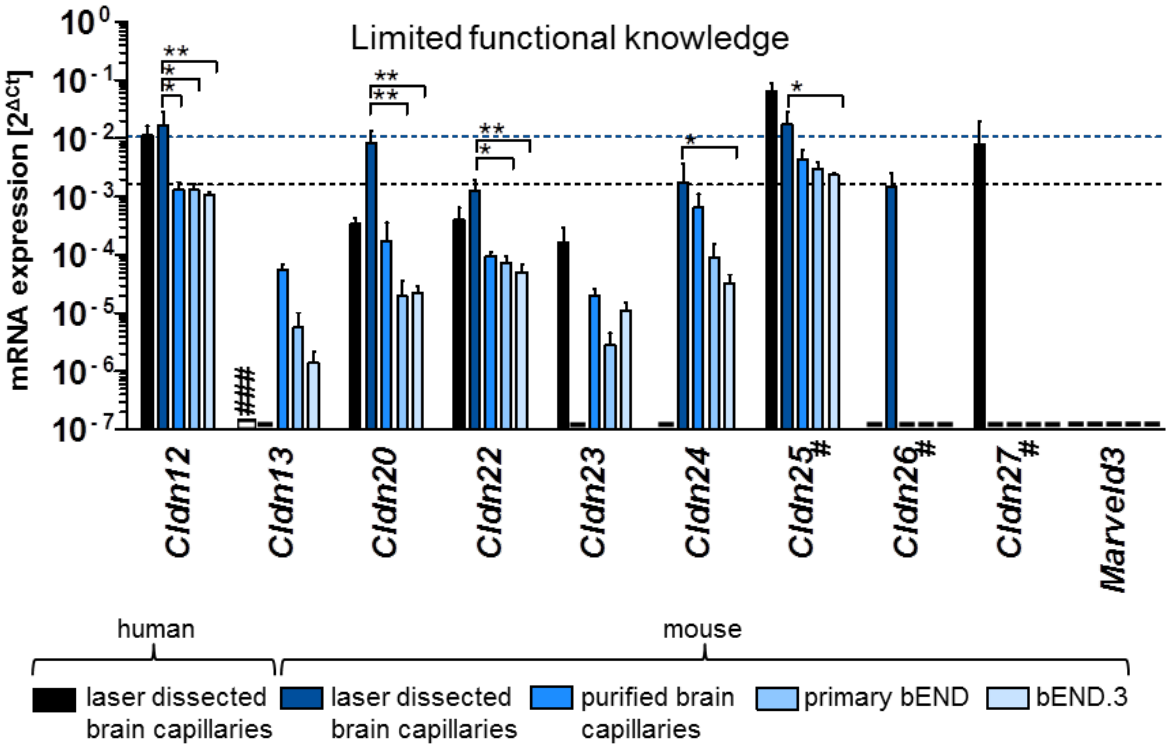


**Figure 13 mRNA expression levels of claudins with limited functional knowledge.** Expression in laser-dissected human and mouse brain capillaries compared with purified mouse brain capillaries, primary mouse brain capillary endothelial cells (primary bEND) and bEND.3, an endothelial cell line of the mouse cerebral cortex. mRNA normalized to β-actin (*Actb*) ($\Delta Ct = Ct_{target} - Ct_{Actb}$). Dashed line, *Ocln* expression of laser-dissected human (black) or mouse (blue) brain capillaries; „-“, not detectable. Kruskal–Wallis test; mean ± SD; n ≥ 4; *, p < 0.05; **, p < 0.01. # synonyms: *Cldn25*, *Cldnd1*; *Cldn26*, *Tmem114*; *Cldn27*, *Tmem235*; ### not found in human. *Cldn*, claudin.

**Table 24 Fold induction with respect to the occludin expression in laser-dissected brain capillaries within the same species.** Fold induction in laser-dissected human and mouse brain capillaries. # not found in human; ## no primer for m*Cldn21* (Table 11); „n.d.“, not detectable. *Cldn*, claudin; *Tric*, tricellulin; *Zo1*, *zonula occludens* protein 1; *Cdh5*, cadherin-5 (VE-cadherin). Positive fold induction (green); negative fold induction (red).

| | human | mouse |
|---|---|---|
| ***Cldn1*** | 1.83E+00 | -2.44E+00 |
| ***Cldn2*** | -1.30E+01 | -7.30E+01 |
| ***Cldn3*** | -2.70E+00 | -2.28E+01 |
| ***Cldn4*** | -3.70E+00 | -2.55E+01 |
| ***Cldn5*** | 1.25E+01 | 6.73E+00 |
| ***Cldn6*** | -2.18E+00 | -8.25E+01 |
| ***Cldn7*** | n.d. | n.d. |
| ***Cldn8*** | n.d. | n.d. |
| ***Cldn9*** | -1.23E+00 | -2.71E+01 |
| ***Cldn10*** | n.d. | n.d. |
| ***Cldn11*** | 9.87E+00 | 5.31E+00 |
| ***Cldn12*** | 6.93E+00 | 1.51E+00 |
| ***Cldn13*** | # | n.d. |
| ***Cldn14*** | n.d. | -6.08E+00 |
| ***Cldn15*** | -2.67E+00 | -1.34E+02 |
| ***Cldn16*** | n.d. | n.d. |
| ***Cldn17*** | -2.80E+00 | -1.31E+01 |
| ***Cldn18*** | n.d. | n.d. |
| ***Cldn19*** | n.d. | n.d. |
| ***Cldn20*** | -4.90E+00 | -1.27E+00 |
| ***Cldn21*** | n.d. | ## |
| ***Cldn22*** | -4.15E+00 | -8.72E+00 |
| ***Cldn23*** | -1.03E+01 | n.d. |
| ***Cldn24*** | n.d. | -6.34E+00 |
| ***Cldn25*** | 3.88E+01 | 1.60E+00 |
| ***Cldn26*** | n.d. | -7.28E+00 |
| ***Cldn27*** | 4.73E+00 | n.d. |
| ***Tric*** | -5.85E+00 | -3.58E+01 |
| ***Marveld3*** | n.d. | n.d. |
| ***Zo1*** | 4.84E+00 | 1.66E+00 |
| ***Cdh5*** | -1.13E+00 | 1.18E+00 |

### *4.1.2* mRNA expression in the brain endothelium *in vitro*

To investigate if isolated endothelial cells *in vitro* exhibit a similar composition of the TJ complex *in vivo*, the expression of TJ proteins was compared. Therefore mouse brain capillaries *ex vivo* (laser capture microdissection from frozen tissue) and *in vitro* in purified capillary preparations from cerebral cortices, primary mouse

brain endothelial cells and the cell line bEND.3 were analyzed. Interestingly, after cultivation of primary endothelial cells a reduced gene transcription of most Cldns was found but not of *Cldn5*. In purified brain capillaries only *Cldn12* was significantly reduced compared to laser-dissected brain capillaries (Figure 13, Table 25). In primary endothelial cells the mRNA levels of seven TJ proteins were significantly decreased with respect to the *ex vivo* expression (*Cldn9*, -*11*, -*12*, -*14*, -17, -*20* and -*22;* Figure 11 - 13; Table 25). This tendency was found for 11 TJ proteins in bEND.3, an immortalized brain endothelial cell line, to an even stronger degree (*Cldn1*, -*3*, -*9*, -*11*, -*12*, -*14*, -*20*, -*22*, -*24*, -*25* and *Ocln*; Figure 10 - 13; Table 25). Further TJ proteins were reduced in mRNA expression *in vitro*, but not significantly (purified brain capillaries, 13 TJ proteins; primary endothelial cells, 8 TJ proteins; bEND.3, 5 TJ proteins; Figure 10 - 13; Table 25). The mouse brain endothelium *ex vivo* was characterized by a percentage of *Cldn5* mRNA of 37% with respect to mRNA of all TJ proteins (Figure 39, 2nd column). Due to cultivation, this dominance of *Cldn5* in the mouse brain endothelium was increased to 84% in purified brain capillaries (Figure 39, 3rd column), 76% in primary brain capillary endothelial cells (Figure 39, 4th column) and even to 95% in bEND.3 cells (Figure 39, 5th column). Importantly, the mRNA level of *Cldn5* itself did not change significantly.

Furthermore, the presence of transcripts in pure endothelial cells *in vitro* could verify those as source of expression. Only the mRNA of *Cldn26* was not expressed in endothelial cells *in vitro* but detected in laser-dissected microvessels (Figure 13).

**Table 25 Fold induction with respect to the expression in laser-dissected mouse brain capillaries.** Fold induction in purified mouse brain capillaries, primary mouse brain capillary endothelial cells (primary bEND) and bEND.3, an endothelial cell line of the mouse cerebral cortex. # not detectable in laser-dissected mouse brain capillaries; ## no primer for m*Cldn21* (Table 11); „n.d.“, not detectable. *Cldn*, claudin; *Tric*, tricellulin; *Ocln*, occludin; *Zo1*, *zonula occludens* protein 1; *Cdh5*, cadherin-5 (VE-cadherin). Positive fold induction (green); negative fold induction (red).

| | purified brain capillaries | primary bEND | bEND.3 |
|---|---|---|---|
| ***Cldn1*** | -1.23E+00 | -9.44E+00 | -2.08E+03 |
| ***Cldn2*** | 1.17E+01 | -2.10E+00 | -1.56E+02 |
| ***Cldn3*** | -3.38E+00 | -1.22E+01 | -1.23E+02 |
| ***Cldn4*** | 1.15E+00 | 1.71E+00 | -5.54E+01 |
| ***Cldn5*** | 1.40E+00 | -1.26E+00 | 1.83E+00 |
| ***Cldn6*** | -1.60E+00 | 1.29E+00 | -5.60E+00 |
| ***Cldn7*** | n.d. | n.d. | n.d. |
| ***Cldn8*** | # | n.d. | # |
| ***Cldn9*** | -3.51E+00 | -9.84E+01 | -1.12E+02 |
| ***Cldn10*** | n.d. | n.d. | n.d. |
| ***Cldn11*** | -1.82E+02 | -2.57E+04 | -6.48E+04 |
| ***Cldn12*** | -1.25E+01 | -1.26E+01 | -1.57E+01 |
| ***Cldn13*** | # | # | # |
| ***Cldn14*** | -3.51E+01 | -3.09E+03 | -1.67E+03 |
| ***Cldn15*** | -3.97E+00 | -1.30E+00 | 2.66E+01 |
| ***Cldn16*** | n.d. | n.d. | n.d. |
| ***Cldn17*** | -6.64E+00 | -2.65E+02 | -6.29E+01 |
| ***Cldn18*** | n.d. | n.d. | # |
| ***Cldn19*** | n.d. | n.d. | n.d. |
| ***Cldn20*** | -4.98E+01 | -4.34E+02 | -3.86E+02 |
| ***Cldn21*** | ## | ## | ## |
| ***Cldn22*** | -1.30E+01 | -1.74E+01 | -2.44E+01 |
| ***Cldn23*** | # | # | # |
| ***Cldn24*** | -2.66E+00 | -1.87E+01 | -5.19E+01 |
| ***Cldn25*** | -3.94E+00 | -5.84E+00 | -7.32E+00 |
| ***Cldn26*** | n.d. | n.d. | n.d. |
| ***Cldn27*** | n.d. | n.d. | n.d. |
| ***Tric*** | 1.28E+00 | -7.35E+00 | -8.81E+01 |
| ***Marveld3*** | n.d. | n.d. | n.d. |
| ***Ocln*** | -1.87E+00 | 1.17E+00 | -9.63E+00 |
| ***Zo1*** | -3.70E+00 | 1.21E+00 | -1.01E+00 |
| ***Cdh5*** | 1.23E+01 | 2.13E+01 | 1.98E+01 |

### 4.1.3 mRNA levels determined by qRT-PCR correlate with those of RNA sequencing

To validate the data shown in chapter 4.1.1, the expression levels determined by qRT-PCR were compared with those of RNA sequencing. RNA sequencing was performed in collaboration with Dr. Jingjing Zhang (Affiliated Hospital of Guangdong Medical College, Zhanjiang, Guangdong, China). Purified mouse brain capillaries were analyzed due to the relatively high RNA yield required for RNA sequencing, which was too low in samples collected by laser capture

microdissection. The values of both quantitative methods plotted in Figure 14 correlated significantly with a spearman's rank correlation coefficient of 0.75.

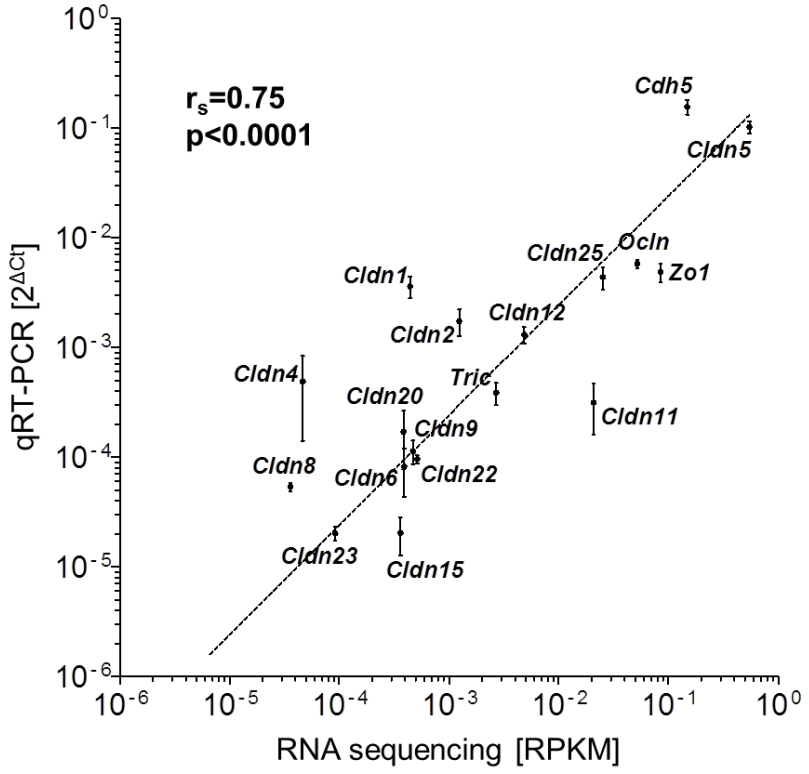


**Figure 14 mRNA levels determined via qRT-PCR correlate with those by RNA sequencing using purified mouse brain capillaries.** mRNA sequencing data is calculated by use of the RPKM ‚Reads Per Kilobase of transcript per Million mapped reads' method. mRNA expression normalized to β-actin (*Actb*). $r_S$, Spearman's rank correlation coefficient. Dashed line, linear regression of correlation data. *Cldn*, claudin; *Tric*, tricellulin; *Ocln*, occludin; *Zo1*, zonula occludens protein 1; *Cdh5*, cadherin-5 (VE-cadherin). Mean ± SD; n ≥ 3.

### 4.1.4 Molality of claudins and occludin in purified mouse brain capillaries

To quantify detected TJ proteins, the MBP tagged epitopes were purified. Knowing the concentration, a dilution series of the epitope was blotted together with the lysate of purified brain capillaries (Figure 15). After densitometric analyses, a calibration curve (Figure S 3) was generated to determine absolute protein quantities (Chapter 3.5.9). Cldn5 was the highest expressed TJ protein in purified brain capillaries with a molality of 509 fmol/µg (Table 26, Table S 2). Followed by the molalities of Cldn25 > Ocln > Cldn1 > -11 > -4 > -12 (98, 36, 15, 8, 5, 4 fmol/µg respectively, Table 26, Table S 2). Cldn1, -11, -25 and Ocln were enriched in the

Triton X-100 insoluble (membrane) fraction whereas Cldn4, -5 and -12 were detected at higher molality in the soluble (non-membrane) fraction. Interestingly, Cldn1 was mainly found as hexamer in the Triton X-100 insoluble fraction, which was also seen in bEND.3 cells (Figure 22).

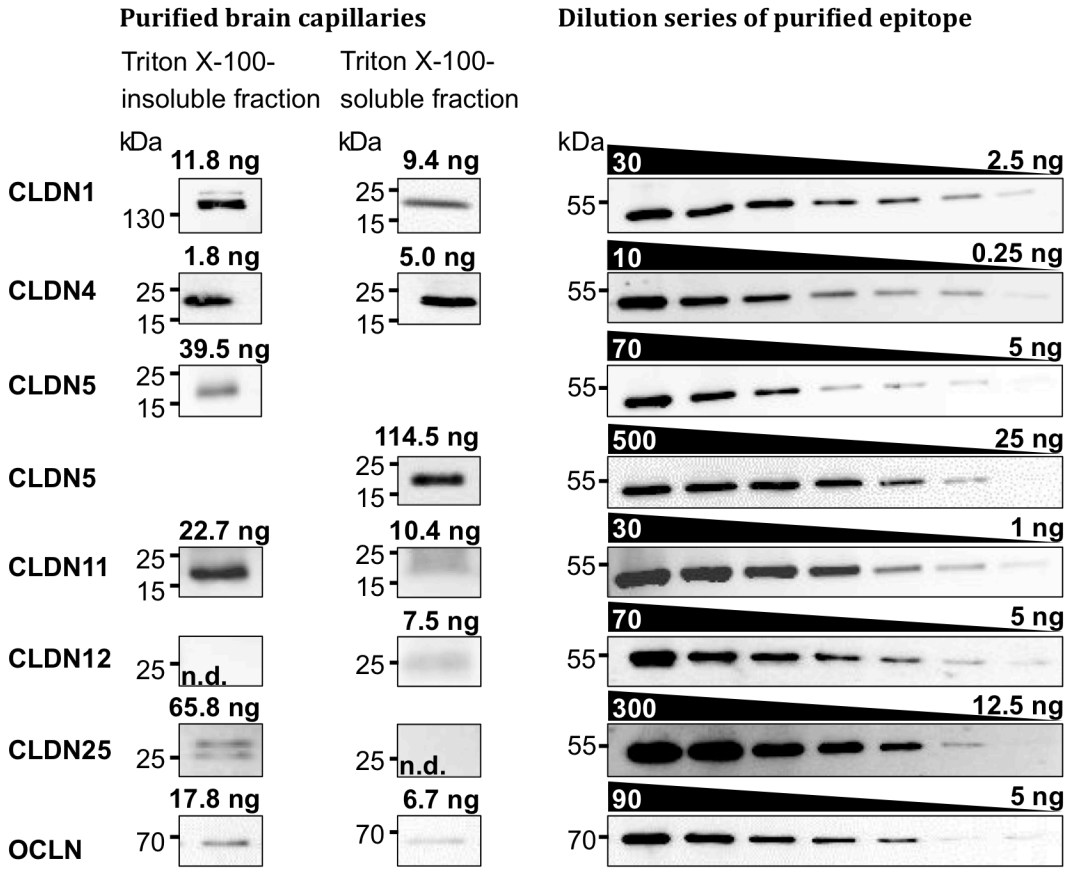


**Figure 15 Epitope dilution assay to determine absolute tight junction protein quantities in purified mouse brain capillaries.** Dilution series of purified recombinant MBP tagged epitopes were blotted (on the right) together with the lysates of purified brain capillaries (on the left). Densitometric analyses and generation of calibration curves (Figure S 3) allowed the determination of the mass of the blotted endogenous TJ proteins (above blots on the right). According to chapter 3.5.9 the molalities were calculated as listed in Table 26 and Table S 2. Examples shown; n = 4; „n.d.“, not detectable.

**Table 26 Molality [fmol/µg protein of mouse brain capillaries] compared between Triton X-100 insoluble and soluble fraction.** The insoluble fraction contains membrane-bound TJ proteins. „n.d.“, not detectable; mean ± SD; n = 4 (single values listed in Table S 2).

| Molality in purified brain capillaries [fmol/µg] | | | |
|---|---|---|---|
| | Total protein | Triton X-100-insoluble fraction | Triton X-100-soluble fraction |
| **CLDN1** | 14.5± 8.1 | 9.7± 6.9 | 4.8± 8.2 |
| **CLDN4** | 5.0± 9.1 | 1.5± 2.9 | 3.4± 6.2 |
| **CLDN5** | 508.9±312.1 | 113.6± 74.0 | 395.3± 291.9 |
| **CLDN11** | 8.0± 5.3 | 6.3± 4.3 | 1.7± 1.2 |
| **CLDN12** | 4.3± 3.5 | n.d. | 4.3± 3.5 |
| **CLDN25** | 97.8±112.7 | 97.8±112.7 | n.d. |
| **OCLN** | 36.1± 12.3 | 26.5± 8.6 | 9.6± 4.3 |

### 4.1.5 Molality and mRNA expression correlate in purified brain capillaries

The mRNA levels of TJ proteins in purified brain capillaries presented in chapter 4.1.1 were blotted against the respective molalities (Chapter 4.1.4) (Figure 16). A significant correlation was found with a Spearman's rank correlation coefficient of 0.82.

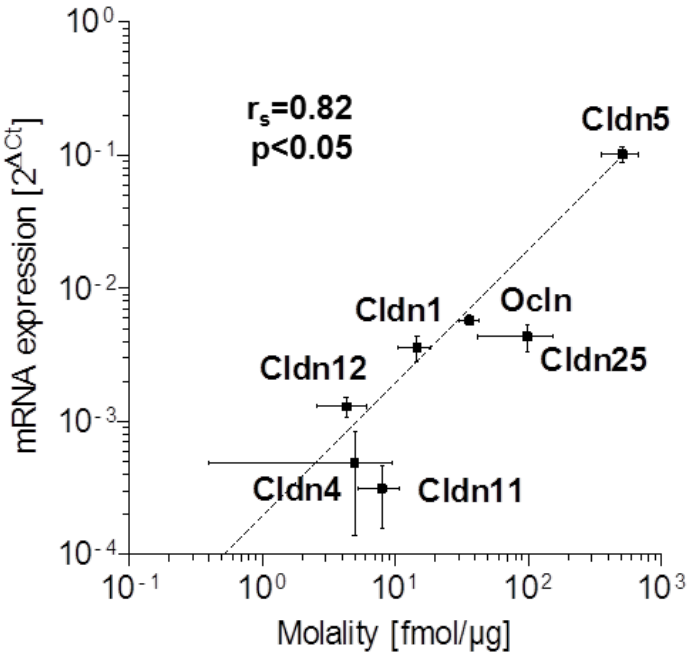


**Figure 16 Correlation of mRNA expression (normalized to β-actin (*Actb*), ΔCt = $Ct_{target}$ - $Ct_{Actb}$; Ct, cycle threshold) and molality in purified mouse brain capillaries.** $r_s$, Spearman's rank correlation coefficient. Dashed line, linear regression of correlation data. Mean ± SEM; n = 4.

## 4.2 Localization of claudins and TAMPs in the brain endothelium

The mRNA expression levels of selected Cldns and TAMPs presented in chapter 4.1.1 correlated with the protein expression as shown in Figure 16. But it is not yet clear to which degree the transmembrane proteins are incorporated into the TJ complex. The enrichment in the membrane fraction determined in chapter 4.1.4 does not differentiate between plasma membrane and membranes of organelles. Thereby, immunoflourescence stainings were indispensable to qualitatively describe the protein composition of the brain endothelial TJ complex.

### 4.2.1 Localization in the human cortex

Cryosections of the human cortex were immunohistochemically labeled and imaged via confocal laser scanning microscopy. Brain capillaries were identified by use of an endothelium specific lectin, RCA1 (Mojsilovic-Petrovic et al., 2004) (Figure 17). Since Zo1 colocalized precisely with Ocln in brain capillaries, it was used as equivalent TJ marker. Cldn3, -4 and -5 localized strictly in TJs and were barely visible in the cytoplasm of capillaries or in the surrounding tissue. Cldn11, -20 and -25 were overlapping with Zo1 but were also visualized in the surrounding tissue. In chapter 4.2.3, cellular structures immunofluorescently labeled exclusively by the antibody for Cldn11 and not for Zo1 were identified as oligodendrocytes. Within the brain capillaries, the Cldn11 staining was restricted to TJs. No clear cellular structures outside the brain capillaries were visible for Cldn20 and -25. Unspecific binding of those antibodies might explain the randomly distributed signal in the surrounding tissue. Within the capillaries, Cldn20 as well as -25 were enriched at the TJs. Cldn1 localized specifically in brain capillaries marked by RCA1, but mainly in the cytoplasm. Earlier Cldn10 was reported as constituent of cerebral endothelial cells (Ohtsuki et al., 2008) but it was stained outside of the capillaries (Figure S 4). A contribution to the BBB can be excluded. No specific antibodies were available to stain further Cldns expressed less than one order of magnitude below *Ocln* in the human cortex (Table S 1, Cldn6, -9, -12, -15, -17, -22 and -27). A mouse specific Cldn12 antibody was available as described in chapter 4.2.2.

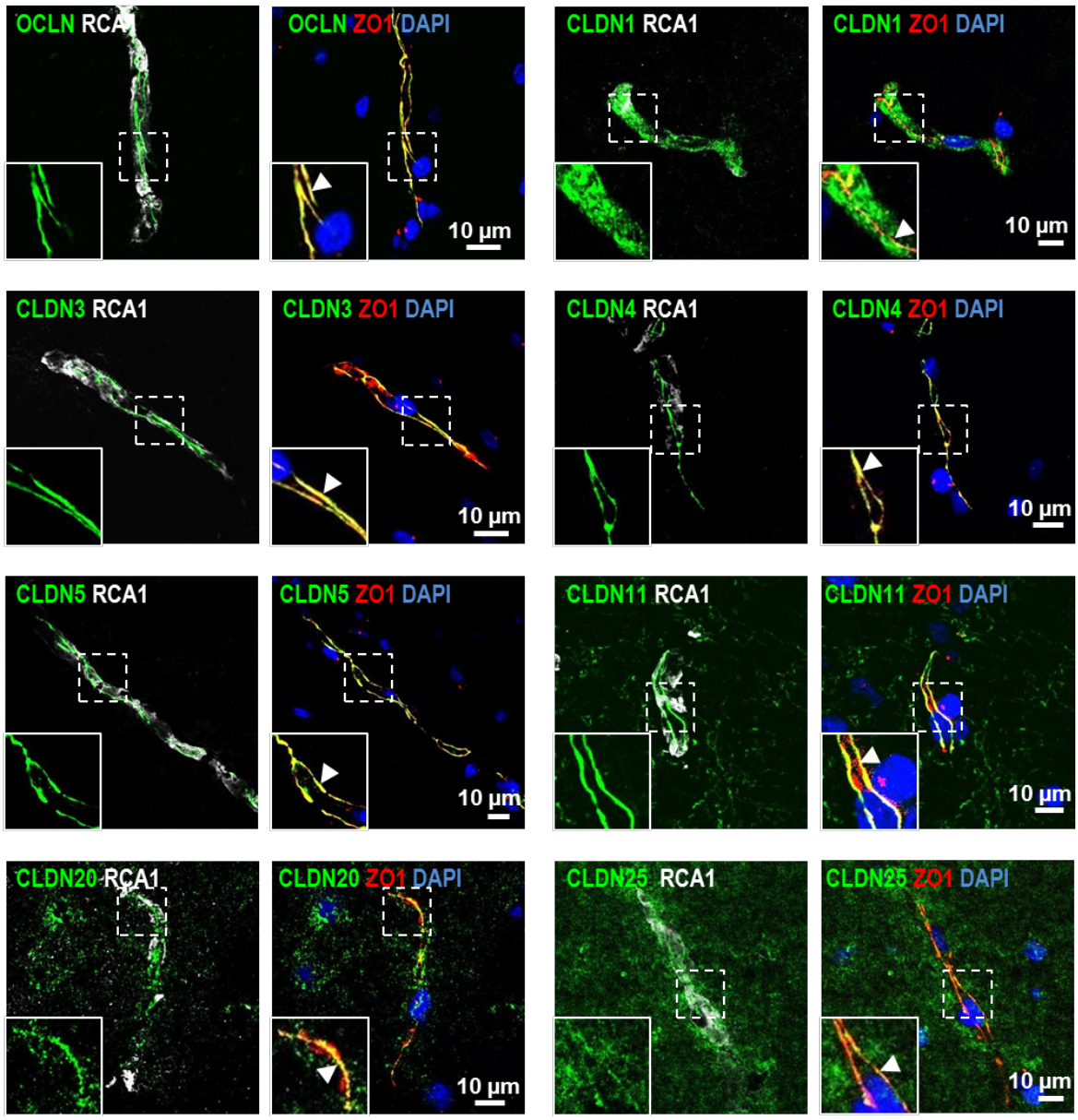


**Figure 17 Claudin (Cldn)-3, -4, -5, -11, -20, -25 and occludin (Ocln) colocalize in the tight junction area of human brain capillaries.** Immunofluorescence stainings of human brain sections against TJ proteins (green). Microvessels stained by RCA1 (white) with *zonula occludens* protein 1 (Zo1) (red), localized in the TJ area. Arrows point to an overlap of TJ proteins with Zo1 (yellow). The nuclei were stained by DAPI (blue). Cldn1 localized mainly in the cytoplasm of brain capillaries.

### 4.2.2 Localization in the mouse cortex

Mouse brain cryosections were immunohistochemically labeled and imaged as described for human cortex cryosections to compare the subcellular localization of Cldns and TAMPs between both species. An accurate overlap between Ocln and ZO1 was also found in the mouse cortex. Cldn5 localized exclusively in TJs of the

brain endothelium while Cldn11 was additionally found in oligodendrocytes, as seen in the human cortex (Figure 17). Unlike its localization in the human cortex, Cldn4 in the mouse brain was not restricted to TJs of brain capillaries, but also observed in the surrounding tissue. Randomly distributed signal outside the capillaries might occur due to unspecific antibody binding in the mouse tissue. Cldn1, as seen in the human cortex was specifically localized in brain capillaries but mainly stained in the cytoplasm. Cldn12 overlapped with Zo1 in the mouse cortex but also showed randomly distributed signal in the brain capillary surrounding tissue. Cldn3, -20 and -25 antibodies used to stain cryosections of the human cortex were not specific to mouse tissue. Taken together, the subcellular localization of all analyzed TJ proteins in the brain endothelium was comparable in human and mouse.

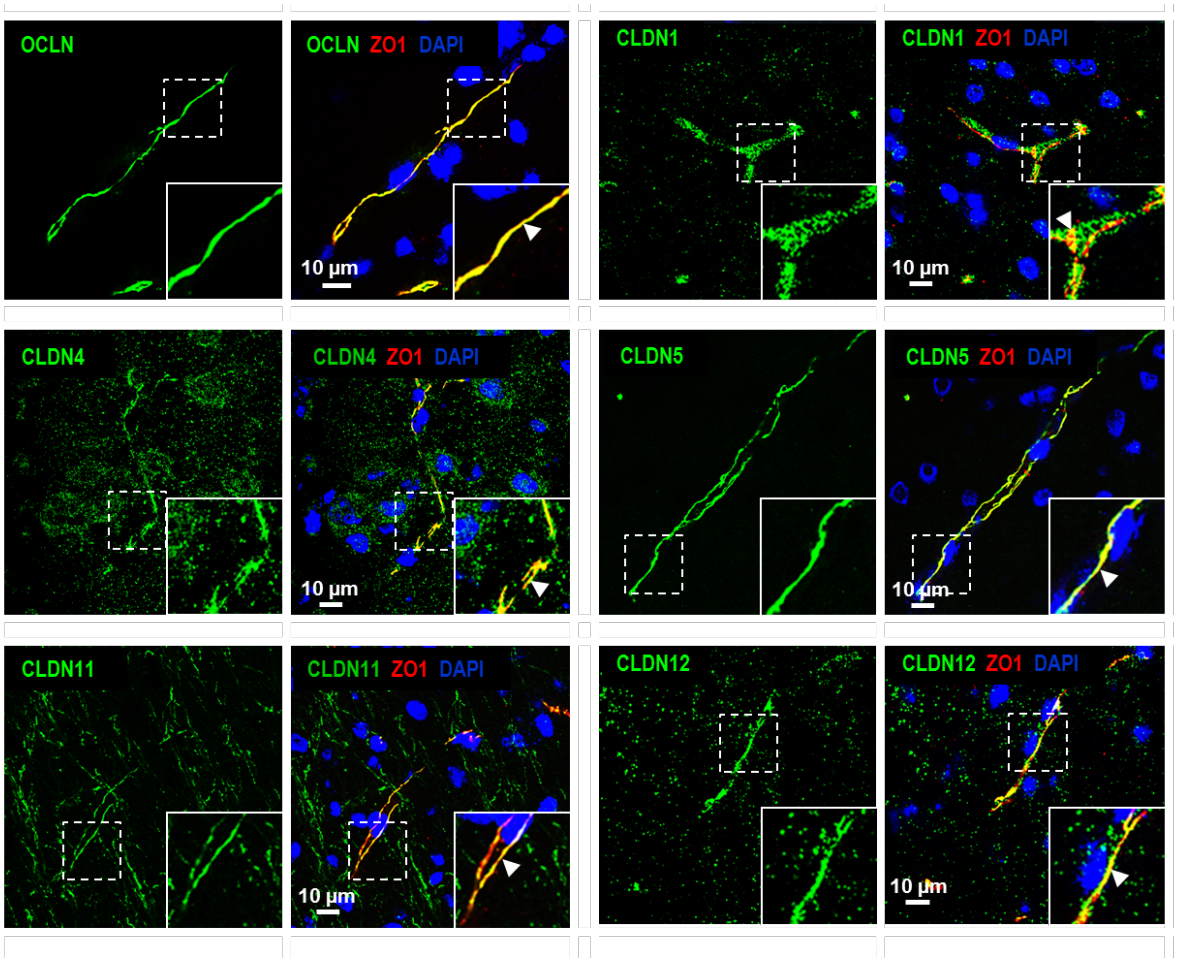


**Figure 18 Claudin (Cldn)-4, -5, -11, -12 and occludin (Ocln) colocalize in the tight junction area of mouse brain capillaries.** Immunofluorescence stainings of mouse brain sections for TJ proteins (green). *Zonula occludens* protein 1 (Zo1) (red), localized in the TJ area. Arrows point to an overlap of TJ proteins with Zo1 (yellow). The nuclei were stained by DAPI (blue). Cldn1 localized mainly in the cytoplasm of brain capillaries.

### 4.2.3 Claudin-11 expression in tight junctions of brain capillaries compared to that of oligodendrocytes

Cldn11 was previously described to be exclusively expressed in oligodendrocytes (Morita et al., 1999b). Contrastingly, mRNA expression was detected in pure brain endothelial cells (primary brain capillary endothelial cells and bEND.3, Figure 11). Additionally, Cldn11 colocalized with Zo1 at the TJ area of human and mouse brain capillaries (Figure 17, 18). As seen in Figure 19, Cldn11 partly overlapped with Cldn5 but also localized separately along the TJ strand. Outside the brain capillaries, Cldn11 was stained in oligodendrocytes wrapping around neuronal processes. Knowing these specific sources of expression, it was of interest if mRNA levels in laser-dissected brain capillaries represent the capillary fraction despite overlapping with oligodendrocytes. After laser capture microdissection mRNA expression levels in tissue stained by RCA1 (brain capillary marker) were compared to those in the surrounding tissue. An enrichment of 1.61 ± 0.88 in capillaries was determined. In human, cortex tissue sections proofed Cldn11 predominantly in blood vessels (Figure 17). Therefore, substantial contamination of oligodendrocytic Cldn11 can be excluded.

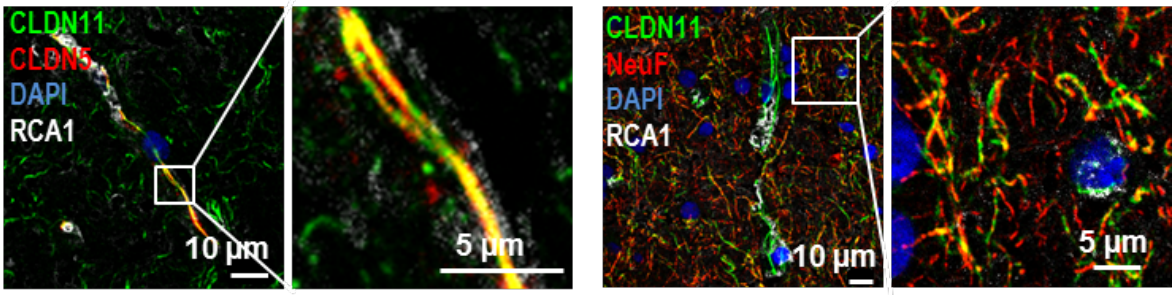


**Figure 19 In immunofluorescence stainings of brain sections, Cldn11 localized in the tight junction (TJ) area of human brain capillaries (marker: RCA1) as well as in oligodendrocytes wrapping around neuronal processes (marker: neurofilament, NeuF).** Cldn11 localized with the TJ marker Cldn5 in brain capillaries.

## 4.3 Barrier properties of Claudin-5 and -25 analyzed in knockdown experiments of bEND.3 cells

Cldn25 was the highest expressed TJ protein in the human brain endothelium (Chapter 4.1.1). Despite recent classification as Cldn (Mineta et al., 2011) it is yet unknown if Cldn25 contributes to the formation of a paracellular barrier, like Cldn5

(Nitta et al., 2003). bEND.3 cells are evaluated as useful model to study BBB function (Watanabe et al., 2013). Additionally, these cells expressed *Cldn5* at mRNA levels comparable to *ex vivo* condition and *Cldn25* in the order of magnitude of the TJ marker *Ocln* (Table S 1). Therefore, this cell line was chosen to study alterations of the paracellular barrier upon silencing of *Cldn5* or *-25*. Short hairpin RNA (shRNA) against mouse *Cldn5* or *-25* as well as a non-mammalian target as control were introduced into bEND.3 cells via lentiviral transduction.

### 4.3.1 Transcriptional regulation of claudins through claudin-5 but not -25

After transduction of shRNA into bEND.3 cells, the knockdown efficiencies were determined by qRT-PCR. For *Cldn25* a knockdown efficiency of 77% and for *Cldn5* of 67% were found. The introduction of control shRNA did not significantly change the mRNA expression of the tested proteins (Figure 20). Remarkably, mRNA expression of other tight junction proteins was altered upon knockdown of *Cldn5,* which was not found upon loss of *Cldn25*. *Cldn1* was 17-fold increased and *Cldn15* 7-fold decreased.

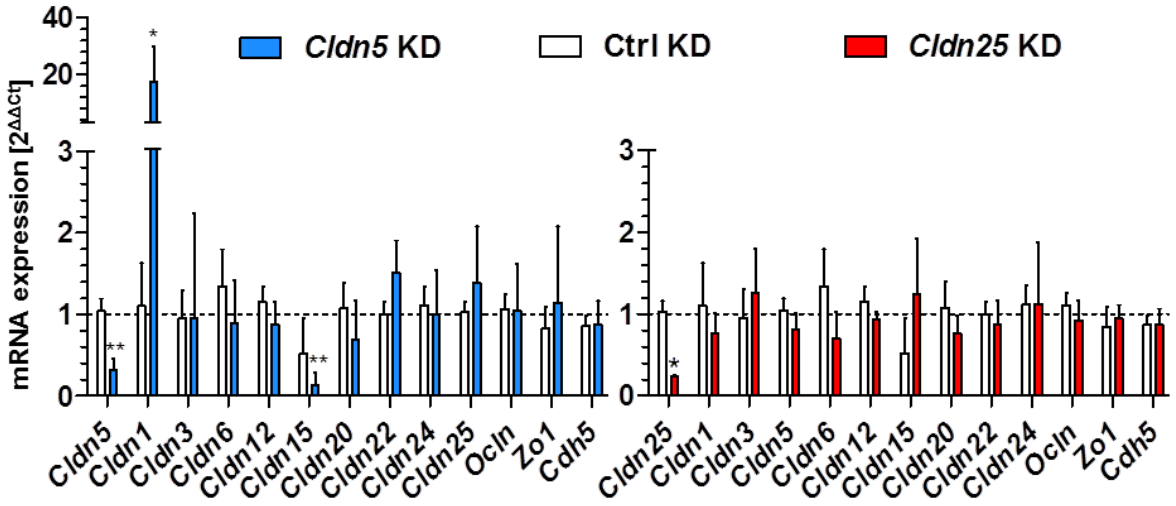


**Figure 20 Alteration of mRNA expression of TJ proteins occurs after knockdown (KD) of Claudin (*Cldn*)-5 but not -25.** mRNA expression in bEND.3 cells after *Cldn5* KD (blue bars) or *Cldn25* KD (red bars) and control (Ctrl) shRNA (white bar). The expression levels were normalized to wild type (wt) cells (dashed line). $\Delta\Delta Ct = (Ct_{target} - Ct_{Actb})_{KD} - (Ct_{target} - Ct_{Actb})_{wt}$, (Ct, cycle threshold). Statistical analyses: Kruskal–Wallis test. Mean ± SD; n ≥ 4; *, $p < 0.05$; **, $p < 0.01$.

Furthermore, bEND.3 cells with different knockdown efficiencies of *Cldn5* were investigated. The degree of Cldn1 up-regulation as well as down-regulation of *Cldn15* was linked to the *Cldn5* expression (Figure 21). Reduced knockdown efficiencies of 43% and 22% increased *Cldn1* around 4- and 2-fold and decreased *Cldn15* around 4- and 2-fold respectively on mRNA level.

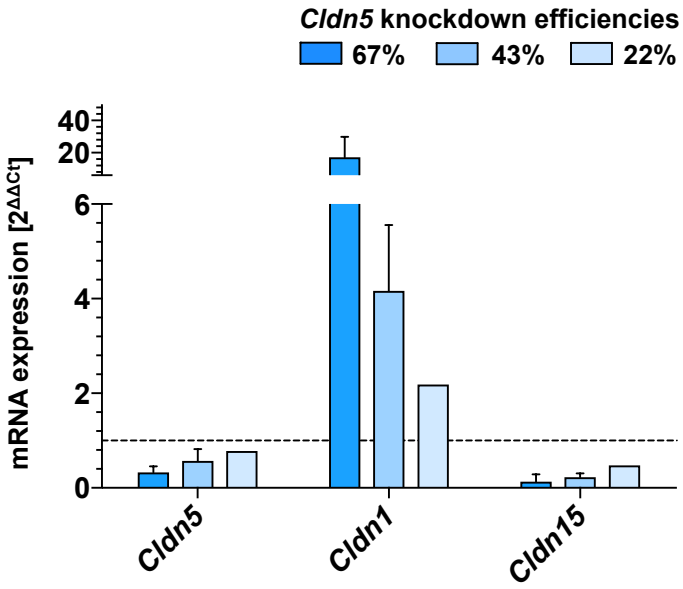


**Figure 21 Altered mRNA level of claudin *(Cldn)-1* and *-15* depend on the expression of *Cldn5*.** mRNA expression in bEND.3 cells upon *Cldn5* knockdown (KD). mRNA normalized to β-actin (*Actb*), ($\Delta Ct = Ct_{target} - Ct_{Actb}$), (Ct, cycle threshold). The expression levels were normalized to wild type (wt) cells (dashed line), ($\Delta\Delta Ct = \Delta Ct_{KD} - \Delta Ct_{wt}$). Mean ± SD; $n_{67\%} = 4$; $n_{43\%} = 3$; $n_{22\%} = 2$.

### 4.3.2 Transcriptional regulation through claudin-5 results in increased claudin-1 and reduced claudin-15 protein

Western blotting was performed to investigate if effects on mRNA expression (Figure 20) upon lentiviral transduction of shRNA were translated to the encoded protein. Transduction of shRNA against *Cldn5* reduced the Cldn5 protein level compared to untransduced or with shRNA against a non-mammalian target transduced cells (Figure 22). A drastic increase was found for the protein band of Cldn1 and a decrease for Cldn15. The same expression pattern was found in the Triton X-100 insoluble (membrane) fraction as well as the soluble (non-membrane) fraction.

As previously described in chapter 4.1.4, Cldn1 was mainly found as hexamer in the insoluble (membrane) fraction. Also Cldn25 was found to be heavily decreased in protein expression after transduction with shRNA against *Cldn25*. Cldn25 was only detected in the Triton X-100 insoluble (membrane) fraction as reported in chapter 4.1.4. This data verifies the knockdown on protein level and in chapter 4.3.1 described effects on the expression of other Cldns.

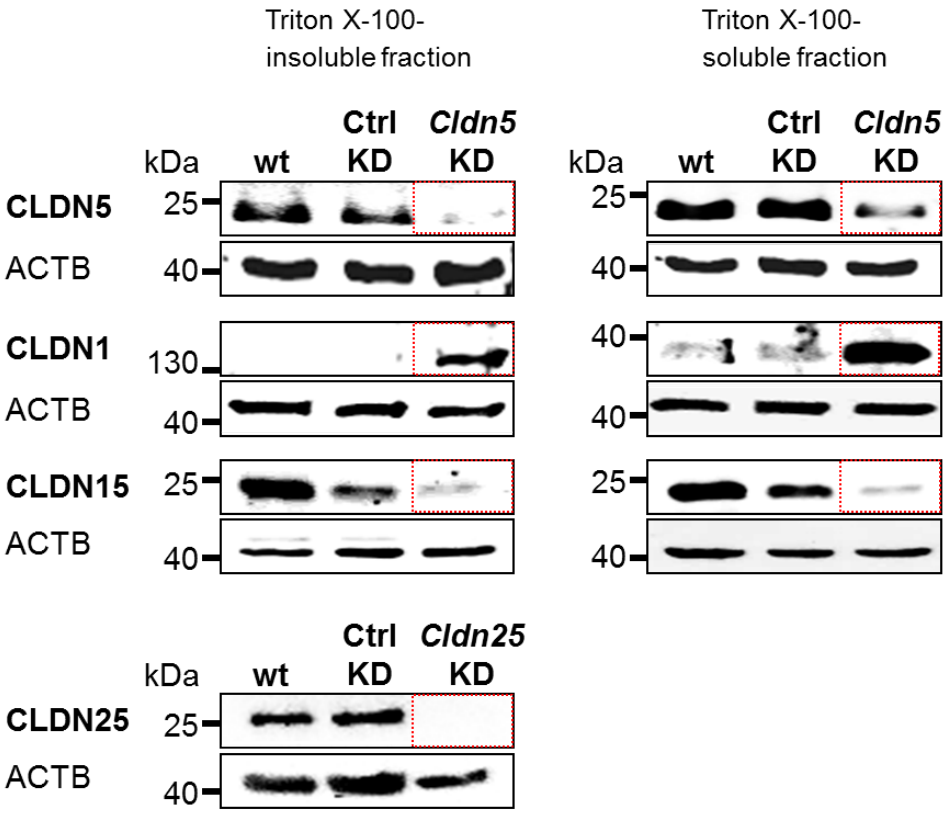


**Figure 22 Western blot of bEND.3 (mouse brain endothelial cell line) cells wt, Ctrl and either *Cldn25* or *Cldn5* KD.** Antibodies for Cldn1, -5, -15 and -25 were used as well as β-Actin (ACTB) as loading control.

### 4.3.3 Extended distribution of claudin-1 within the cytoplasm upon claudin-5 knockdown

To understand if the up-regulation of Cldn1 in bEND.3 cells upon *Cldn5* knockdown can functionally compensate a loss of Cldn5, the localization in TJs was analyzed. As described in chapter 4.2, Cldn1 was visible mainly in the cytoplasm of human and mouse brain capillaries.

Also in bEND.3 cells Cldn1 localized mainly in the cytoplasm enriched around the nucleus and barely in TJs marked by Ocln (Figure 23, wt and Ctrl KD). Upon *Cldn5* knockdown, a slight decrease in signal intensity as well as an increased number of gaps along the Cldn5 stained cell-cell contacts were found. The *Cldn5* knockdown showed a more extended distribution of Cldn1 within the cytoplasm and no enrichment at the nucleus. Taken together, a functional compensation of the loss of Cldn5 by Cldn1 can be excluded.

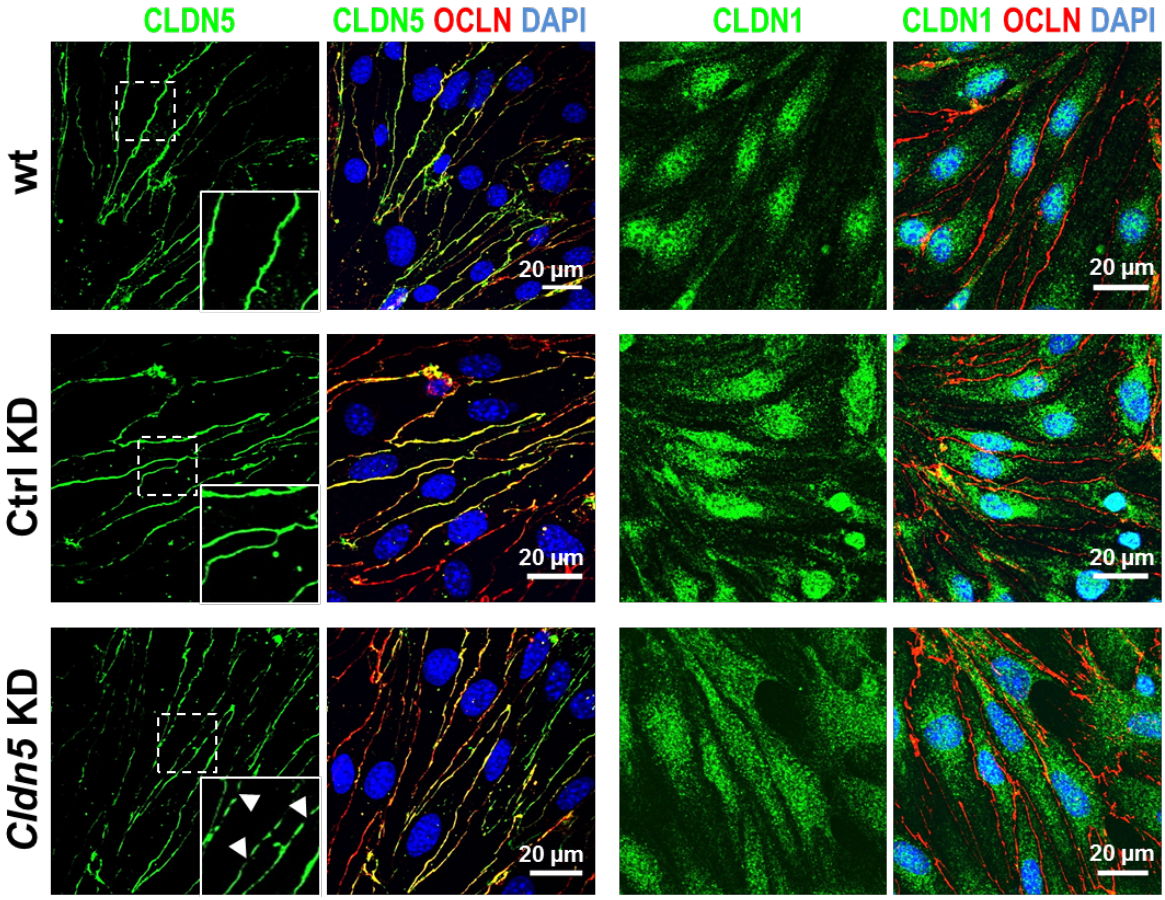


**Figure 23 Increased number of gaps along the claudin (Cldn)-5 stained cell-cell contacts and more extended distribution of Cldn1 within the cytoplasm upon *Cldn5* knockdown (KD).** Immunocytochemical staining of bEND.3 cells against occludin (Ocln) used as tight junction marker and Cldn1 or Cldn5. Nuclei stained by DAPI. Subcellular localization of Cldns was compared between wild type (wt), control (Ctrl) transduced and *Cldn5* KD. White arrows point to gaps along the Cldn5 stained cell-cell contacts.

### 4.3.4 Altered tight junction strand morphology upon knockdown of claudin-5 and -25

To analyze TJ strand morphology upon knockdown of *Cldn5* or *-25,* freeze fracture electron microscopy was performed in collaboration with Prof. Dr. Hartwig Wolburg (University of Tübingen, Germany). This technique allows examination of lipid membranes and the incorporated proteins. Cldn5 based TJs strands are characterized by chains of particles associated to the extracellular fracture-face (EF) (Morita et al., 1999c; Piontek et al., 2008). The control knockdown exhibited TJ strands on the EF, characteristic for Cldn5 (Figure 24). But also on the protoplasmatic fracture-face (PF) chains of particles were present, most likely formed by other TJ proteins than Cldn5. Upon knockdown of *Cldn5* the count of strands was dramatically reduced and thereby the size of meshes increased. Also the proper orientation of strands was disturbed. The particles, arranged as discontinuous chains on the EF as well as PF, were still existent. The *Cldn25* knockdown did not exhibit altered strand morphology on the EF but on the PF. The PF was characterized by particles randomly distributed. Also more unstructured strands and a reduced mesh number were found. This data suggests a contribution of Cldn25 to the TJ strand arrangement on the PF.

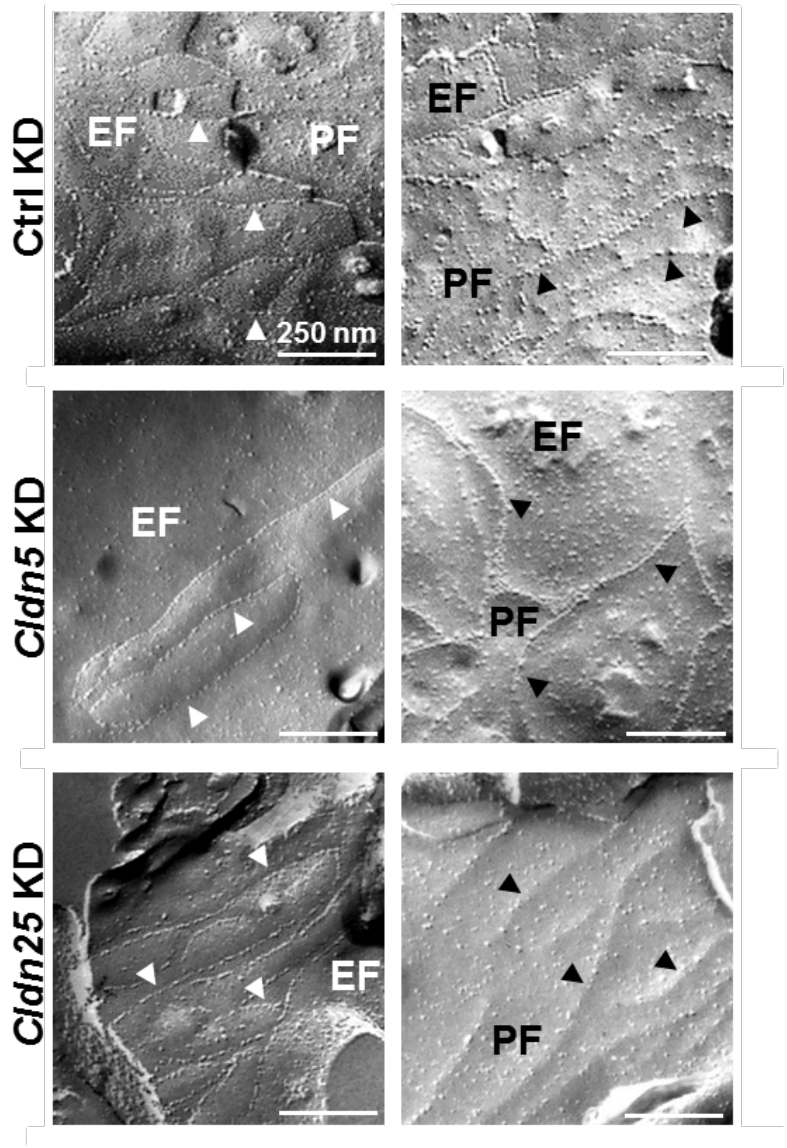


**Figure 24 Freeze fracture microscopy.** *Cldn5* KD weakened the TJ strand network on the extracellular fracture-face (EF) and protoplasmatic fracture-face (PF) in bEND.3, i.e. enlarged and more round-shaped meshes. *Cldn25* KD led to more unstructured strands and a reduced mesh number as well as more randomly distributed particles on the PF.

### 4.3.5 Transendothelial electrical resistance is reduced upon knockdown of claudin-5 but not -25

The knockout of *Cldn5* is known to increase paracellular permeability of the mouse BBB for molecules up to 800 Da (Nitta et al., 2003). The impact of the loss of Cldn25 on the paracellular barrier is yet unknown. The transendothelial electrical resistance (TEER) was monitored via ECIS (Chapter 3.4.6) to investigate paracellular ion flux. The *Cldn5* knockdown led to a reduction of 29% in TEER, 48 h after seeding (Figure 25). The time point was chosen since TJ development

was fully completed. The significant decrease was stable till termination of the experiment. On the contrary, no significant change in TEER was detected upon *Cldn25* knockdown.

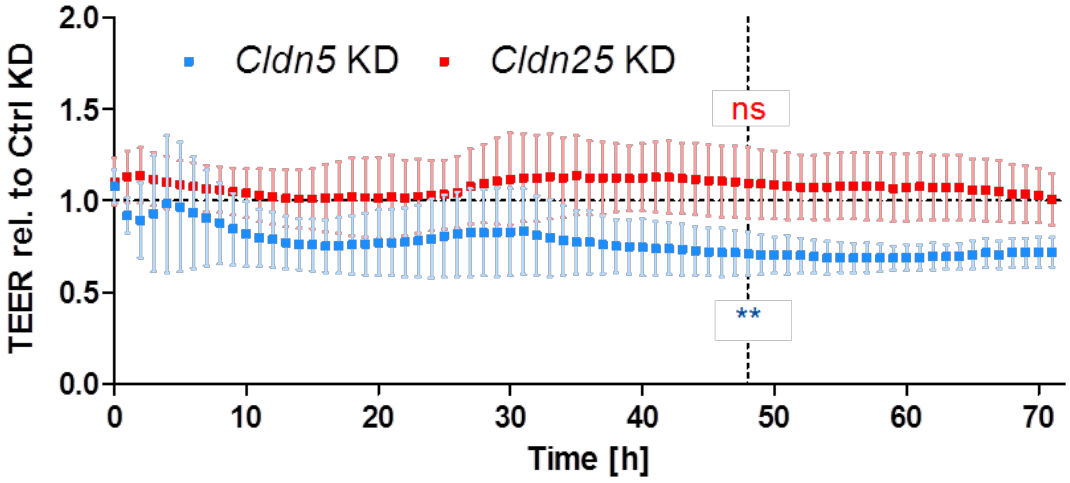


**Figure 25 Transendothelial electrical resistance (TEER) of bEND.3 cells is reduced upon knockdown (KD) of claudin (*Cldn*)-5 but not -25.** The values are normalized to the control KD (Ctrl KD; dashed horizontal line). Statistical analyses 48 h after seeding (dashed vertical line); Kruskal–Wallis test. Mean ± SD; n ≥ 8; **, $p < 0.01$.

## 4.4 Characterization of the extracellular loops of claudin-25

The paracellular sealing function of Cldns is realized through interaction of their extracellular loops. Cldn enrichment in cell-cell contacts can be used as a measure for interaction between Cldns of neighboring cells (Piontek et al., 2008). Cldn25 did not enrich at cell-cell contacts when transfected into HEK-293 cells as seen in Figure 29. Also the knockdown did not alter the TEER in bEND.3 cells (Figure 25). The first extracellular loop of Cldn25 (115 amino acids) differs greatly in size compared to those of all other Cldns (e.g. Cldn5, 53 amino acids). Additionally, association of glycans at two amino acid residues was found (Wollscheid et al., 2009) that might sterically hinders loop association. It remains still unclear if these structural properties of Cldn25 prohibit barrier formation and if the presence of post-translational modifications varies with respect to tissue or pathology.

### 4.4.1 Homo- and heteromeric association of the extracellular loops

The second extracellular loop of Cldn5 is described to be crucial for barrier formation (Krause et al., 2009). The short loop with 16 amino acids exhibits residues required for *trans*-interaction that are conserved among the classic Cldns. The extracellular loops of Cldn25 do not share a high sequence homology with those of classic Cldns (Figure 26). Substitution of aromatic amino acids (F147, Y148, and Y158) in the second extracellular loop of Cldn5 leads to disturbed *trans*-interaction (Krause et al., 2009).

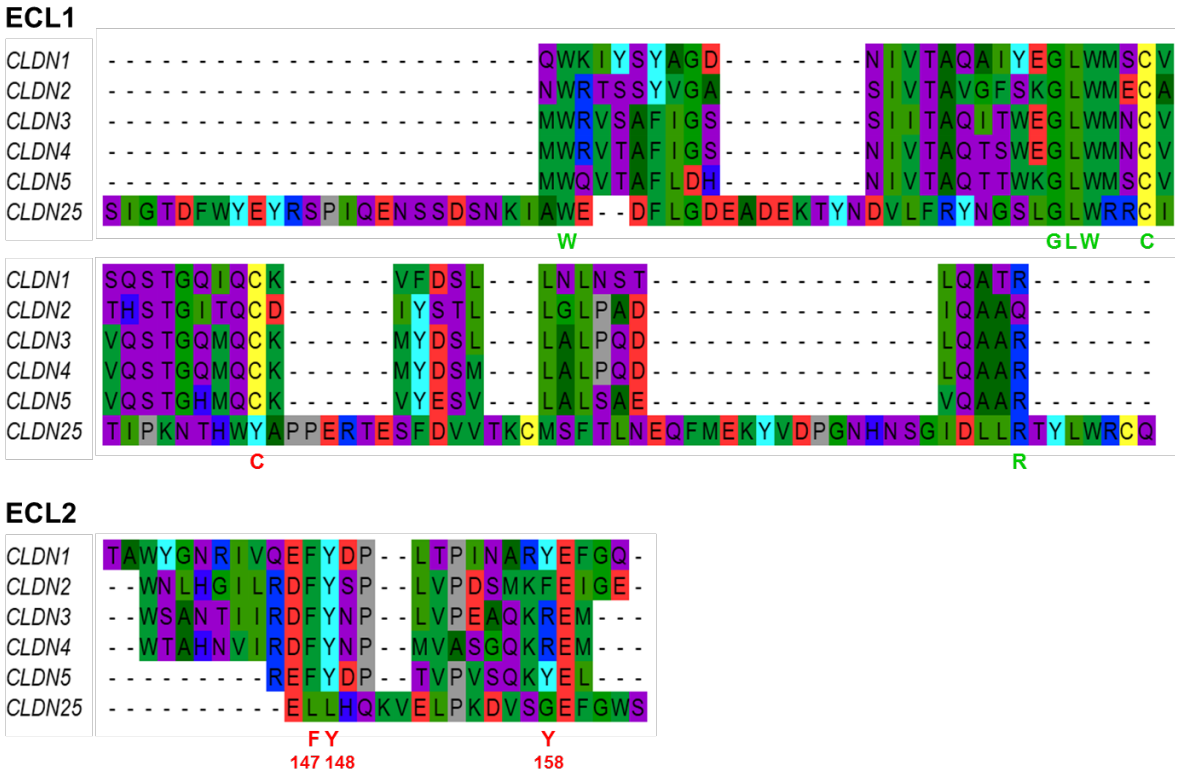


**Figure 26 Low sequence homology of the first and second extracellular loops (ECLs) of claudin (Cldn)-25 with those of classic Cldns.** (Clustal Omega) Green: hydrophobic, blue: basic, magenta: acidic, violet: hydrophilic residues, yellow: cysteine, cyan: tyrosine, black: proline. Residues in green indicate conservation among Cldns including Cldn25 in contrast to those highlighted in red. Those residues (F147, Y148, and Y158) in the ECL2 are reported to be crucial for *trans*-interaction (Krause et al., 2009). The alignment is based on sequences taken from UniProtKB/ Swiss-Prot, calculated by ClustalW2 (http://www.ebi.ac.uk/Tools/clustalw2/index.html) and edited with Jalview (http://www.jalview.org).

Binding affinities of the extracellular loops of Cldn25 were analyzed to investigate if loop association can occur despite lack of sequence homology with classic Cldns. MBP tagged Cldn loops were purified and labeled (Chapter 3.5.2 and 3.6.1.1). A dilution series of the unlabeled loop was titrated against the labeled Cldn loop. The thermophoretic motion behavior was monitored via microscale thermophoresis. The dissociation constants ($K_d$) were determined for homo- and heteromers of the Cldn25 loops and compared with that of the homomer of the second loop of Cldn5. As shown in Figure 27, the homomeric binding affinity of the second loop of Cldn5 was the strongest with a $K_d$ of 9.1 nM. The homomeric affinity of the second loop of Cldn25 was with a $K_d$ of 1504 nM significantly lower. A $K_d$ of 332.1 nM was calculated for the homomer of the first loop of Cldn25. The association of the first and second loop was characterized by a $K_d$ of 1579 nM. Taken together, a lack of *trans*-interaction due to relatively low binding affinities of the Cldn25 loops can be assumed.

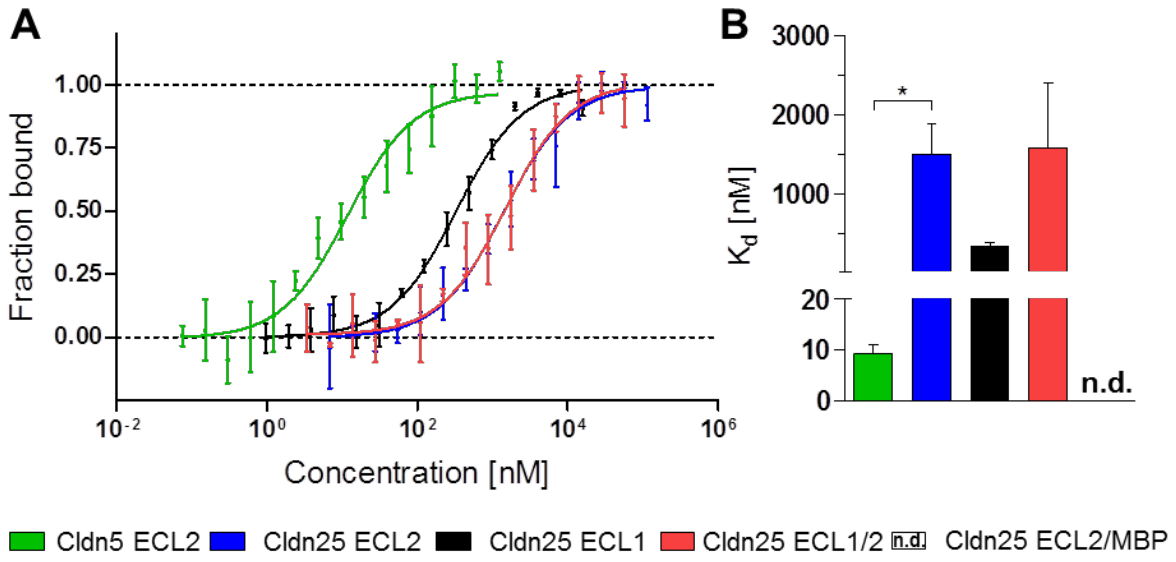


**Figure 27 Homomer and heteromer of the extracellular loops (ECLs) of claudin (Cldn)-25 have a higher dissociation constant than the homomer of the ECL2 of Cldn5.** Dissociation constants ($K_d$) were determined by microscale thermophoresis. Mean ± SD; n ≥ 3; *, p < 0.05 (A) The ordinate represents the fraction bound (1 = bound/ 0 = unbound). $K_d$: Cldn5 ECL2, 9.1 ± 1.8 nM; Cldn25 ECL1, 332.1 ± 56.1 nM; Cldn25 ECL2, 1504.0 ± 377.7 nM; Cldn25 ECL1/ ECL2, 1579.0 ± 823.7 nM. n.d., not detected. (B) $K_d$ increase indicates lower binding affinity. Homomeric association of the ECL2 of Cldn5 between two neighboring cells is known to support homophilic *trans*-interaction (Krause et al., 2009). The ECL1 and -2 of Cldn25 bound homo- as well as heteromeric with a higher dissociation constant. MBP alone did not associate with the ECL.

### 4.4.2 Glycosylation of the first extracellular loop of claudin-25

Post-translational modifications are crucial for proper Cldn function including oligomerization, trafficking, interaction with binding partners, subcellular localization or Cldn homeostasis (Liu et al., 2016). Yet experimental evidence for Cldn glycosylation is limited. The first extracellular loop of Cldn25 is found to be glycosylated at the asparagine at position 42 as well as 72 in human T lymphocytes (Wollscheid et al., 2009). As seen in Figure S 6, only these two positions exhibit the consensus tripeptide crucial for *N*-glycosylation consisting of an asparagine followed by any amino acid except proline and serine or threonine (Kaplan et al., 1987; Marshall, 1972). No *O*-glycosylation sites were predicted using the NetOGlyc 4.0 Server (Center for biological sequence analyses, Technical University of Denmark).

#### 4.4.2.1 Verification of the glycosylation sites of claudin-25 in HEK-293 cells

In western blots of purified brain capillaries a double band was found for Cldn25 (Figure 15). This result suggested that Cldn25 glycosylation occurred also *in vivo* in the brain endothelium. To understand the functional importance of glycosylation occurring at the stated positions, mutants of YFP tagged Cldn25 were generated. Via site directed mutagenesis asparagine was substituted by glutamine with similar chemical and physical properties. The YFP tagged Cldn25 lacking either one or both of the glycosylation sites were transfected into HEK-293 cells. After western blotting, the wild type Cldn25 exhibited a double band whereas the upper band, the glycosylated fraction, was more prominent. A mutation of either position 42 or 72 led to a shift of the prominent band to a lower molecular weight pointing to the existence of glycosylation events at both residues. The double mutant showed only the fraction with lower molecular weight (Figure 28). To specifically stain glycans, the YFP tagged proteins were enriched and purified as described in chapter 3.5.3. A positive glycoprotein staining for the wild type as well as both single mutants was detected whereby the staining of the N72Q mutant was less pronounced. No staining was detected for the double mutant (Figure 28). The coomassie gel showed quantitative differences of the proteins presumably due to impaired purification of the unglycosylated Cldn25 (Figure 28). These results proofed that *N*-glycosylation at both positions of Cldn25 also occurred in HEK-293

cells. Thereby, this cell line was chosen as model to investigate the impact of *N*-glycosylation on subcellular localization of Cldn25.

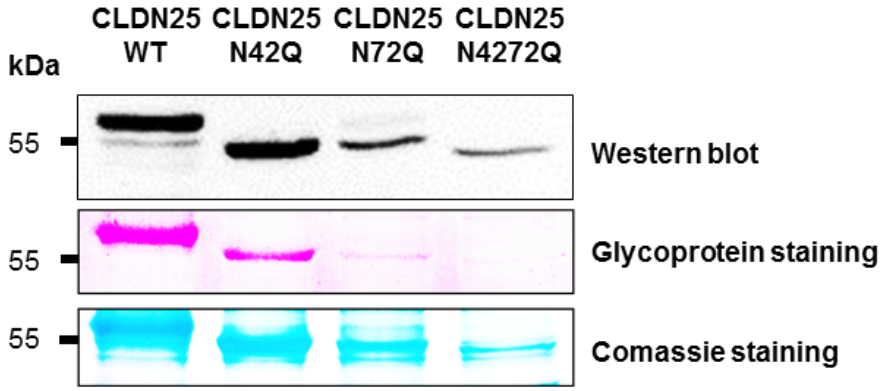


**Figure 28 The first extracellular loop (ECL1) of claudin (Cldn)-25 is glycosylated at position 42 and 72 in HEK-293 cells.** YFP-Cldn25 wt, asparagine to glutamine mutation in position 42 (N42Q), N72Q and N4272Q were purified from transiently monotransfected HEK-293 cells. Western blotting against yellow fluorescent protein (YFP). Staining of glycosylated proteins in polyacrylamide gels (PAGE) using the periodic acid-Schiff method. Coomassie staining of PAGE as loading control.

#### 4.4.2.2 Claudin-25 does not localize in the plasma membrane after deletion of the N-linked glycosylation site in position 72

Cldn25 is glycosylated at position 42 as well as 72. The subcellular localization of the mutants lacking either one or both glycosylation sites was analyzed to investigate the biological impact of glycans at these positions. Life cell imaging of HEK-293 cells monotransfected with YFP tagged Cldn25 wild type and mutants lacking the glycosylation sites was performed. Both wild type and the N42Q mutant were enriched at the plasma membrane stained with trypan blue. The N72Q as well as the N4272Q mutant localized exclusively in the cytoplasm and did not overlap with trypan blue at the plasma membrane (Figure 29). The asparagine at position 42 is glycosylated as described in chapter 4.4.2.1 but was not crucial for localization at the plasma membrane. The deletion of the glycosylation site at position 72 alone led to exclusion of Cldn25 from the plasma membrane.

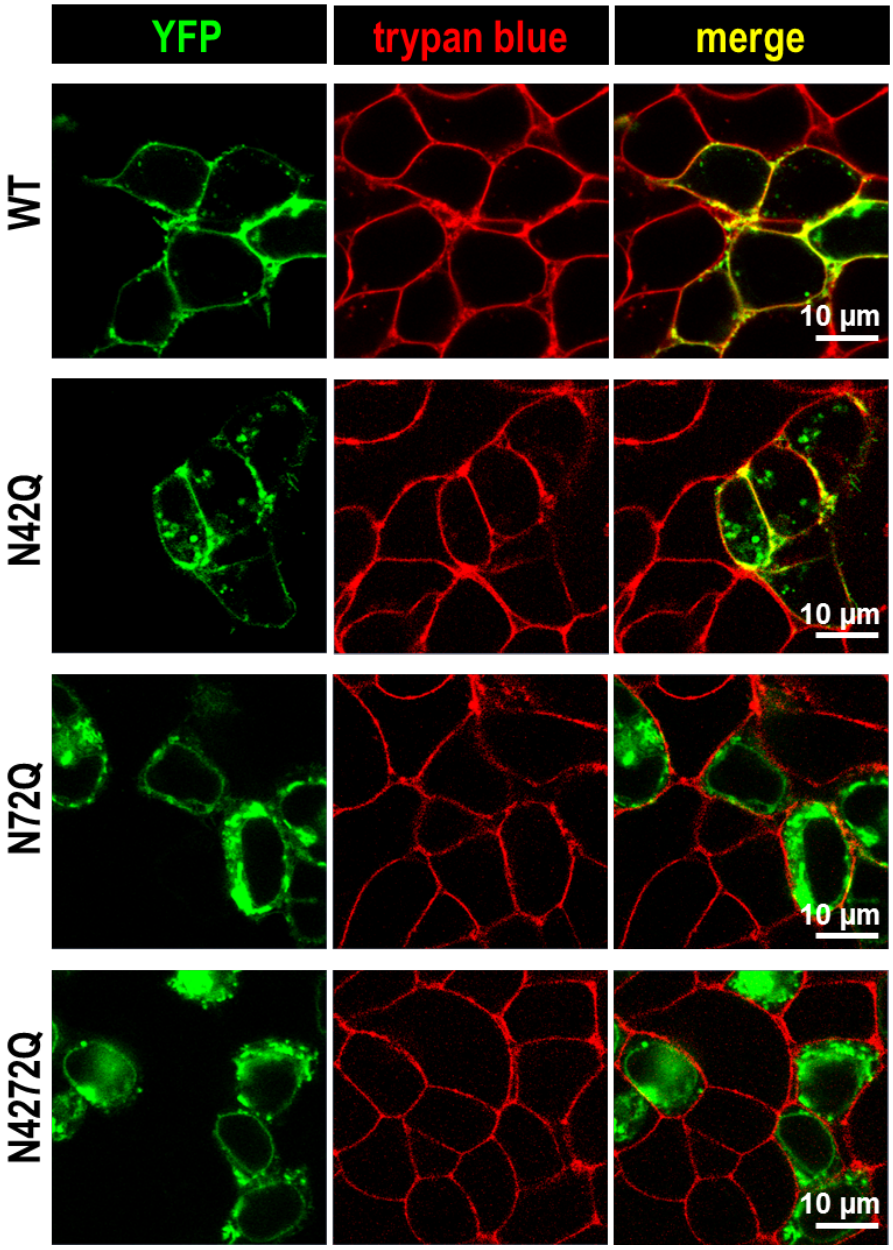


**Figure 29 Claudin (Cldn)-25 does not localize in the plasma membrane after deletion of the N-linked glycosylation site in position 72.** Live-cell images of HEK-293 cells transiently monotransfected with YFP-Cldn25 wt, asparagine to glutamine mutation in position 42 (N42Q), N72Q or N4272Q (green). The plasma membrane was stained by trypan blue (red).

### 4.4.2.3 N-Glycosidase F activity leads to internalization of Claudin-25 through cleavage of asparagine bound *N*-glycans in position 72.

Glycosylation is a regulated process (Stowell et al., 2015). The exclusion of Cldn25 from the plasma membrane led to the impairment of the Cldn25 function as transmembrane protein. The question rose if glycosidase activity results in the

same phenotype as shown in Figure 29. N-Glycosidase F was used to specifically cleave N-linked glycans from glycoproteins. HEK-293 cells were monotransfected with YFP tagged Cldn25 wild type or N42Q mutant. After 24 h of treatment with N-Glycosidase F, the localization of the YFP tagged Cldn25 was examined by use of life cell imaging. Both wild type as well as the N42Q mutant exhibited reduced localization at the plasma membrane after treatment with N-Glycosidase F (Figure 30).

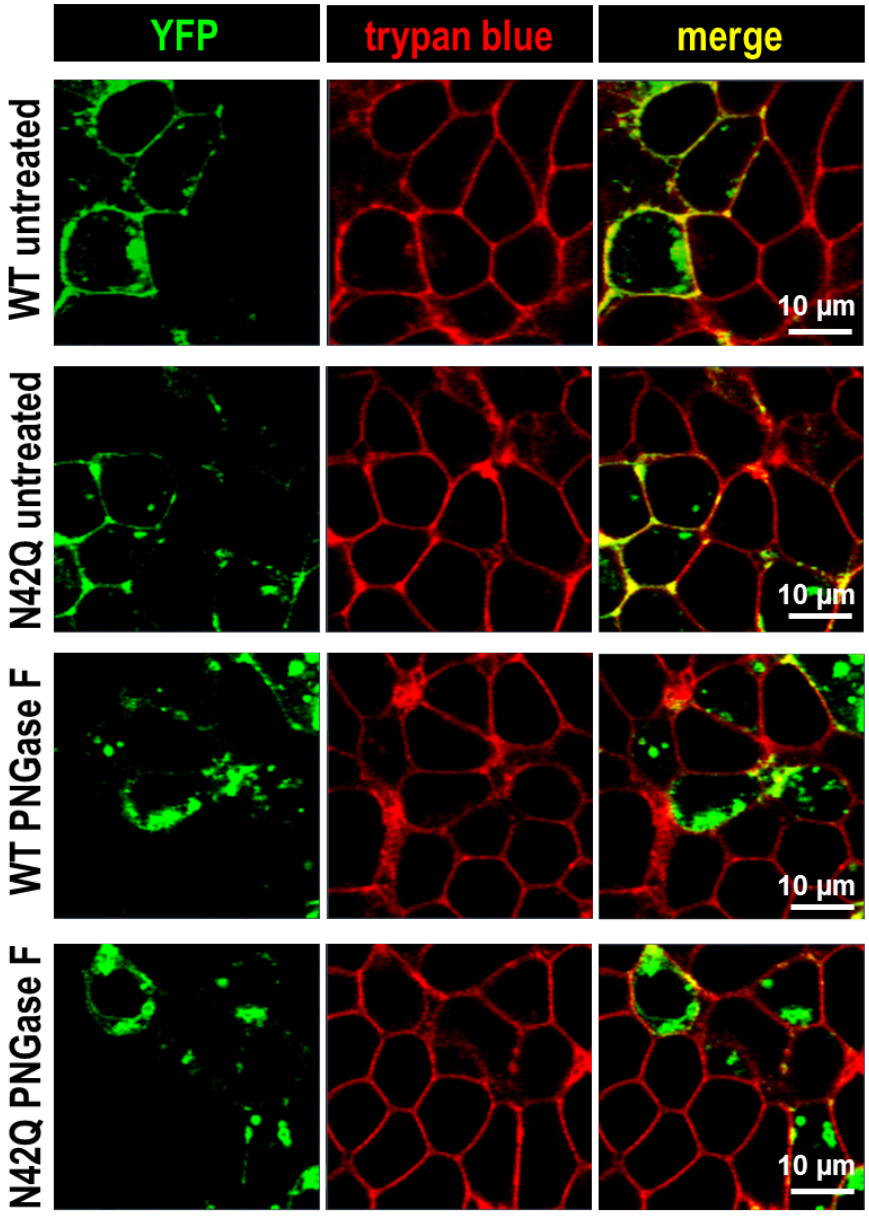


**Figure 30 N-Glycosidase F (PNGase F) activity leads to internalization of claudin (Cldn)-25 through cleavage of asparagine bound N-glycans in position 72.** Live-cell image of HEK-293 cells transiently mono-transfected with YFP-Cldn25 wt or asparagine to

glutamine mutation in position 42 (N42Q) untreated or treated with PNGase F for 24 h. The plasma membrane was stained by trypan blue (red).

The localization at the plasma membrane was reduced after N-Glycosidase F treatment. Both WT and N42Q mutant exhibited a weighted colocalization coefficient of 0.75, which decreased significantly to 0.37 (wild type) or 0.34 (N42Q) (Figure 31).

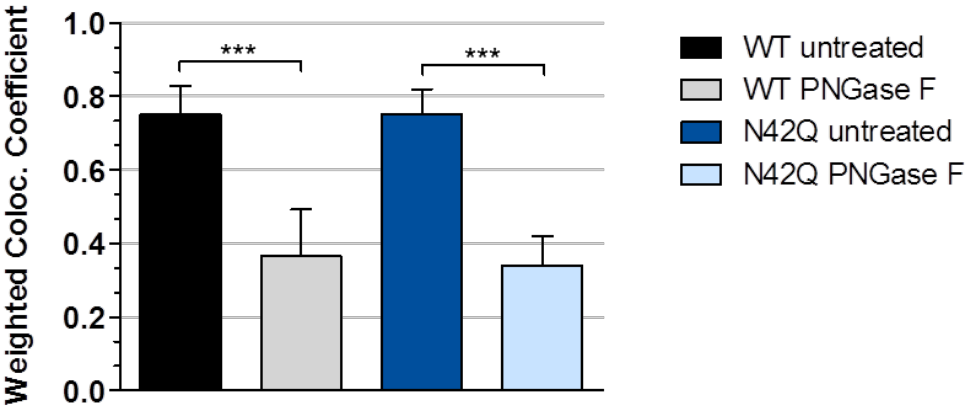


**Figure 31 Weighted colocalization coefficient of claudin (Cldn)-25 and the plasma membrane is significantly reduced after treatment with N-Glycosidase F (PNGase F).** In order to quantify membrane association of YFP-Cldn25 wt or asparagine to glutamine mutation in position 42 (N42Q), the colocalization coefficient was determined which compares the YFP to the trypan blue signal. Kruskal-Wallis test, mean ± SD; n ≥ 16; *** $p < 0.001$.

### 4.5 Binding of claudin-25 to *zonula occludens* protein 1

Zo1 associates with the TJ complex via interaction of its PDZ1 domain with the COOH terminus of Cldns (Itoh et al., 1999). So far it is still under discussion if Zo1 is crucial for the recruitment of Cldns to TJs (Itoh et al., 1999; Kausalya et al., 2006; Muller et al., 2003; Ruffer and Gerke, 2004; Umeda et al., 2006). Binding of Cldn25 to PDZ1 of Zo1 is theoretically excluded due to absence of the conserved PDZ-binding motif (Gunzel and Yu, 2013). Zo1-PDZ1 binding sequences contain valine, isoleucine or leucine at position$^{0}$; tryptophan or tyrosine at position$^{-1}$; threonine or serine at position$^{-2}$ and arginine, lysine, serine or threonine at position$^{-3}$. Strong preferences for hydrophobic residues at position$^{-4}$ and aromatic residues at position$^{-6}$ but no clear preferences at position$^{-5}$ are reported (Zhang et al., 2006). Despite disagreement with the Zo1-PDZ1 sequence preferences shown

in Table 27, Cldn25 co-localizes with Zo1 after transfection into epithelial cells (Mineta et al., 2011) as well as endogenously in brain capillaries (Figure 17). The insertion of arginine at position$^{-1}$ results in a shift of tyrosine from position$^{-1}$ to $^{-2}$ as well as lysine from position$^{-3}$ to $^{-4}$ compared to the binding motif. Also alanine at position$^{+1}$ is atypical but its physical properties might not hinder a binding to PDZ1 (Table 27).

To quantify binding affinities, microscale thermophoresis was applied. Changes in the thermophoretic motion behavior of purified MBP tagged Zo1-PDZ1 were monitored depending on the concentration of the MBP tagged Cldn-COOH-terminus.

### 4.5.1 The binding affinity of claudin-25 to PDZ1 of *zonula occludens* protein 1 is comparable to claudins with higher agreement to the binding motif

Additionally to Cldn25, the Zo1-PDZ1 binding was quantified for Cldns varying in their COOH-terminal sequences. The highest agreement with the Zo1-PDZ1 sequence preference exhibits Cldn5 (at position$^{0/\ -1/\ -3/\ -4/\ -6}$), followed by Cldn4 (at position$^{0/\ -1/\ -3/\ -6}$), Cldn1 (at position$^{0/\ -1/\ -3}$) and Cldn25 (at position$^{0}$). Compared to mouse (Table 27), the human Cldn1 sequence exhibits alanine instead of threonine at position$^{-8}$. The human Cldn4 sequence is characterized by alanine at position$^{-5}$ and $^{-6}$. The COOH-terminal sequences for Cldn5 and -25 shown in Table 27 are conserved between human and mouse. Contrary to Cldn4, -5 and -25, Cldn1 was mainly stained in the cytoplasm of human (Figure 17) or mouse (Figure 18) brain capillaries as well as bEND.3 cells (Figure 23). Competitive Cldn association with Zo1 followed by recruitment to the TJs might explain this observation.

**Table 27 COOH terminal mouse (m) claudin (Cldn) sequences exhibit different agreement with the Zo1-PDZ1 binding motif.** The Zo1-PDZ1 binding motif ([Φ]$^{-6}$ [X]$^{-5}$ [Φ]$^{-4}$ [R/K/S/T]$^{-3}$ [T/S]$^{-2}$ [W/Y]$^{-1}$ [V/I/L]$^{0}$ -COOH) consists of six of the last seven amino acids (Φ=aromatic/aliphatic (F, Y, W, L, I, V, K, R). Lysine and arginine are included because of the aliphatic portions of their side chains) (Zhang et al., 2006). Stars indicate an agreement with the binding motif. Cldn1, -4 and -5 share an agreement with the PDZ binding motif at postion$^{0,\ -1}$ and $^{-3}$ and are conserved in position$^{0}$ and $^{-1}$. On the contrary Cldn25 exhibits only the valine at postion$^{0}$. Arginine at position$^{-1}$ resulting in a shift of

tyrosine from position$^{-1}$ to $^{-2}$ as well as alanine at position$^{+1}$ do not agree with the binding motif. The colors indicate the chemical and physical properties of the amino acids.

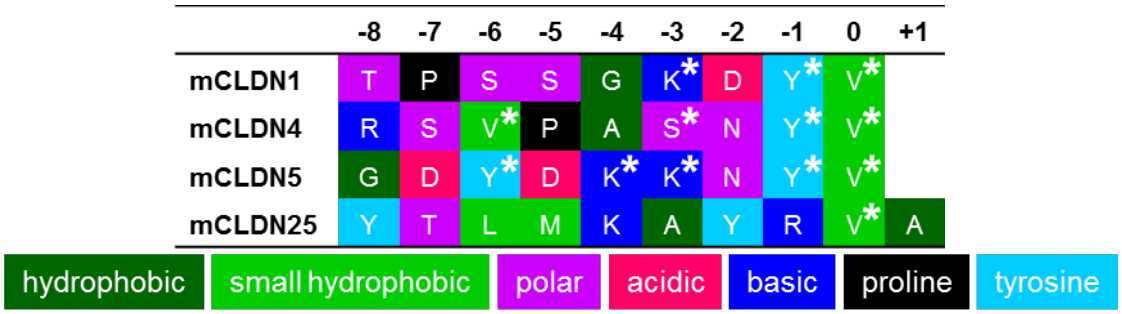


The MBP tagged protein domains were purified as described in chapter 3.5.2. The purity was verified via Coomassie Blue staining after SDS-PAGE (Figure S 8). MBP-Zo1-PDZ1 was fluorescently labeled to monitor its thermophoretic motion behavior (Figure S 9).

All tested Cldn COOH-termini bound to the PDZ1 domain. Cldn4 showed the lowest dissociation constant ($K_d$) with 62.6 nM. Cldn25 was not significantly different in its binding behavior with a $K_d$ of 164.2 nM. Cldn1 and -5 (1007.0, 944.6, respectively) exhibited a significantly higher $K_d$ than Cldn4. In the concentration range of PDZ1-bound MBP tagged Cldn-COOH-termini, no binding of the negative control, the purified MBP tag was detected (Figure 32).

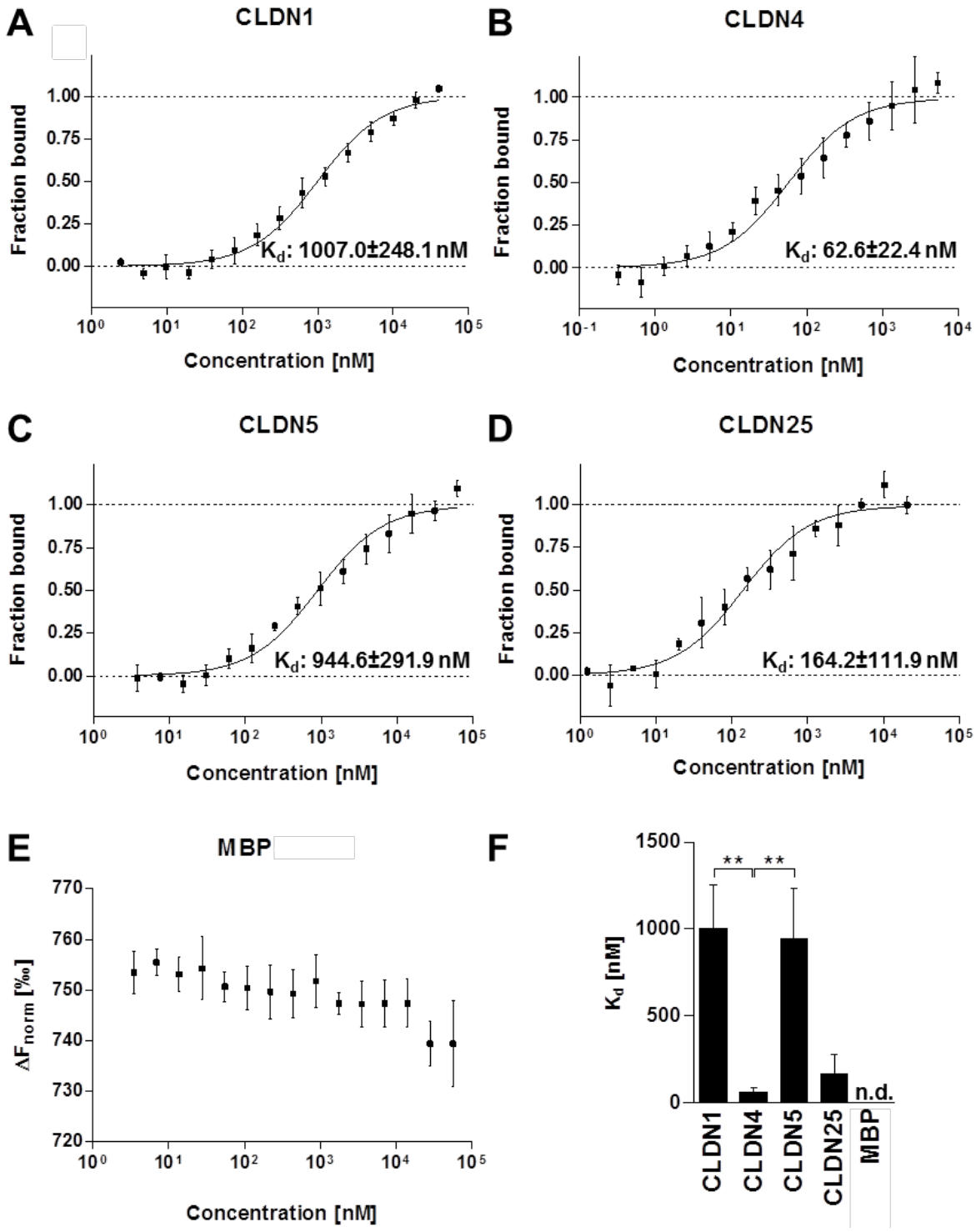


**Figure 32 Zo1-PDZ1 binding to claudins (Cldns) expressed in the brain endothelium.** Binding affinities were quantified via microscale thermophoresis. (A-D) Maltose binding protein (MBP) tagged COOH-termini of Cldns were titrated against the fluorescently labeled MBP tagged PDZ1 domain of Zo1. Relative values (1 = bound/ 0 = unbound) define the ordinate and therefore the fraction of proteins bound to Zo1-PDZ1. Mean ± SD; n = 5 (E) MBP alone did not associate with the PDZ1 domain of Zo1. The two values with the highest concentrations showed a slight decrease, indicating the beginning of a binding curve. However, potential binding was above the concentration range of the COOH-termini of all Cldns. The ordinate shows the normalized fluorescence intensity

($F_{norm}$). Mean ± SD; n = 5 (F) $K_d$ increase indicates lower binding affinity. Kruskal–Wallis test. **, p < 0.01.

### 4.5.2 Deletion of tyrosine at position$^{-2}$ reduces binding affinity of claudin-25 to PDZ1 of *zonula occludens* protein 1

Cldn25 exhibited a high affinity to Zo1-PDZ1 (Figure 32). To determine residues crucial for this interaction, binding of deletion mutants of the MBP tagged COOH-terminus of Cldn25 were analyzed. Via site directed mutagenesis, mutants with a stop codon at position$^{+1, 0, -1, -2}$ and $^{-4}$ were generated (Table 28). The deletion of alanine at position$^{+1}$ increased the $K_d$ around 7-fold, but not significantly. The value of 1164 nM was still in the range of that detected for Cldn1 and -5 (Table 27). The deletion of residues at position$^{0}$ and $^{-1}$ did not further increase the $K_d$. The deletion of tyrosine at position$^{-2}$ increased the $K_d$ significantly, 22-fold to 3611 nM. No further significant increase of the $K_d$ was detected after deletion of residues at position$^{-3}$ and $^{-4}$.

**Table 28 Truncated derivates of the Cldn25 COOH-terminus.** COOH-terminal amino acids were deleted by replacing the coding triplet with a stop codon through site directed mutagenesis.

| | -8 | -7 | -6 | -5 | -4 | -3 | -2 | -1 | 0 | +1 |
|---|---|---|---|---|---|---|---|---|---|---|
| mCLDN25$_{237-253}$ | Y | T | L | M | K | A | Y | R | V | A |
| mCLDN25$_{237-252}$ | Y | T | L | M | K | A | Y | R | V | |
| mCLDN25$_{237-251}$ | Y | T | L | M | K | A | Y | R | | |
| mCLDN25$_{237-250}$ | Y | T | L | M | K | A | Y | | | |
| mCLDN25$_{237-249}$ | Y | T | L | M | K | A | | | | |
| mCLDN25$_{237-247}$ | Y | T | L | M | | | | | | |

hydrophobic | small hydrophobic | polar | acidic | basic | proline | tyrosine

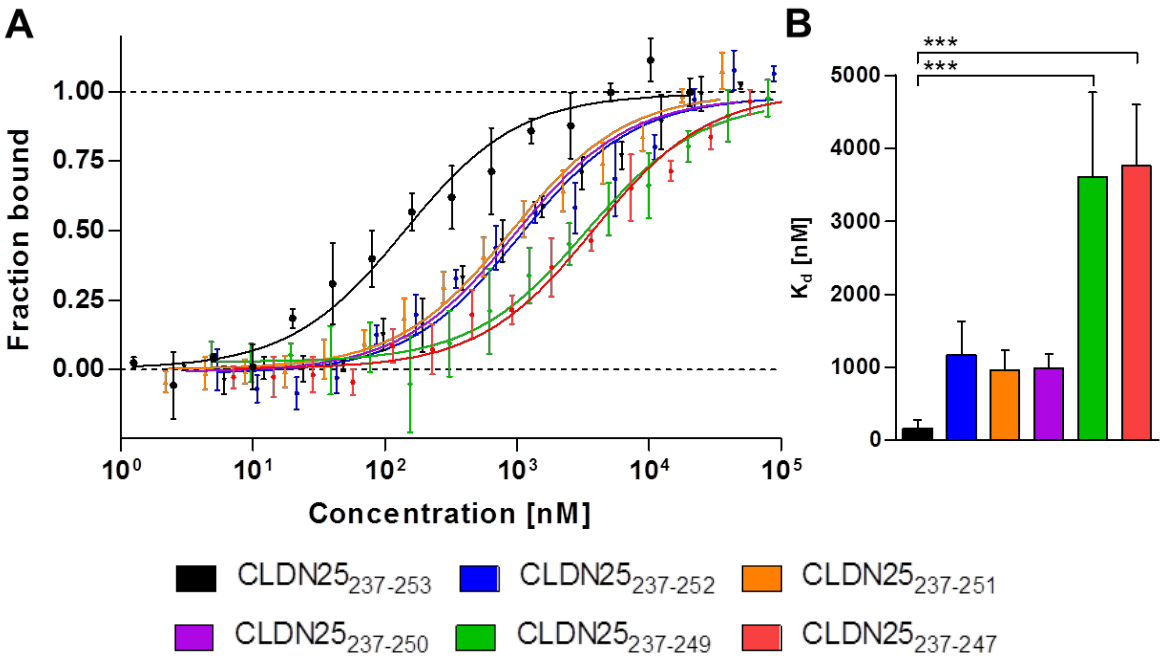


**Figure 33 Binding of the MBP tagged COOH-terminus of claudin (Cldn)-25 and its truncated derivates to PDZ1 of Zo1.** Binding affinities were determined by microscale thermophoresis. (A) The ordinate represents the fraction of proteins bound to Zo1-PDZ1. A series of COOH-terminal deletion mutants of Cldn25 was analyzed. (B) The $K_d$ values: $Cldn25_{237-253}$ (164.2 ± 111.9 nM), $Cldn25_{237-252}$ (1164 ± 461.1 nM), $Cldn25_{237-251}$ (958.9 ± 280.0 nM), $Cldn25_{237-250}$ (990.5 ± 196.2 nM), $Cldn25_{237-249}$ (3611 ± 1153 nM) and $Cldn25_{237-247}$ (3757 ± 841.2 nM). Mean ± SD; n = 5. The association of the MBP tagged COOH-terminus of Cldn25 with Zo1-PDZ1 significantly decreases when tyrosine at position$^{-2}$ is deleted. Kruskal–Wallis test; ***; $p < 0.001$.

### 4.5.3 Localization of claudin-25 at the plasma membrane is reduced after deletion of tyrosine at position$^{-2}$

Cldn25 bound to Zo1-PDZ1 (Chapter 4.5.1) and this interaction was disturbed by deletion of tyrosine at position$^{-2}$ (Chapter 4.5.2). These findings gave rise to the question if impaired association of Cldn25 with Zo1 alters the subcellular localization. Mutants of YFP tagged full length Cldn25 with a stop codon at position$^{-2}$ or $^{-4}$ were generated as for the MBP tagged COOH-termini (Table 28). These mutations increased the $K_d$ at least 22-fold, determined by microscale thermophoresis. After transfection into the epithelial cell lines HEK-293 and MDCK-II, the localization of YFP tagged Cldn25 was microscopically analyzed via life cell imaging. The colocalization of Cldn25 with the plasma membrane is given as weighted colocalization coefficient. The deletion of tyrosine at position$^{-2}$ led in

both cell lines to an accumulation of Cldn25 in the cytoplasm and reduced localization at the plasma membrane (Figure 34). Both cell lines expressed Zo1 (Figure S 7), but only MDCK-II cells form TJ strands visualized by freeze fracture microscopy (Piontek et al., 2008). The weighted colocalization coefficient of Cldn25 lacking tyrosine at position$^{-2}$ with the plasma membrane was significantly reduced in HEK-293 cells (Cldn25$_{1-253}$, 0.71; Cldn25$_{1-249}$, 0.53) as well as in MDCK-II cells (Cldn25$_{1-253}$, 0.58; Cldn25$_{1-249}$, 0.43). In HEK-293, but not MDCK-II cells a further significant decrease was detected after deletion of the residues at position$^{-3}$ and $^{-4}$ (Cldn25$_{1-247}$, 0.35, 0.37 respectively).

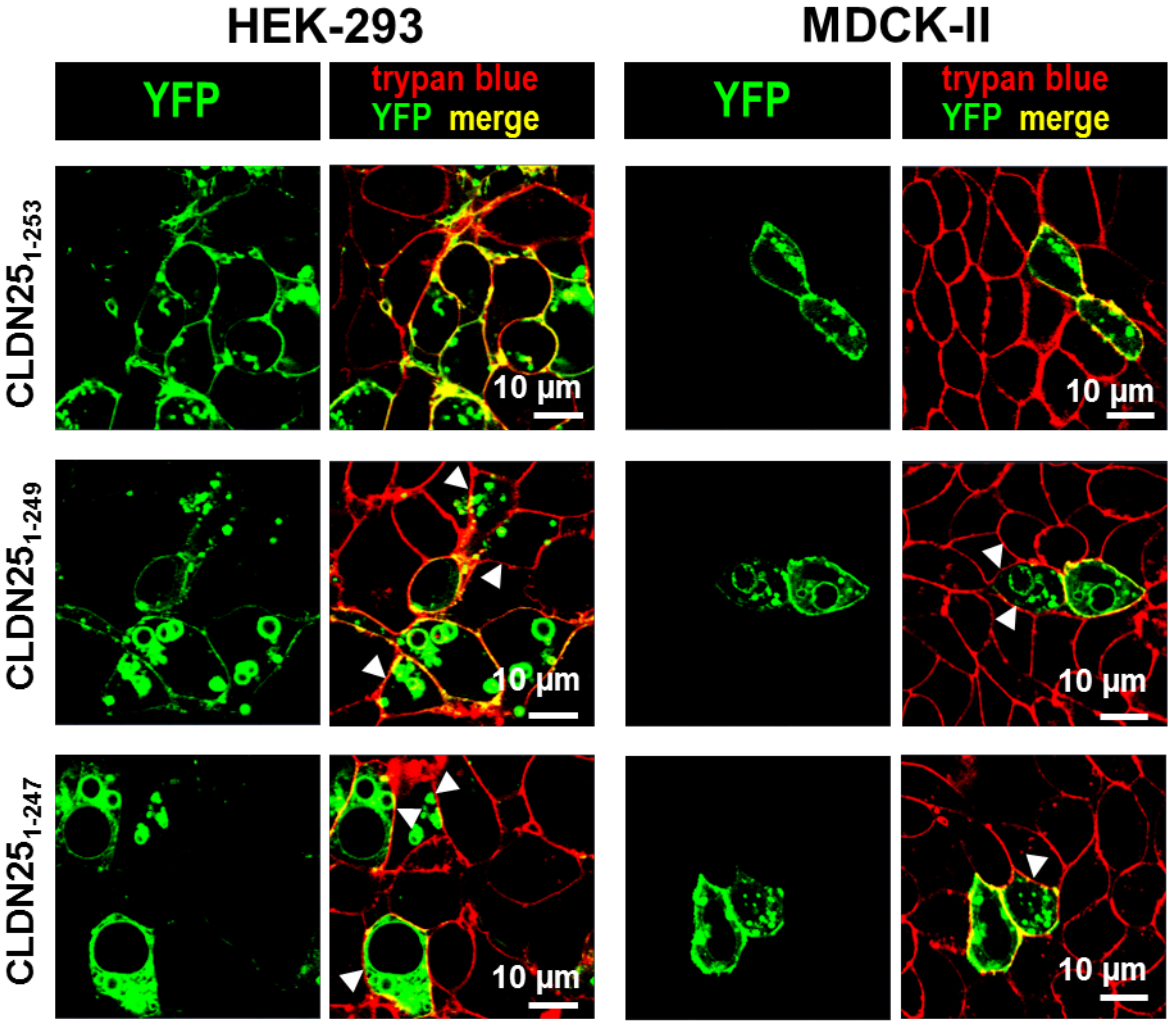


**Figure 34 Deletion of tyrosine at position$^{-2}$ reduces localization of claudin (Cldn)-25 at the plasma membrane of HEK-293 and MDCK-II cells.** YFP tagged Cldn25 (YFP-Cldn25$_{1-253}$) and the COOH-terminal deletion mutants missing the last four amino acids, YRVA (YFP-Cldn25$_{1-249}$) or the last six amino acids, KAYRVA (YFP-Cldn25$_{1-247}$) were transfected into HEK-293 and MDCK-II cells. YFP signal (green) was observed 48 h later

by live-cell microscopy. Cell membranes were stained by trypan blue (red). Arrows point to the plasma membrane lacking Cldn25 in transfected cells.

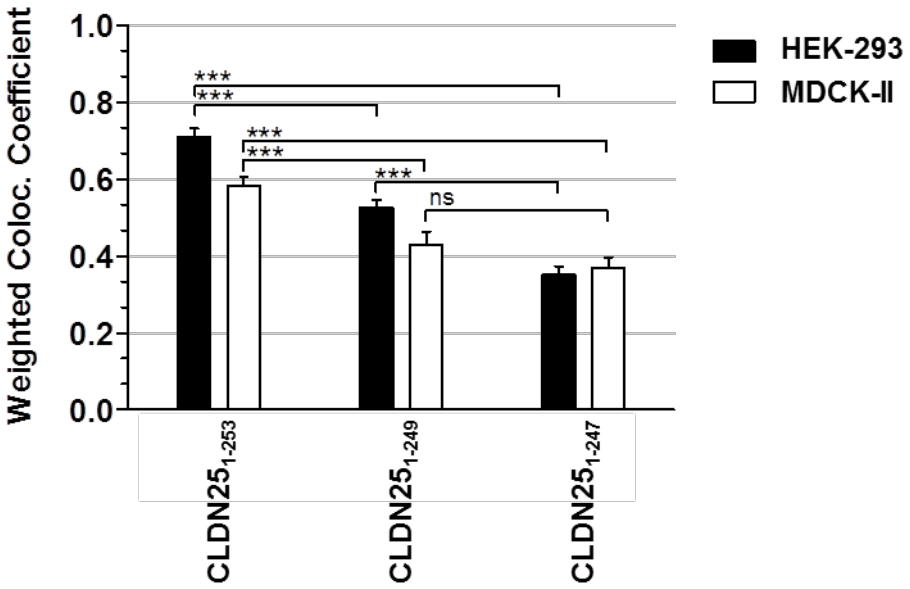


**Figure 35 Plasma membrane fraction of claudin (Cldn)-25 is reduced upon deletion of tyrosine at position$^{-2}$.** In order to quantify the membrane association of YFP-Cldn25 and the COOH-terminally truncated mutants, the colocalization coefficient was determined, which compares the YFP to the trypan blue signal. The Kruskal-Wallis test showed significant differences between Cldn25 and its mutants. *** $p < 0.001$; „ns“ = not significant. Mean ± SD; $n_{HEK-293} \geq 34$, $n_{MDCK-II} \geq 5$.

## 4.6 Cerebral ischemia impairs the integrity of the blood-brain barrier endothelium

Ischemic stroke occurs under permanent or temporary restriction of cerebral blood flow to parts of the brain, resulting in a deficit of oxygen and nutrients as well as an accumulation of metabolic products. Several pathological conditions including neuronal depolarization, intracellular calcium increase, metabolic function loss, oxidative stress and inflammation are induced under the progression of stroke (Sandoval and Witt, 2008). Molecular changes of the blood-brain barrier upon cerebral ischemia are not yet fully understood. In this chapter, transcriptional regulation of Cldns and TAMPs in the mouse brain endothelium after surgically induced middle cerebral artery occlusion (MCAO) was investigated.

### 4.6.1 Evaluation of the MCAO affected brain

The MCAO surgery and evaluation of the mouse brains were performed in collaboration with PD Dr. André Rex (Charité, Center Neurology, Berlin, Germany). In Figure 36, the diffusion-weighted magnetic resonance imaging (DWI) of a mouse brain after one hour of MCAO is shown. The apparent diffusion coefficient (ADC) is a measure for diffusion of water molecules within the tissue. The blue area, striatal and cortical located indicates the area with reduced diffusion due to artery occlusion. The use of DWI allows the precise localization of the affected brain region. Infarct sizes between 1.05 and 29.99% per hemisphere were determined for mice after surgically induced MCAO (Table 15).

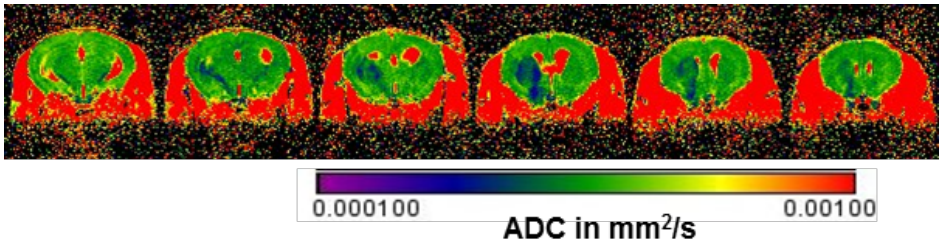


**Figure 36 Diffusion-weighted magnetic resonance imaging of a mouse brain after middle cerebral artery occlusion (MCAO).** The occlusion was surgically induced for 30 to 60 min. The imaging was performed directly after removing of the intraluminal filament. The apparent diffusion coefficient (ADC), a measure for water diffusion indicates reduced movement of molecules in the (MCAO) affected brain area.

### 4.6.2 mRNA expression of tight junctions proteins changes under post ischemic reperfusion *in vivo*

Due to biphasic changes of the BBB permeability during post ischemic reperfusion (Figure 8), two time points were chosen to evaluate the transcriptional regulation of TJ proteins. Those are during the initial reperfusion phase at 3 h as well as the final phase at 48 h after surgically induced MCAO (for 60 to 30 min, respectively). After defining the localization of the MCAO affected brain region (Table 15), cryosections were prepared (Chapter 3.2.1). Brain capillaries visualized by RCA1 staining were isolated via laser capture microdissection in the ipsi- and contralateral area. Following mRNA isolation and cDNA synthesis, qRT-PCR was

performed to determine the mRNA expression of *Cldns* and *Ocln* relative to *Rn28s*. The target mRNAs were selected due to their expression levels in the mouse brain (Chapter 4.1.1). The expression levels (Figure 37) were normalized to those of the contralateral region. The mRNA level of *Hbegf* was previously shown to be up-regulated in the cerebral cortex upon ischemia and reperfusion (Oyagi et al., 2011) and thereby chosen as marker for this study. In the initial phase of 3 h post ischemic reperfusion, mRNA of *Hbegf* as well as *Cldn5*, *-25* and *Cdh5* were significantly up-regulated (2.3-, 1.7-, 1.6- and 2.4-fold, respectively). Contrastingly, the mRNA of *Cldn1, -3, -12* and *Ocln* were significantly down-regulated (-1.3-, -4.3-, -1.7- and -1.3-fold, respectively). *Cldn11, -20* and *Zo1* did not change significantly in mRNA expression. Upon 48 h of reperfusion, *Hbegf* as well as *Cldn5* and *Cdh5* were significantly up-regulated (2.4-, 2.1- and 2.9-fold, respectively), slightly stronger than in the initial phase, but not *Cldn25*. Only the mRNA of *Cldn12* was significantly down-regulated (-1.4-fold). *Cldn1, -3* and *Ocln,* down-regulated in the acute stage were not significantly altered in mRNA expression after 48 h of reperfusion as for *Cldn11, -20* and *Zo1*. Taken together, the reduced number of down-regulated *Cldns* and a higher degree of up-regulation upon 48 h of reperfusion suggests a molecular re-establishment of TJs after ischemia induced breakdown.

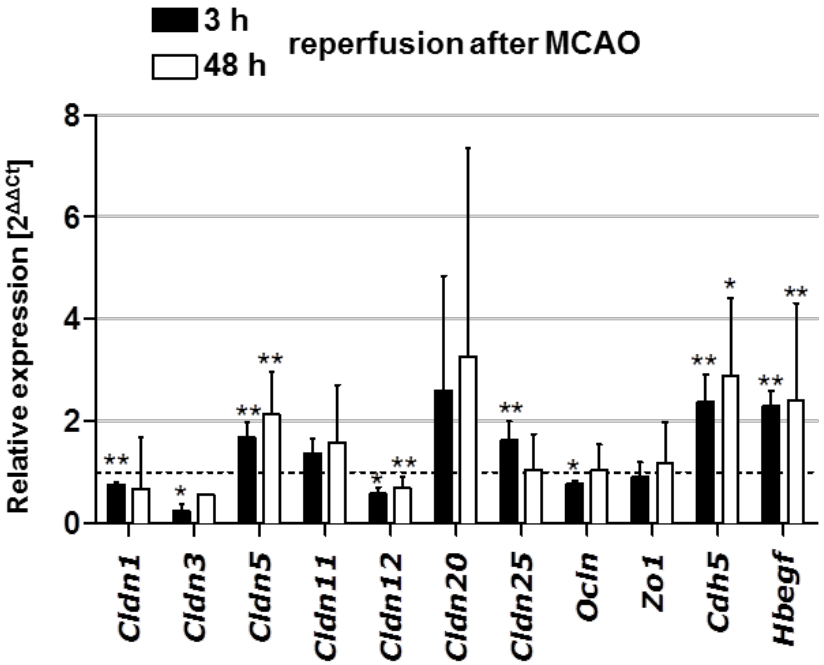

**Figure 37 mRNA expression in laser-dissected mouse brain capillaries 3 or 48 h of reperfusion after middle cerebral artery occlusion (MCAO).** The expression levels were normalized to that of the contralateral region. $\Delta\Delta Ct = (Ct_{target} - Ct_{Rn28s})_{ipsilateral} - (Ct_{target} - Ct_{Rn28s})_{contralateral}$. Heparin-binding EGF-like growth factor (*Hbegf*) is the ischemia control. Mean ± SD; n ≥ 4 (except *Cldn3* 48 h reperfusion, n = 1); Mann–Whitney U test. *Cldn*, claudin; *Ocln*, occludin; *Zo1*, *zonula occludens* protein 1; *Cdh5*, cadherin-5.

### 4.6.2.1 Enhanced down-regulation of claudin-1 mRNA expression upon post ischemic reperfusion in claudin-3 deficient mice

The strongest reduction in mRNA expression upon post ischemic reperfusion was found for *Cldn3* (Figure 37, -4.3-fold in the initial phase of reperfusion). As previously described (Chapter 4.3.1), transcriptional regulation of Cldns can occur upon loss of certain members of the Cldn family. A 1.7-fold reduction of the *Cldn1* mRNA level was already found under physiological conditions in brain capillaries of Cldn3 deficient mice (Figure S 10). To investigate if the loss of Cldn3 alters the expression profile upon post ischemic reperfusion, mRNA expression levels were examined in brain capillaries of *Cldn3* deficient mice under the same reperfusion conditions described in chapter 4.6.2. The down-regulation of *Cldn1* upon post ischemic reperfusion was enhanced, significantly by 9.6-fold at 3 h and by 3.1-fold at 48 h reperfusion (Figure 38).

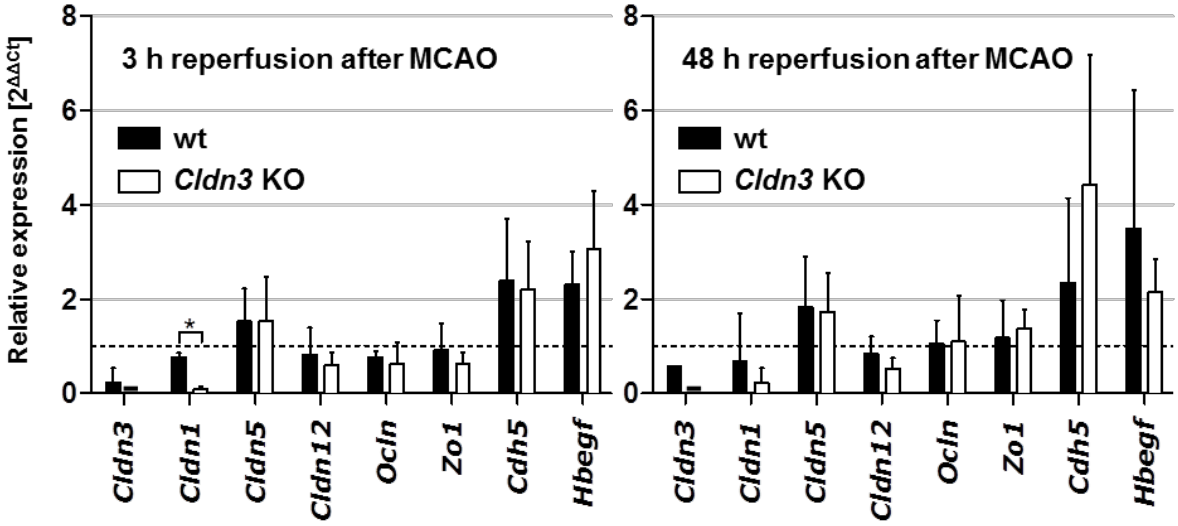


**Figure 38 Down-regulation of claudin (*Cldn)*-1 mRNA expression upon reperfusion after middle cerebral artery occlusion (MCAO) is enhanced in *Cldn3* deficient (KO) mice.** The expression levels in laser-dissected brain capillaries were normalized with respect to that of the contralateral region. $\Delta\Delta Ct = (Ct_{target} - Ct_{Rn28s})_{ipsilateral} - (Ct_{target} -$

$Ct_{Rn28s})_{contralateral}$. Heparin-binding EGF-like growth factor (*Hbegf*) is the ischemia control. Mean ± SD; n ≥ 4 (except *Cldn3* 48 h reperfusion, n = 1); Mann–Whitney U test; statistical differences between wt and *Cldn3* KO, * $p < 0.05$. *Ocln*, occludin; *Zo1*, *zonula occludens* protein 1; *Cdh5*, cadherin-5.

# 5 Discussion

## 5.1 The claudin and TAMP profile of the human and mouse blood-brain barrier exhibits only few qualitative and quantitative differences

Quantitative analyses of TJ proteins in the brain endothelium *in* or *ex vivo* is still missing. In all studies that investigate brain capillary or endothelial cell preparations from tissue homogenates, *Cldn5* is the dominant Cldn subtype (> 80% of total *Cldn* and *TAMPs*) (Bocsik et al., 2016; Daneman et al., 2010; Ohtsuki et al., 2008). An impairment of the mouse BBB upon loss of Cldn5 was reported (Nitta et al., 2003). Ever since, numerous publications correlate BBB dysfunction e.g. in inflammation, stroke or brain tumours with the integrity of TJs, particularly with the quantity and subcellular localization of Cldn5 (Bai et al., 2014; Balbuena et al., 2011; Liu et al., 2012; Podjaski et al., 2015; Shi et al., 2016; Tominaga et al., 2015). This study provides qualitative and quantitative information about the TJ protein expression at the BBB and compares the human with the mouse model (*ex vivo* and *in vitro*), commonly used in BBB research.

### 5.1.1 mRNAs of 16 tight junction proteins are detected in both human and mouse

The detection of mRNA of 16 TJ proteins (*Cldn1, -2, -3, -4, -5, -6, -9, -11, -12, -15, -17, -20, -22, -25, Ocln* and *Tric*) in laser-dissected brain capillaries is consistent between human and mouse. Only *Cldn23* and *-27* are exclusively detected in human whereas *Cldn14, -24* and *-26* are found solely in mouse. Probably due to an expression level below the detection limit in laser-dissected mouse brain capillaries, *Cldn8, -13, -18* and *-23* are detected only *in vitro* (Figure 10 - 13). To proof the mRNA expression by use of an independent method, RNA sequencing was performed in collaboration with Dr. Jingjing Zhang (Affiliated Hospital of Guangdong Medical College, Zhanjiang, Guangdong, China). Transcripts of all TJ proteins detected by qRT-PCR in purified mouse brain capillaries were found except for *Cldn13, -17* and *-24*, although *Cldn3* and *-14* were below the limit of quantification. In human as well as mouse no expression was found for *Cldn7, -10, -16, -19, -21* and *Marveld3.* Transcript amplification was proven for the respective

primers (Table 11) using cDNA of Caco-2 cells (Figure S 2, except for Cldn21). In contrast, mRNA of *Cldn10 and -19* was previously reported to be enriched in the mouse brain endothelium (Ohtsuki et al., 2008). However, *Cldn10* was later found to be enriched in the cerebral cortex compared to brain capillaries and *Cldn19* in the choroid plexus (Kratzer et al., 2012). In accordance, Cldn10 localized outside of brain capillaries (Figure S 4). The mRNAs of *Cldn1, -2, -3, -9, -11* and *-12* were stated as detected but not concentrated in endothelial cells. Besides, *Cldn4, -6* and *-14* were not detected (Ohtsuki et al., 2008). But in addition to Cldn5 and -20, immunohistochemistry unveiled an expression specifically in the brain endothelium for Cldn1, -3, -4, -11 and -12 (Figure 17, 18). Furthermore, the localization in brain capillaries was reported for Cldn1 and -3 (Wolburg et al., 2003) as well as Cldn12 (Nitta et al., 2003). *Cldn1, -2, -3, -4, -6, -9, -11, -12* and *-14* were also detected in pure endothelial cells *in vitro,* additionally to *Cldn5, -15, -17, -20 and -22* reported to be concentrated in brain endothelial cells (Ohtsuki et al., 2008). These findings further confirmed the brain endothelium as source of expression with regard to mRNA detected in laser-dissected brain capillaries. In accordance with the discovered mRNA, the transcript of *Cldn1* was detected in human brain capillaries (Kooij et al., 2014). *Cldn3* mRNA was reported in human (Kooij et al., 2014) as well as in rat brain microvessels (Kratzer et al., 2012). mRNA expression of *Cldn5* was found in human (Kooij et al., 2014), rat (Kooij et al., 2014) and mouse brain endothelial cells (Brown et al., 2007; Daneman et al., 2010; Ohtsuki et al., 2008; Urich et al., 2012). *Cldn12* and *-25* transcription was proven in mouse brain endothelial cells (Daneman et al., 2010) as well as for Cldn15, -17, -20 and -22 (Ohtsuki et al., 2008). Taken together, despite controversy with literature, this data suggests 16 TJ proteins (*Cldn1, -2, -3, -4, -5, -6, -9, -11, -12, -15, -17, -20, -22, -25, Ocln* and *Tric*) to be expressed in the brain endothelium due to detection of mRNA in both human and mouse *ex vivo* as well as *in vitro* in pure endothelial cells.

### 5.1.2 In the brain endothelium, low expression of pore forming claudins is found compared to epithelial cells

Among the 16 TJ proteins expressed in the brain endothelium of human and mouse, only *Cldn2*, *-15* and *-17* have an additional function in formation of

paracellular ion pores (Table 1). None of those were expressed above the level of Ocln (Table S 1). The functions of *Cldn12*, *-20*, *-22* and *-25* remain still unclear (Table 1). On the contrary, in Caco-2 cells (human colon epithelial cells) mRNAs of six pore-forming Cldns (*Cldn2, -7, -8, -10, -15, -16*) as well as *Cldn12, -20, -22, -23, -24, -25, -27* and *Marveld3*, with yet unknown function was found. *Cldn7* was detected even above the expression level of *Ocln* (Figure S 2). Accordingly, the mRNA expression of *Cldn7* was previously described as the highest amongst the pore forming Cldns in Caco-2 cells (Bocsik et al., 2016). A high expression of *Cldn7* was also reported in the corneal epithelium (Ban et al., 2003) as well as alveolar epithelium (Overgaard et al., 2012). Increasing the chloride permeability (Hou et al., 2006), Cldn7 might be specific to epithelial cells. Like *Cldn7*, the expression of *Cldn16* was only found in Caco-2 cells, not in brain endothelial cells (Bocsik et al., 2016). However, relatively low *Cldn16* expression in rat brain capillaries was reported (Kratzer et al., 2012). Cldn8 was described as the most abundant Cldn in the bladder epithelium (Acharya et al., 2004). In the brain endothelium, mRNA of *Cldn8* was detected only *in vitro* and at low levels (Figure 12). It can be assumed that a low paracellular ion flux is characteristic for brain endothelial cells supporting a stable environment for neuronal signaling.

### 5.1.3 Unlike mouse, the human blood-brain barrier is not dominated by claudin-5

Among the stated 16 TJ proteins, a significant difference in the mRNA expression level between human and mouse was found only for *Ocln* (6.6-fold lower in human). But mRNAs of ten TJ proteins were expressed at lower (*Cldn1, -2, -5, -11, -12, -17, -20, -22, Ocln* and *Tric*) and six at higher levels (*Cldn3, -4, -6, -9, -15, -25*) in human compared to mouse (Figure 10 - 13). Considering the high abundance of Cldn5 and -11, known to seal the paracellular cleft, these findings suggest qualitative differences of the BBB between human and mouse. The human BBB was characterized by a percentage of *Cldn5* mRNA of 16% with respect to mRNA of all TJ proteins. In mouse, with 37% more than the double in quantity, *Cldn5* was the most abundant mRNA (Figure 39). The dominance of *Cldn5* in the mouse brain endothelium was previously reported (Ohtsuki et al., 2008). A relatively low *Cldn5* mRNA level in human was described for cultured

brain endothelial cells in comparison to isolated mouse brain capillaries (Urich et al., 2012). Considering a similar quantity of the *Cldn5* transcript *ex vivo* and *in vitro* (Figure 11), this result supports the finding that *Cldn5* does not dominate the human BBB. *Cldn11* exhibited an expression pattern similar to *Cldn5* (in human 13% and mouse 29%). On the contrary *Cldn25* was with 49% the strongest expressed Cldn in the human brain endothelium, 5.6-times higher compared to mouse. mRNAs of 8 further TJ proteins (*Cldn2, -3, -4, -6, -15, -17, -22* and *Tric*) were below 1% of all TJ proteins in both species. Expression above 1% was found for *Cldn9* only in human and for *Cldn20* only in mouse (Figure 39). *Cldn1* and *-12* were above 1% in both, human (*Cldn1*, 2%; *Cldn12*, 9%) and mouse (*Cldn1*, 2%; *Cldn12*, 8%). Accordingly, mRNA expression levels below *Cldn5* were previously reported for *Cldn1*, *-3* and *-12* (Kooij et al., 2014; Ohtsuki et al., 2008; Urich et al., 2012). In addition, a significant correlation of mRNA levels determined by qRT-PCR and RNA sequencing in purified mouse brain capillaries confirmed quantitative differences of expression between Cldn subtypes and TAMPs (Figure 14). Taken together, these quantitative differences could lead to varying barrier properties. Furthermore, the use of drugs targeting specific Cldn subtypes (Staat et al., 2015) might not lead to the same success in both species. Additionally, differences of the human and mouse BBB with regard to transporter expression were previously reported. E.g. the drug transporter, breast cancer resistance protein is 2-fold higher and P-glycoprotein 2-fold lower expressed in human than in mouse. Importantly, the multidrug resistance-associated proteins, organic anion transporter and organic anion-transporting polypeptide family members found in the rodent BBB, were under the limit of quantification in human (Uchida et al., 2011). Hence, the use of mice as model to investigate BBB properties is questionable.

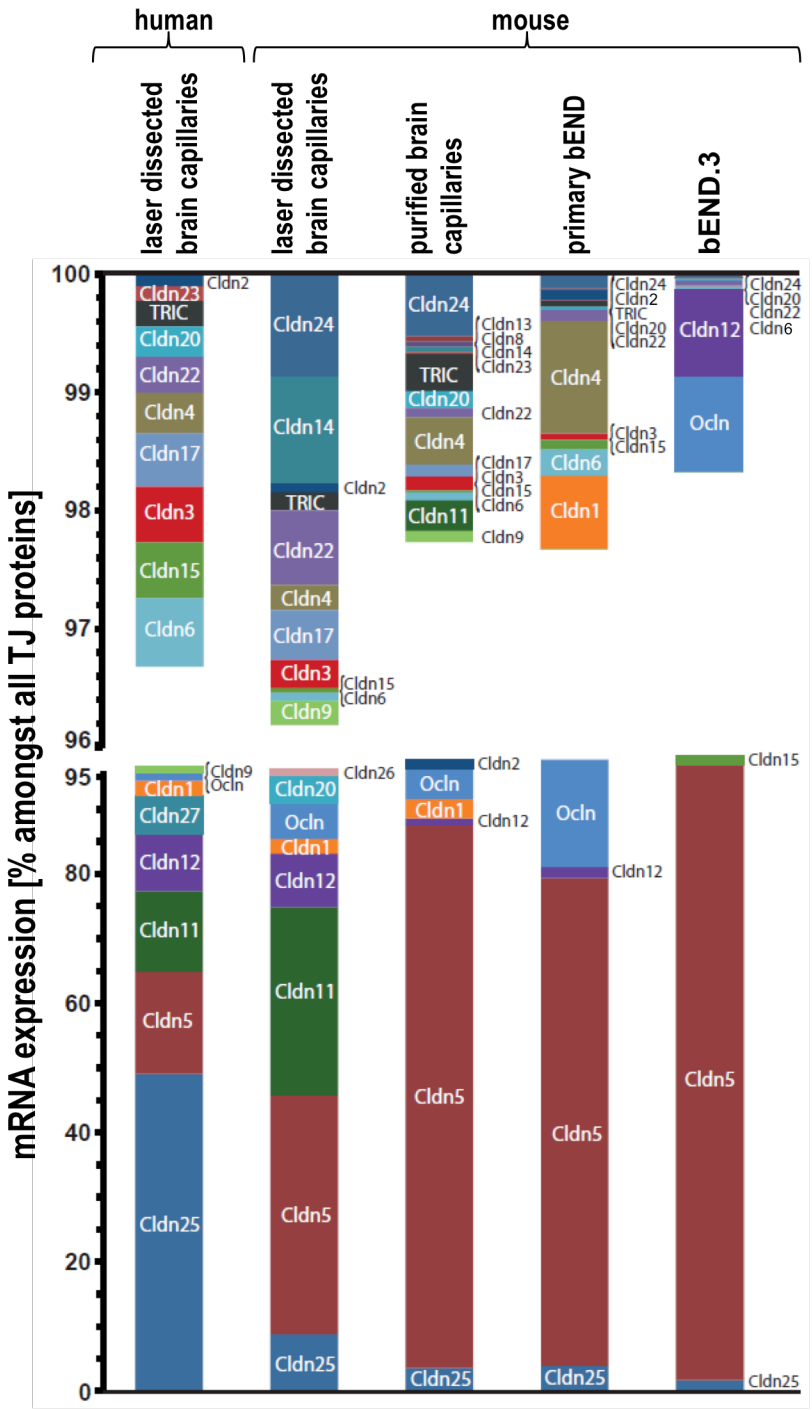


**Figure 39 Percentage of mRNA expressed amongst all tight junction proteins in the human and mouse brain endothelium.** Expression in laser-dissected human and mouse brain capillaries, purified mouse brain capillaries, primary mouse brain capillary endothelial cells (primary bEND) and bEND.3, an endothelial cell line of the mouse cerebral cortex. *Cldn*, claudin; *Tric*, tricellulin; *Ocln*, occludin. Percentage of total mRNA expression amongst TJ proteins. High abundant > 1% and low abundant mRNA < 1% of total mRNA. Mean, n ≥ 4.

## 5.2 mRNA expression levels of claudins and TAMPs reflect abundance of the encoded proteins

mRNA expression levels (Chapter 4.1.1) were often criticised when used as quantitative measure for protein abundance. Most studies that compare the expression of various TJ proteins in the brain endothelium described only the mRNA level (Kooij et al., 2014; Ohtsuki et al., 2008; Urich et al., 2012). Translational control of existing transcripts often leads to changes in the expression of the encoded proteins, which consequently might not correlate with mRNA levels (Sonenberg and Hinnebusch, 2009). But information about the correlation of mRNA and protein level was missing. Moreover, recent approaches to quantify any other TJ protein than Cldn5 failed. In a study applying mass spectrometry-based quantitative absolute proteomics of purified brain capillaries, the Ocln expression was revealed as below the limit of quantification (Hoshi et al., 2013). Certainly, all Cldns except *Cldn5* were expressed below the mRNA expression level of *Ocln* in purified brain capillaries (Figure 11 - 13). To address this issue an epitope dilution assay was developed to quantify the expressed protein in the brain endothelium. Quantification was realized by western blotting of purified brain capillaries. All Cldns detectable by specific antibodies were quantified by use of the purified recombinant expressed epitope (Figure 15). Cldn5 was the highest abundant TJ protein (509 fmol/µg, Table 26). Followed by Cldn25 > Ocln > Cldn1 > -11 > -4 > -12 (98, 36, 15, 8, 5, 4 fmol/µg respectively; Table 26). These values correlated with mRNA levels determined in purified brain capillaries (Figure 16). Taken together, mRNA levels determined by qRT-PCR (Figure 10 - 13) were representative for protein abundance with regard to TJ proteins in the brain endothelium. However, the Cldn5 molality was higher than previously determined by mass spectrometry-based quantitative absolute proteomics. In human brain microvessels, the Cldn5 quantity was 4 fmol/µg (Shawahna et al., 2011), in cynomolgus monkeys 7 fmol/µg (Ito et al., 2011) and in rats and common marmosets 8 fmol/µg (Hoshi et al., 2013). So far the Cldn5 quantity in mouse brain capillaries was not determined using this technique. As previously described, the mRNA expression of *Cldn5* was found to be higher in mouse compared to human (Figure 11). Additionally, the results of absolute proteomics, especially of transmembrane proteins, using different lysate protocols should be compared

critically. For mass spectrometry-based quantitative absolute proteomics, microvessels were sonicated in hypotonic buffer (10 mM Tris–HCl, 10 mM NaCl, 1.5 mM $MgCl_2$, pH 7.4) (Uchida et al., 2011). Instead, a lyses buffer containing 1% Triton X-100 (Table 6) was used to purify proteins of brain capillaries for western blotting. Also varying blotting efficiency of proteins with different molecular weight with respect to endogenous Cldns (22 - 29 kDa) and recombinant epitopes (46 - 58 kDa) could lead to determination of higher quantities (Figure 15). Nevertheless, endogenous Ocln (60 kDa) has a comparable molecular weight as the recombinant epitope (65 kDa) and the determined molality fits to the correlation that includes the values for Cldns (Figure 16). Differences in blotting efficiency do not explain values at least 60-fold higher for Cldn5. In summary, molalities of all investigated TJ proteins were between 4 and 509 fmol/µg in the brain endothelium such as the quantities for Cldn5, determined by mass spectrometry-based quantitative absolute proteomics (Hoshi et al., 2013; Ito et al., 2011; Shawahna et al., 2011). Differences with respect to the molality of Cldn5 might be due to varying species and lysate protocols.

## 5.3 mRNA expression of most claudins except claudin-5 decrease under exclusion of *in vivo* stimuli

Upon cultivation of brain endothelial cells, the mRNA expression profile of TJ proteins changed drastically. The mRNA levels of 14 TJ proteins were reduced in purified brain capillaries *in vitro* (significantly for *Cldn12;* Figure 13; Table 25). The expression of mRNAs of 15 TJ proteins decreased in primary endothelial cells (*Cldn9*, *-11*, *-12*, *-14*, -17, *-20* and *-22;* Figure 11 - 13; Table 25) and of 16 TJ proteins in bEND.3 cells (significantly for *Cldn1*, *-3*, *-9*, *-11*, *-12*, *-14*, *-20*, *-22*, *-24*, *-25* and *Ocln;* Figure 10 - 13; Table 25) Interestingly, *Cldn15*, coding for a sodium channel (Colegio et al., 2002) was 27-fold up-regulated in bEND.3 cells (Figure 12; Table 25). Taken together, the total transcript quantity of TJ proteins was drastically reduced *in vitro* but not for *Cldn5* and *-15*. As a consequence, *Cldn5* dominated the mRNA expression of TJ proteins in endothelial cells *in vitro* (Figure 39; mouse brain endothelium *ex vivo,* 37% < purified brain capillaries, 84% and primary brain capillary endothelial cells, 76% < bEND.3 cells, 95%) The overall reduction in *Cldn* expression accompanied with an increase of *Cldn15 in vitro*

could explain the reduced barrier properties compared to the brain endothelium *in vivo*.

The BBB is established in an environment of constant blood flow and interaction with other cell types like astrocytes and pericytes (Abbott, 2013). The cultivation of bEND.3 cells exposed to constant unidirectional flow of medium changes the expression of transcription factors and gasotransmitter-synthesizing enzymes and increases NO production supporting a vasoprotective phenotype. Importantly, NFκB localization in the nucleus and thereby its activation is reduced (Mao et al., 2014). NFκB is a transcription factor known to regulate *Cldn* expression. TNF-α induced down-regulation of Cldn1 is mediated by NFκB (Amasheh et al., 2010). NFκB activation leads also to disruption of Cldn5 dependent TJs in human dermal microvascular endothelial cells (Clark et al., 2015). Suppression of this transcription factor by use of Tanshinone II A improves BBB tightness in rat brains (Wang et al., 2010). Flow can be considered as one of the key factors determining BBB tightness by inactivation of NFκB. In accordance several pathologies including ischemia, HIV infection and inflammation known to compromise BBB integrity lead to an increased NFκB activation (Aslam et al., 2012; Brown et al., 2003; Epple et al., 2009). Static cultures of endothelial cells exhibit features typically found in pathology, resulting in an altered *Cldn* expression profile.

Co-cultures with astrocytes become important when stimulated with e.g. transforming growth factor β1. A decrease in TEER and expression of Cldn5 upon treatment is only found in endothelial cells co-cultured with astrocytes (Hawkins et al., 2015). In summary, isolated cultures of brain capillary endothelial cells being not exposed to unidirectional flow are characterized by a reduced TJ protein expression. The complex interplay of Cldn regulation is disturbed and could lead to a phenotype that does not reflect the situation *in vivo*. Expression of *Cldn1* depending on *Cldn3* abundance is previously shown in cultured keratinocytes (Tokumasu et al., 2016). This finding could further explain the overall reduction of *Cldns*. It remains still unclear, why *Cldn5* expression does not decrease *in vitro*. But a reduction of Cldn5 in pathology might rely on co-culture with astrocytes (Hawkins and Davis, 2005) which could explain the stable expression in isolated cultures of endothelial cells.

Cultures of isolated primary capillary endothelial cells of human, rodents, pigs or cattle as well as cell lines like bEND.3 or hCMEC/D3 are used to evaluate BBB

permeability and integrity after treatment with drugs or under stress conditions. Besides permeability, which is much higher in cell cultures compared to *in vivo*, Cldn5 reduction is the major goal to evaluate the effect of the treatment. Thus, the value of those model systems to represent the BBB is questionable. Co-cultures of primary endothelial cells with astrocytes and pericytes under exposure of unidirectional flow are highly recommended to better reflect the barrier properties *in vivo.* Overall Cldn expression of static isolated endothelial cell cultures could be compared to those, qualitatively and quantitatively varying in co-culture with other cell types or degree of flow. This could further reveal key factors of specific transcriptional Cldn regulation.

## 5.4 Highly abundant claudin-11 and -25 localize in brain endothelial tight junctions

Cldn3, -5 and -12 are previously described to localize in TJs of the brain endothelium (Nitta et al., 2003; Wolburg et al., 2003). Cldn3 interacts homophilically as well as heterophilically with Cldn5 (Krause et al., 2008). Due to its potential to polymerize in brain endothelial TJ strands, a contribution to the paracellular barrier can be assumed despite its relatively low expression. With respect to the lack of homophilic and heterophilic interactions of Cldn12, a function in TJs is still unclear (Krause et al., 2008). Besides those reported, Cldn4, -11, -20 and -25 are newly found to localize in brain endothelial TJs (Figure 17, 18). Of all TJ protein transcripts *ex vivo*, 13% were of *Cldn11* in human and 29% in mouse (Figure 39). Thus, *Cldn11* was as highly abundant as *Cldn5*. Absence of TJ strands upon loss of Cldn11, was reported in the CNS myelin and between Sertoli cells (Gow et al., 1999). Accordingly, silencing of Cldn11 in Sertoli cells reduces the TER (McCabe et al., 2016). Unpublished data reveals that Cldn11 decreases paracellular ion permeability in canine kidney epithelial cells. Remarkably, Cldn11 interacts homophilically in *cis* and *trans* but not with any other Cldn. TJs exclusively formed by Cldn11, localizing separately from others could increase the number of brain endothelial TJ strands and further tighten the paracellular cleft (Research group for molecular cell physiology, PD Dr. Ingolf E. Blasig, unpublished data). Thereby, a contribution to TJs of the brain endothelium can be assumed. Cldn4, known to tighten the paracellular cleft (Van Itallie et al., 2001) as

well as Cldn20 with unclear function (Martin et al., 2013), were expressed below 1% of all TJ proteins in human brain capillaries (Figure 39). Just minor contribution to barrier tightness can be assumed. *Cis*-interaction of Cldn4 and -3 was reported which supports the incorporation of Cldn4 into TJs of the BBB (Daugherty et al., 2007). *Cldn25* was with 49% of all TJ protein transcripts the strongest expressed Cldn in the human brain endothelium (Figure 39). It is not yet reported if Cldn25 is capable to form TJs. To address this question, barrier properties of the brain endothelium were analyzed upon silencing of *Cldn25* (Chapter 4.3). Cldn10 previously reported be expressed in the brain endothelium (Ohtsuki et al., 2008) was stained outside the brain capillaries (Figure S 4), but the origin remains unidentified. Cldn1 was localized in brain capillaries of human and mice but localized mainly in the cytoplasm. Despite its function as paracellular barrier (Inai et al., 1999), a contribution of Cldn1 to the BBB might be minor. No specific commercial antibodies were available to stain further Cldns expressed less than one order of magnitude below *Ocln* in the human cortex (Table S 1, Cldn6, -9, -15, -17, -22 and -27). The contribution of those Cldns to the BBB remains still unclear. The generation of antibodies to identify specifically a Cldn subtype might be difficult due to high sequence homology within the protein family. Except for *Cldn15,* a knockdown *in vitro* might not lead to a barrier phenotype that can be quantified by ion permeability since all *Cldns* are very low expressed in cell cultures.

## 5.5 Loss of claudin-5 compromises tight junction strand integrity and alters the expression of tight junction proteins

bEND.3, an immortalized cell line of the mouse brain endothelium was described as useful model to evaluate BBB function due to high expression of Cldn5 (Watanabe et al., 2013). Despite the drastic reduction in expression of most other *Cldns*, the *Cldn5* mRNA level is comparable to that of laser-dissected mouse brain capillaries (Figure 11). The lentivirally induced knockdown of Cldn5 in bEND.3 cells exhibited a reduction of 29% in TEER (Figure 25). In accordance, it was shown that overexpression of Cldn5 in canine kidney epithelial cells increases TER and reduces paracellular flux of monovalent cations (Wen et al., 2004). In freeze fracture electron micrographs a drastically simplified TJ strand network was

visible upon loss of Cldn5 (Figure 24). The count of strands as well as size of meshes were reduced and their proper orientation disturbed. The arrangement of particles as discontinuous chains was not altered on the EF as well as PF. Cldn5 based TJs strands are described as chains of particles mainly associated to the EF (Morita et al., 1999c; Piontek et al., 2008). Importantly, in the control knockdown, the TJ strands were associated with the EF but also with the PF (Figure 23). This result further proved the contribution of other proteins to brain endothelial TJs. However, upon kockdown of Cldn5 the number of TJ strands was also reduced on the PF. Cldn5 might contribute to PF associated TJ strands through interaction with other Cldns such as Cldn1 and -3 (Piontek et al., 2011). Direct interaction with Cldn25 can be excluded since no heterophilic *trans*-interaction is found in co-cultures of transfected HEK-293 cells (Research group for molecular cell physiology, PD Dr. Ingolf E. Blasig, unpublished data). An interaction with Cldn15 still needs to be proven but might explain this phenotype due to a relatively high expression level (Figure 12). In electron micrographs of the upper small intestine of Cldn15 knockout mice, TJs are found comparable to the wild type. But a decrease of TJ strands becomes visible upon freeze-fracture electron microscopy (Tamura et al., 2008). This observation reflects the finding that TJs of the BBB appear normal in electron micrographs of Cldn5 deficient mice (Nitta et al., 2003).

Besides this expected phenotype, the expression of Cldn1 and -15 was drastically changed. On mRNA level, *Cldn1* is 17-fold increased and *Cldn15* 7-fold decreased (Figure 20). This effect was further proven on protein level (Figure 22). Since the reduction of *Cldn5* and *-15* was associated in a concentration dependent manner (Figure 21), a regulatory mechanism can be assumed. Cldn15 might be involved in ion homeostasis in the brain due to its function as sodium channel. Sodium plays a key role in e.g. regulation of the kainite-receptor activity, a major neurotransmitter receptor, crucial for normal brain function (Dawe et al., 2013). The impact of the elevated Cldn1 level on barrier function is questionable. Cldn1 is known to tighten the paracellular barrier by increase of TER (Inai et al., 1999) but in brain capillaries this protein localizes mainly in the cytoplasm (Figure 17, 18). Also upon loss of Cldn5 the increased Cldn1 level did not lead to improved localization in TJs. The Cldn1 localization was rather extended within the cytoplasm and the enrichment at the nucleus, seen in wild type bEND.3 cells was reduced (Figure 23). A regulatory

function of Cldn1 in recruitment of TAMPs was previously suggested (Cording et al., 2013; Furuse et al., 1998b).

### 5.6 Cldn25 does not exhibit classical claudin function

Unlike Cldn5, silencing of Cldn25 did not alter the TEER in bEND.3 cells (Figure 25). A reduction in TEER upon silencing indicates the involvement of a Cldn in paracellular sealing (Gan et al., 2013). Whereas an increase in TEER indicates the formation of ion pores (Buzza et al., 2010). Also the expression of other TJ proteins was not effected (Figure 20). As for Cldn5, changes in Cldn expression were previously described upon loss of Cldn1 (Tokumasu et al., 2016). In mono-transfected HEK-293 cells, Cldn25 did not enrich in cell-cell-contacts and was rather equally distributed along the plasma membrane (Figure 29), though a tendency to *trans*-interact with Ocln is found (Research group for molecular cell physiology, PD Dr. Ingolf E. Blasig, unpublished data). Typically Cldns, with either paracellular sealing or ion pore-forming function, enrich in cell-cell-contacts through homo- or heterophilic *trans*-interactions (Furuse et al., 1999). Sequence alignment of the ECL1 and 2 of Cldn25 with those of classic Cldns revealed a very low homology. Aromatic amino acids (F147, Y148 and Y158) in the ECL2, known to be crucial for *trans*-interaction of Cldn5 (Krause et al., 2009) are not conserved in the sequence of Cldn25 (Figure 26). In accordance, homomeric binding of the ECL2 of Cldn25 ($K_d$ of 1504 nM) was significantly lower than that of Cldn5 ($K_d$ of 9.1 nM). In addition, homomeric binding of the ECL1 ($K_d$ of 332.1 nM) as well as heteromeric association of the ECL1 and 2 ($K_d$ of 1579 nM) were also not in the $K_d$ range of the binding of the ECL2 of Cldn5 (Figure 27). These findings explain the lack of homophilic *trans*-interaction of Cldn25. In freeze fracture electron micrographs, the Cldn25 knockdown exhibited altered strand morphology on the PF but not on the EF. On the PF, particles were randomly distributed and did not follow the strand orientation. Furthermore, unstructured strands as well as a reduced number of meshes were found. The mechanism that could explain the incorporation of Cldn25 into the TJs is unclear. It might be possible through interaction with TAMPs such as Ocln or with Zo1 (Chapter 4.5).

### 5.6.1 Claudin-25, exhibits glycan features in the first extracellular loop, at asparagine in position 72 essential for localisation at the plasma membrane

*N*-glycosylation occurs typically at the ECL1 of voltage-dependent calcium channel gamma subunits, which are like Cldns members of the PMP-22/EMP/MP20/Cldn family (Price et al., 2005). Experimental evidence for *N*-glycosylation of the ECL1 of Cldns other than Cldn25 is still missing (Price et al., 2005).

Cldn25 is glycosylated in human T lymphocytes at the asparagine in position 42 and 72 in the ECL1 (Wollscheid et al., 2009). In western blots of brain capillary preparations, a double band for Cldn25 indicates a glycosylation at the BBB *in vivo* (Figure 15). After proof of glycosylation at both positions (Figure 28), YFP tagged Cldn25 lacking either one or both of the glycosylation sites were analyzed for subcellular distribution in HEK-293 cells. *N*-glycosylation at position 72 was found to be essential for localization of Cldn25 at the plasma membrane (Figure 29). This result was confirmed by a significantly reduced localization of YFP tagged Cldn25 wild type or N42Q mutant at the plasma membrane upon treatment of transfected HEK-293 cells with N-Glycosidase F (Figure 30, 31).

Cell membrane glycans are involved in numerous cellular processes like cell signaling and undergo alterations during carcinogenesis. Specific glycan features are associated with epithelial ovarian cancer, namely the “bisecting N-acetyl-glucosamine” type *N*-glycans, increased levels of α 2–6 sialylated *N*-glycans and “N,N’-diacetyllactosamine” type *N*-glycans (Anugraham et al., 2014). Silencing of Cldn25 is reported to induce apoptosis in several breast cancer cell lines (Achari et al., 2015). However, this effect was not found upon knockdown of Cldn25 in bEND.3 cells. No delay in endothelial proliferation was recorded (Figure S 5). These differences might be explained by a function of Cldn25 that is induced by changes of the glycan features during carcinogenesis. *N*-glycans of Cldn25 could be characterized based on molecular mass and tandem MS fragmentation patterns after cleavage using N-Glycosidase F. For this approach, it would be especially of interest to perform immunoprecipitation of Cldn25 in physiological tissues and those undergoing carcinogenesis and to compare the glycan features. In the acute stage of post ischemic reperfusion, the mRNA level of Cldn25 was significantly 1.6-fold increased, but normalized after 48 h (Figure 37). This result

further points to an involvement of Cldn25 in pathology. Despite being highly expressed at the BBB (Figure 13, 17; Table 26), the function of Cldn25 under physiological conditions remains unclear.
In addition to Cldn25, Cldn1 as well as -12 are predicted to be *N*-glycosylated in the ECL1 (Price et al., 2005). However, western blots of brain capillaries have shown predominantly a single band (Figure 15), which further points to glycosylation as a regulated process.

### 5.6.2 Like the classic claudin-1, -4 and -5, claudin-25 associates with *zonula occludens* protein 1, supporting a localization at the plasma membrane

Zo1 is known to associate with the TJ complex via interaction of its PDZ1 domain with the COOH terminus of Cldns (Itoh et al., 1999). The role in recruitment of TJ proteins is yet unclear. In epithelial cells that do not form TJs due to silencing of Zo1 and -2, exogenously expressed Zo1 and -2 are recruited to the junctional area and induce Cldn polymerization (Umeda et al., 2006). A mutation in the PDZ binding motif is reported to lead to intracellular retention and lysosomal mistargeting of Cldn16 (Kausalya et al., 2006; Muller et al., 2003). On the contrary, recombinant Cldns, COOH-terminally tagged with YFP, are hindered to interact with Zo1 but still incorporate into TJs (Piontek et al., 2008). The lack of the PDZ-binding motif is reported not to impair the localization of Cldns at TJs. Only upon truncation of the entire COOH-terminus, Cldns do not incorporate in TJs and accumulate in the cytoplasm (Ruffer and Gerke, 2004).
Despite different agreement to the PDZ binding motif (Table 27), all Cldn COOH-termini bound to Zo1-PDZ1. Cldn5 that exhibits the highest agreement with the Zo1-PDZ1 sequence preference (at position$^{0/\ -1/\ -3/\ -4/\ -6}$) bound with a $K_d$ of 944.6 nM, Cldn4 (at position$^{0/\ -1/\ -3/\ -6}$) with a $K_d$ of 62.6 nM, Cldn1 (at position$^{0/\ -1/\ -3}$) with a $K_d$ of 1007.0 and Cldn25 (at position$^{0}$) with a $K_d$ of 164.2 nM (Figure 32). The binding of Cldn25 to Zo1-PDZ1 was theoretically excluded due to the absence of the conserved PDZ-binding motif (Gunzel and Yu, 2013), but was not significantly different compared to those with higher agreement to the PDZ binding motif (Figure 32). The deletion of alanine at postion$^{+1}$ reduced the binding affinity of Cldn25 around 7-fold, but not significantly. The $K_d$ value of 1164 nM was still in the range of that detected for Cldn1 and -5, which do not exhibit alanine in

postion$^{+1}$. Tyrosine at position$^{-2}$ was critical to bind to Zo1-PDZ1 and its deletion reduced the $K_d$ significantly 22-fold to 3611 nM. This finding is consistent with recent data that describes tyrosine in position$^{-1}$ and not valine in position$^{0}$ as crucial for PDZ1 binding (Wu et al., 2015). The deletion of tyrosine at position$^{-2}$ led to accumulation of transfected YFP tagged Cldn25 in the cytoplasm of MDCK-II and HEK-293 cells. The localization at the plasma membrane was reduced (Figure 34). This finding suggests a contribution of Zo1 to membrane association of Cldn25. In accordance, Cldn25 co-localized with Zo1 in TJs of the BBB (Figure 17).

A recent study found tyrosine in position$^{-6}$ to be critical for the interaction of the COOH-terminus with Zo1-PDZ1. Furthermore, the phosphorylation of this residue is reported to reduce the binding affinity (Nomme et al., 2015). Only nine human Cldns, excluding Cldn1 and -4 exhibit a tyrosine is this position. The sequence of Cldn25 is characterized by a tyrosine at position$^{-8}$. Although the COOH-terminus of Cldn5 exhibits tyrosine at position$^{-6}$, the binding affinity is significantly lower than that of Cldn4. Furthermore, a comparable binding of the COOH-termini of Cldn1-8 is reported and a $K_d$ of 13 nM quantified for Cldn1 (Itoh et al., 1999). Therefore it is questionable if the tyrosine in position$^{-6}$ is crucial for a binding to Zo1-PDZ1.

A cytoplasmic localization of Cldn1 in the brain endothelium (Figure 17, 18, 23) due to competitive association of Cldn subtypes with Zo1 can be excluded due to a $K_d$ comparable to Cldn5 (Figure 32).

## 5.7 Transcriptional up-regulation of claudin-5 after ischemic reperfusion supports re-establishment of the blood-brain barrier and compensates the reduction of claudin-1, -3 -12 and occludin

The disruption of the BBB due to ischemia has been known for a long time (Sandoval and Witt, 2008). Increased permeability is in accordance with a reduction of Cldn5 and Ocln in TJs and Cdh5 in AJs of brain capillaries (Teng et al., 2013; Yang et al., 2007). Previously, a reduction of the mRNA level of *Cldn1, -3, -12* and *Ocln* was found in purified mouse brain capillaries upon exposure to 3 h of hypoxia (Research group for molecular cell physiology, PD Dr. Ingolf E. Blasig, unpublished data). Opening of the BBB upon restriction of oxygen and nutrient supply might support the survival of the surrounding tissue.

In the initial phase, 3 h after ischemic reperfusion, the mRNA expression of *Cldn1, -3, -12* and *Ocln* was down-regulated (-1.3-, -4.3-, -1.7- and -1.3-fold, respectively). Only the mRNA of *Cldn12* was still significantly down-regulated in the final phase, 48 h post reperfusion, although to a lower degree (-1.4-fold). Taken together, the reduction of the mRNA levels of *Cldn1, -3, -12* and *Ocln* 3 h after ischemic reperfusion might be due to restriction of oxygen. Ocln was previously reported to regulate the assembly of TJs redox dependently (Bellmann et al., 2014; Cording et al., 2015). A reduction of Ocln is thereby associated with disruption of the TJ complex. A loss of Cldn3 from TJs of the BBB was previously found in a mouse model of experimental autoimmune encephalomyelitis and in human tissue with glioblastoma multiforme (Wolburg et al., 2003). Reduction of Cldn3, localized at TJs of brain capillaries (Figure 17) might contribute to increased BBB permeability. The consequence of decreased Cldn1 level in the cytoplasm are not yet clear, but a reduction in TJs might also increase permeability with respect to the reported sealing function (Inai et al., 1999). An impact of Cldn12 on BBB permeability is questionable despite constantly reduced mRNA levels in both phases after reperfusion. The incapability of Cldn12 to interact homophilically or heterophilically with Cldns (Krause et al., 2008) suggests a role beyond the typical barrier function of Cldns.

In contrast to the decrease in mRNA expression of TJ proteins, a significant increase of *Cldn5* (1.7-fold) and *Cdh5* transcripts (2.4-fold) was detected in the initial phase after reperfusion. In the final phase after reperfusion, the up-regulation of *Cldn5* (2.1-fold) and *Cdh5* (2.9-fold) was even stronger. Contrastingly, hypoxia is not found to induce up-regulation of both mRNAs (Research group for molecular cell physiology, PD Dr. Ingolf E. Blasig, unpublished data). Therefore, a transcriptional regulation of *Cldn5* and *Cdh5* in response to reperfusion can be assumed. Cdh5 controls the Cldn5 expression through inhibition of the nuclear accumulation of FoxO1 and β-catenin, which are repressors of the Cldn5 promoter (Gavard and Gutkind, 2008). Changes of the nuclear level of FoxO1 and β-catenin during ischemic reperfusion and thereby the impact on the Cldn5 expression remain to be investigated. An increase of the encoded proteins would support the re-establishment of the BBB. Furthermore, Cldn5 might compensate a reduced level of Cldn1, -3, -12 and Ocln in TJs. To further proof these results, the mRNA expression of *Cldn5* and *Cdh5* needs to be

evaluated during ischemia as well as time-dependently in the initial phase of reperfusion. The elevated *Cldn5* mRNA level is crucial to ensure the rapid assembly of TJs. The disassembly during reperfusion could be explained by degradation of Cldn5 at TJs. Both mechanisms together might explain the biphasic permeability upon post ischemic reperfusion, accompanied with regulated disassembly and assembly of TJs at the BBB.

Furthermore, the transcript of *Cldn25* was significantly increased (1.6-fold) in the initial phase, but not in the final phase after reperfusion. It was previously shown that *Cldn25* is regulated by protein kinase-C (PKC)-δ (Achari et al., 2015). PKC-δ is activated under hypoxic conditions (Baek et al., 2001; Kim et al., 2004). An up-regulation of *Cldn25,* hypothetically by PKC-δ in response to ischemia could promote proliferation of endothelial cells as shown for breast cancer cells (Achari et al., 2015). However, a contribution of Cldn25 to cell proliferation was not found in brain endothelial cells under physiological conditions (Figure S 5). A change of the function of Cldn25 with respect to the alteration of glycan features in pathology remains to be investigated as discussed in chapter 5.6.1.

### 5.7.1 Claudin-1 down-regulation in response to ischemia is enhanced upon loss of claudin-3

The strongest mRNA reduction after ischemic reperfusion was found in the initial phase for *Cldn3* (-4.3-fold). Also *Cldn1* mRNA was reduced (-1.3-fold). This reduction of *Cldn1* was drastically enhanced, by 9.6-fold (Figure 38) upon loss of *Cldn3*. A down-regulation of *Cldn1* mRNA was already detected under physiological conditions in brain capillaries of Cldn3 deficient mice (Figure S 10). These results suggest a coupled transcriptional regulation of these Cldn subtypes. Accordingly, a reduced mRNA expression of *Cldn3* was reported upon silencing of Cldn1 in cultured mouse keratinocytes (Tokumasu et al., 2016). The signal transduction pathway involved in regulation of both *Cldns* remains still unclear. Interactions between the encoded proteins are reported. Cldn1 and -3 interact homophilically as well as heterophilically in *cis* and *trans* (Coyne et al., 2003; Furuse et al., 1999).

# 6 Conclusion

Based on mRNA expression, previous studies have speculated about the quantitative contribution of Cldn1, -3, -12 and Ocln to brain endothelial TJs. A major goal of this study was to clarify if the reported dominance of Cldn5 transcripts among all Cldns and TAMPs in the brain endothelium reflects the protein abundance. By use of a novel epitope dilution assay, a correlation was found. Translational regulation did not significantly alter the protein expression of members within the Cldn and TAMP families. Furthermore, TJ proteins were usually chosen as drug targets based on immunohistological stainings. The quantitative comparison of Cldns and TAMPs of the brain endothelial TJ complex is necessary to assess the impact when only a single protein is targeted.

BBB integrity is commonly thought to be maintained by high expression of Cldn5 and its localization in TJs. Upon evaluation of BBB models, cell lines expressing high Cldn5 levels are chosen for further investigations without consideration of other TJ proteins. In this work, it was shown that the transcript abundance of Cldn5 in cultured brain endothelial cells is comparable to *ex vivo*. But *in vitro* BBB models are known to be less impermeable than the BBB *in vivo*. This can be explained by *ex vivo* expression of 16 TJ proteins in the human and mouse brain endothelium, which was drastically reduced upon culturing. Cldn11 was detected in laser-dissected brain capillaries at similar levels like Cldn5. On the contrary, in cell culture, a significant contribution to the formation of TJs can be excluded due to its drastically reduced expression. Drugs designed to target only Cldn5 might affect the paracellular barrier in the brain to a much lesser degree. Cldn11 should be included for future investigations of the BBB, especially with respect to its strong and exclusively homophilic interactions. Furthermore, factors that induce Cldn11 expression remain to be identified and could reveal new therapeutical targets. Besides, the use of mice in BBB research is problematic due to the complexity and quantitative differences of proteins expressed in the brain endothelium compared to human. These proteins include members of the Cldn and TAMP families but also drug transporters. The use of 3D cell cultures of primary human brain endothelial cells might be a more useful model to investigate BBB function e.g. upon treatment with drugs. Microvascular networks, fully

enclosed and perfusable in a bioremodelable hydrogel were recently developed (Morgan et al., 2013) and provide a promising alternative to common BBB models.
Cldn25 is found to be the most abundant TJ protein in the human brain endothelium. Still, the physiological role at the BBB is unclear whereas an involvement in tumor progression was previously described. Alterations of glycan features associated with the ECL1 might induce functional changes that remain to be investigated. Especially due to its high expression, Cldn25 might be a drug target to intervene carcinogenesis of endotheliomas.
During post ischemic reperfusion, transcriptional up-regulation of *Cldn5* supports the re-establishment of TJs that are disassembled and assembled in a phasic manner. *Cldn1, -3, -12* and *Ocln* were down-regulated in the early onset of reperfusion associated with the breakdown of brain endothelial TJs in response to ischemia. These results point to distinct functions of Cldn subtypes in pathology. The analyses of single components of the TJ complex might lead to wrong assumptions and should be expanded with respect the Cldn and TAMP expression profile at the BBB.
In summary, this work breaks with the former belief that the TJs of the BBB are less complex with respect to Cldn expression then those of epithelia. Cldn5 alone cannot reflect the TJ integrity of the BBB under pathological conditions. Furthermore, members of the Cldn family were shown to compensate each other in their expression. Differences in TJ protein expression of mouse and *in vitro* BBB models compared to the human BBB *ex vivo* were revealed. Considering the identification of highly expressed Cldns such as Cldn11, new potential drug targets to modulate the permeability of the BBB were introduced for future BBB research.

## Summary

Claudin (Cldn)-5 is thought to dominate the tight junctions (TJs) of the blood-brain barrier (BBB) with minor contribution of Cldn3, -12 and occludin (Ocln). However, in Cldn5 knockout mice the BBB appears ultrastructurally normal (Nitta et al., 2003). Therefore, the involvement of further Cldns and TJ-associated MARVEL proteins (TAMPs) can be hypothesized. Laser-dissected brain capillaries exhibit a high expression of *Cldn1, -5, -11, -12, -25* and *Ocln*, as well as *Cldn20* and *-26* in mice or *Cldn9* and *-27* in human. Below one percent of total *Cldn/ TAMP* mRNA, tricellulin and 10 further *Cldns* in mice and 9 partially different *Cldns* in human are found. mRNA values correlate with protein expression, quantified by a novel epitope dilution assay. In brain sections, Cldn3, -4, -5, -11, -12, -20 and -25 are enriched at TJs of capillaries. Cldn25 with ~50% of total *Cldn/ TAMP* mRNA, the strongest expressed TJ protein at the human BBB, neither tightens the paracellular barrier nor interconnects opposing cells through loop interactions. But a contribution to the proper TJ strand morphology, possibly through interactions with other TJ associated proteins is found. Despite lack of the typical PDZ binding motif, interaction of Cldn25 with the PDZ1 domain of *zonula occludens* protein 1 is as pronounced as for classic Cldns. Besides, glycosylation of the extracellular loop of Cldn25 is found to be crucial for the localization at the plasma membrane. During post ischemic reperfusion *Cldn5* is transcriptionally up-regulated, supporting a re-establishment of TJs at the BBB. *Cldn1, -3, -12* and *Ocln* are down-regulated in the early phase of reperfusion associated with disassembly of TJs due to ischemia. Inversely, *Cldn1* expression is strongly up-regulated in brain endothelial cells upon silencing of *Cldn5*. Collectively, in the first complete *Cldn/ TAMP* profile, in addition to Cldn5, seven high and eleven low abundant TJ proteins in the brain endothelium become evident and new insights in their interdependent regulation are found. Human and mouse share a common profile *ex vivo* but differ substantially in quantity. Moreover, *in vitro* BBB models of isolated endothelial cells are missing *ex vivo*-complexity and hence, are of limiting informational value. A misconception of the complexity of BBB TJs with respect to Cldn expression was revealed. Furthermore new potential drug targets to modulate the permeability of the BBB were identified.

## Zusammenfassung

Derzeit wird angenommen, dass die Tight Junctions (TJs) der Blut-Hirn-Schranke (BHS) hauptsächlich von Claudin (Cldn)-5 und nur zu geringem Anteil von Cldn3, -12 und Occludin (Ocln) gebildet werden. Die elektronenmikroskopische Analyse der BHS in einem Cldn5 Knockout-Maus Modell zeigt jedoch strukturell normale TJs (Nitta et al., 2003). Daher kann die Beteiligung weiterer Claudine und TJ-assoziierter MARVEL Proteine (TAMPs) angenommen werden. In Gehirnkapillaren, die mittels Laser-Mikrodissektion isoliert wurden, konnte eine relativ starke Expression von *Cldn1, -5, -11, -12, -25* und *Ocln* sowie *Cldn20* und *-26* in der Maus oder *Cldn9* und *-27* im Menschen gefunden werden. Tricellulin sowie 10 weitere Claudine in der Maus und 9 zum Teil andere Claudine im Menschen sind unter einem Prozent der Gesamttranskriptmenge aller Claudine und TAMPs exprimiert. Eine Korrelation von Transkriptmenge und Proteingehalt, welcher mittels einer neuen Epitop Verdünnungsanalyse ermittelt wurde, konnte festgestellt werden. In Hirnschnitten sind Cldn3, -4, -5, -11, -12, -20 und -25 an den TJs von Kapillaren angereichert. Cldn25 ist mit ~50% der Gesamttranskriptmenge aller Claudine und TAMPs das höchst exprimierte TJ Protein der humanen BHS. Es hat weder eine parazellulär abdichtende Funktion, noch trägt es zur Adhäsion benachbarter Zellen durch Assoziation der extrazellulären Schleifen bei. Es konnte allerdings ein Einfluss auf die TJ Strang Morphologie, möglicherweise über Bindung an TJ assoziierte Proteine, nachgewiesen werden. Cldn25 bindet, trotz Abweichung vom PDZ Bindungsmotiv, gleichermaßen an *Zonula Occludens* Protein 1 wie klassische Claudine. Außerdem konnte eine Glykosylierung der ersten extrazellulären Schleife von Cldn25 als essentiell für die Lokalisation in der Plasmamembran identifiziert werden. Bei Reperfusion der Blutgefäße nach zerebraler Ischämie konnte eine Erhöhung der Transkriptmenge von *Cldn5* in Kapillaren festgestellt werden. Erhöhte Synthese von Cldn5 ist für die Bildung neuer TJs erforderlich und erklärt die phasische Entwicklung der BHS Durchlässigkeit. Die mRNAs von *Cldn1, -3, -12* und *Ocln* waren dagegen in der frühen Phase der Reperfusion als Folge zerebraler Ischämie reduziert. In Kultur von Hirnendothelzellen führt die Reduktion von Cldn5 zu einer stark erhöhten Transkription von Cldn1. In dieser Arbeit wurde erstmals die Expression aller Claudine und TAMPs untersucht. Neben Cldn5

konnten sieben stark und elf schwach exprimierte TJ Proteine im Hirnendothel nachgewiesen werden und Hinweise auf eine gegenseitige Regulation gefunden werden. Die BHS von Mensch und Maus ist in ihrer Claudin Komposition vergleichbar, unterscheidet sich aber in der Quantität einzelner TJ Proteine. BHS Modelle isolierter Hirnendothelzellen *in vitro* sind in ihrer Komplexität bezogen auf die TJ Komposition eingeschränkt, weshalb deren Einsetzbarkeit kritisch betrachtet werden sollte.

Die Annahme, dass die TJs der BHS in Bezug auf die Expression von Claudinen weniger komplex als TJs von Epithelien sind, konnte widerlegt werden. Des Weiteren wurden neue Zielproteine für die Modulation der BHS Permeabilität identifiziert.

## Bibliography

Abbott, N.J. 2013. Blood-brain barrier structure and function and the challenges for CNS drug delivery. *Journal of inherited metabolic disease*. 36:437-449.

Abbott, N.J., L. Ronnback, and E. Hansson. 2006. Astrocyte-endothelial interactions at the blood-brain barrier. *Nature reviews. Neuroscience*. 7:41-53.

Achari, C., S. Winslow, and C. Larsson. 2015. Down Regulation of CLDND1 Induces Apoptosis in Breast Cancer Cells. *PloS one*. 10:e0130300.

Acharya, P., J. Beckel, W.G. Ruiz, E. Wang, R. Rojas, L. Birder, and G. Apodaca. 2004. Distribution of the tight junction proteins ZO-1, occludin, and claudin-4, -8, and -12 in bladder epithelium. *American journal of physiology. Renal physiology*. 287:F305-318.

Amasheh, M., A. Fromm, S.M. Krug, S. Amasheh, S. Andres, M. Zeitz, M. Fromm, and J.D. Schulzke. 2010. TNFalpha-induced and berberine-antagonized tight junction barrier impairment via tyrosine kinase, Akt and NFkappaB signaling. *Journal of cell science*. 123:4145-4155.

Amasheh, S., N. Meiri, A.H. Gitter, T. Schoneberg, J. Mankertz, J.D. Schulzke, and M. Fromm. 2002. Claudin-2 expression induces cation-selective channels in tight junctions of epithelial cells. *Journal of cell science*. 115:4969-4976.

Anugraham, M., F. Jacob, S. Nixdorf, A.V. Everest-Dass, V. Heinzelmann-Schwarz, and N.H. Packer. 2014. Specific glycosylation of membrane proteins in epithelial ovarian cancer cell lines: glycan structures reflect gene expression and DNA methylation status. *Molecular & cellular proteomics : MCP*. 13:2213-2232.

Aslam, M., N. Ahmad, R. Srivastava, and B. Hemmer. 2012. TNF-alpha induced NFkappaB signaling and p65 (RelA) overexpression repress Cldn5 promoter in mouse brain endothelial cells. *Cytokine*. 57:269-275.

Baek, S.H., U.Y. Lee, E.M. Park, M.Y. Han, Y.S. Lee, and Y.M. Park. 2001. Role of protein kinase Cdelta in transmitting hypoxia signal to HSF and HIF-1. *Journal of cellular physiology*. 188:223-235.

Bai, Y., G. Xu, M. Xu, Q. Li, and X. Qin. 2014. Inhibition of Src phosphorylation reduces damage to the blood-brain barrier following transient focal cerebral ischemia in rats. *International journal of molecular medicine*. 34:1473-1482.

Balbuena, P., W. Li, and M. Ehrich. 2011. Assessments of tight junction proteins occludin, claudin 5 and scaffold proteins ZO1 and ZO2 in endothelial cells of the rat blood-brain barrier: cellular responses to neurotoxicants malathion and lead acetate. *Neurotoxicology*. 32:58-67.

Balda, M.S., J.A. Whitney, C. Flores, S. Gonzalez, M. Cereijido, and K. Matter. 1996. Functional dissociation of paracellular permeability and transepithelial electrical resistance and disruption of the apical-basolateral intramembrane diffusion barrier by expression of a mutant tight junction membrane protein. *The Journal of cell biology*. 134:1031-1049.

Ballabh, P., A. Braun, and M. Nedergaard. 2004. The blood-brain barrier: an overview: structure, regulation, and clinical implications. *Neurobiology of disease*. 16:1-13.

Ban, Y., A. Dota, L.J. Cooper, N.J. Fullwood, T. Nakamura, M. Tsuzuki, C. Mochida, and S. Kinoshita. 2003. Tight junction-related protein expression and distribution in human corneal epithelium. *Experimental eye research*. 76:663-669.

Bazzoni, G., and E. Dejana. 2004. Endothelial cell-to-cell junctions: molecular organization and role in vascular homeostasis. *Physiological reviews*. 84:869-901.

Begley, D.J., and M.W. Brightman. 2003. Structural and functional aspects of the blood-brain barrier. *Progress in drug research. Fortschritte der Arzneimittelforschung. Progres des recherches pharmaceutiques*. 61:39-78.

Bellmann, C., S. Schreivogel, R. Gunther, S. Dabrowski, M. Schumann, H. Wolburg, and I.E. Blasig. 2014. Highly conserved cysteines are involved in the oligomerization of occludin-redox dependency of the second extracellular loop. *Antioxidants & redox signaling*. 20:855-867.

Ben-Yosef, T., I.A. Belyantseva, T.L. Saunders, E.D. Hughes, K. Kawamoto, C.M. Van Itallie, L.A. Beyer, K. Halsey, D.J. Gardner, E.R. Wilcox, J. Rasmussen, J.M. Anderson, D.F. Dolan, A. Forge, Y. Raphael, S.A. Camper, and T.B. Friedman. 2003. Claudin 14 knockout mice, a model for

autosomal recessive deafness DFNB29, are deaf due to cochlear hair cell degeneration. *Human molecular genetics*. 12:2049-2061.

Blasig, I.E., L. Winkler, B. Lassowski, S.L. Mueller, N. Zuleger, E. Krause, G. Krause, K. Gast, M. Kolbe, and J. Piontek. 2006. On the self-association potential of transmembrane tight junction proteins. *Cellular and molecular life sciences : CMLS*. 63:505-514.

Bocsik, A., F.R. Walter, A. Gyebrovszki, L. Fulop, I. Blasig, S. Dabrowski, F. Otvos, A. Toth, G. Rakhely, S. Veszelka, M. Vastag, P. Szabo-Revesz, and M.A. Deli. 2016. Reversible Opening of Intercellular Junctions of Intestinal Epithelial and Brain Endothelial Cells With Tight Junction Modulator Peptides. *Journal of pharmaceutical sciences*. 105:754-765.

Boussif, O., F. Lezoualc'h, M.A. Zanta, M.D. Mergny, D. Scherman, B. Demeneix, and J.P. Behr. 1995. A versatile vector for gene and oligonucleotide transfer into cells in culture and in vivo: polyethylenimine. *Proceedings of the National Academy of Sciences of the United States of America*. 92:7297-7301.

Brown, R.C., K.S. Mark, R.D. Egleton, J.D. Huber, A.R. Burroughs, and T.P. Davis. 2003. Protection against hypoxia-induced increase in blood-brain barrier permeability: role of tight junction proteins and NFkappaB. *Journal of cell science*. 116:693-700.

Brown, R.C., A.P. Morris, and R.G. O'Neil. 2007. Tight junction protein expression and barrier properties of immortalized mouse brain microvessel endothelial cells. *Brain research*. 1130:17-30.

Bustin, S.A. 2000. Absolute quantification of mRNA using real-time reverse transcription polymerase chain reaction assays. *Journal of molecular endocrinology*. 25:169-193.

Butt, A.M., H.C. Jones, and N.J. Abbott. 1990. Electrical resistance across the blood-brain barrier in anaesthetized rats: a developmental study. *The Journal of physiology*. 429:47-62.

Buzza, M.S., S. Netzel-Arnett, T. Shea-Donohue, A. Zhao, C.Y. Lin, K. List, R. Szabo, A. Fasano, T.H. Bugge, and T.M. Antalis. 2010. Membrane-anchored serine protease matriptase regulates epithelial barrier formation and permeability in the intestine. *Proceedings of the National Academy of Sciences of the United States of America*. 107:4200-4205.

Clark, P.R., R.K. Kim, J.S. Pober, and M.S. Kluger. 2015. Tumor necrosis factor disrupts claudin-5 endothelial tight junction barriers in two distinct NF-kappaB-dependent phases. *PloS one*. 10:e0120075.

Colegio, O.R., C.M. Van Itallie, H.J. McCrea, C. Rahner, and J.M. Anderson. 2002. Claudins create charge-selective channels in the paracellular pathway between epithelial cells. *American journal of physiology. Cell physiology*. 283:C142-147.

Cording, J., J. Berg, N. Kading, C. Bellmann, C. Tscheik, J.K. Westphal, S. Milatz, D. Gunzel, H. Wolburg, J. Piontek, O. Huber, and I.E. Blasig. 2013. In tight junctions, claudins regulate the interactions between occludin, tricellulin and marvelD3, which, inversely, modulate claudin oligomerization. *Journal of cell science*. 126:554-564.

Cording, J., R. Gunther, E. Vigolo, C. Tscheik, L. Winkler, I. Schlattner, D. Lorenz, R.F. Haseloff, K.M. Schmidt-Ott, H. Wolburg, and I.E. Blasig. 2015. Redox Regulation of Cell Contacts by Tricellulin and Occludin: Redox-Sensitive Cysteine Sites in Tricellulin Regulate Both Tri- and Bicellular Junctions in Tissue Barriers as Shown in Hypoxia and Ischemia. *Antioxidants & redox signaling*. 23:1035-1049.

Correale, J., and A. Villa. 2007. The blood-brain-barrier in multiple sclerosis: functional roles and therapeutic targeting. *Autoimmunity*. 40:148-160.

Coyne, C.B., T.M. Gambling, R.C. Boucher, J.L. Carson, and L.G. Johnson. 2003. Role of claudin interactions in airway tight junctional permeability. *American journal of physiology. Lung cellular and molecular physiology*. 285:L1166-1178.

Cserr, H.F., and M. Bundgaard. 1984. Blood-brain interfaces in vertebrates: a comparative approach. *The American journal of physiology*. 246:R277-288.

Cummings, R.D., and J.M. Pierce. 2014. The challenge and promise of glycomics. *Chemistry & biology*. 21:1-15.

Dabrowski, S., C. Staat, D. Zwanziger, R.S. Sauer, C. Bellmann, R. Gunther, E. Krause, R.F. Haseloff, H. Rittner, and I.E. Blasig. 2015. Redox-sensitive structure and function of the first extracellular loop of the cell-cell contact protein claudin-1: lessons from molecular structure to animals. *Antioxidants & redox signaling*. 22:1-14.

Daneman, R. 2012. The blood-brain barrier in health and disease. *Annals of neurology*. 72:648-672.

Daneman, R., and A. Prat. 2015. The blood-brain barrier. *Cold Spring Harbor perspectives in biology*. 7:a020412.

Daneman, R., L. Zhou, D. Agalliu, J.D. Cahoy, A. Kaushal, and B.A. Barres. 2010. The mouse blood-brain barrier transcriptome: a new resource for understanding the development and function of brain endothelial cells. *PloS one*. 5:e13741.

Daugherty, B.L., C. Ward, T. Smith, J.D. Ritzenthaler, and M. Koval. 2007. Regulation of heterotypic claudin compatibility. *The Journal of biological chemistry*. 282:30005-30013.

Dawe, G.B., M. Musgaard, E.D. Andrews, B.A. Daniels, M.R. Aurousseau, P.C. Biggin, and D. Bowie. 2013. Defining the structural relationship between kainate-receptor deactivation and desensitization. *Nature structural & molecular biology*. 20:1054-1061.

Ebnet, K., C.U. Schulz, M.K. Meyer Zu Brickwedde, G.G. Pendl, and D. Vestweber. 2000. Junctional adhesion molecule interacts with the PDZ domain-containing proteins AF-6 and ZO-1. *The Journal of biological chemistry*. 275:27979-27988.

Engel, O., S. Kolodziej, U. Dirnagl, and V. Prinz. 2011. Modeling stroke in mice - middle cerebral artery occlusion with the filament model. *Journal of visualized experiments : JoVE*.

Epple, H.J., T. Schneider, H. Troeger, D. Kunkel, K. Allers, V. Moos, M. Amasheh, C. Loddenkemper, M. Fromm, M. Zeitz, and J.D. Schulzke. 2009. Impairment of the intestinal barrier is evident in untreated but absent in suppressively treated HIV-infected patients. *Gut*. 58:220-227.

Fanning, A.S., and J.M. Anderson. 1996. Protein-protein interactions: PDZ domain networks. *Current biology : CB*. 6:1385-1388.

Fanning, A.S., B.J. Jameson, L.A. Jesaitis, and J.M. Anderson. 1998. The tight junction protein ZO-1 establishes a link between the transmembrane protein occludin and the actin cytoskeleton. *The Journal of biological chemistry*. 273:29745-29753.

Fanning, A.S., C.M. Van Itallie, and J.M. Anderson. 2012. Zonula occludens-1 and -2 regulate apical cell structure and the zonula adherens cytoskeleton in polarized epithelia. *Molecular biology of the cell*. 23:577-590.

Furuse, M., K. Fujita, T. Hiiragi, K. Fujimoto, and S. Tsukita. 1998a. Claudin-1 and -2: novel integral membrane proteins localizing at tight junctions with no sequence similarity to occludin. *The Journal of cell biology*. 141:1539-1550.

Furuse, M., T. Hirase, M. Itoh, A. Nagafuchi, S. Yonemura, S. Tsukita, and S. Tsukita. 1993. Occludin: a novel integral membrane protein localizing at tight junctions. *The Journal of cell biology*. 123:1777-1788.

Furuse, M., M. Itoh, T. Hirase, A. Nagafuchi, S. Yonemura, S. Tsukita, and S. Tsukita. 1994. Direct association of occludin with ZO-1 and its possible involvement in the localization of occludin at tight junctions. *The Journal of cell biology*. 127:1617-1626.

Furuse, M., H. Sasaki, K. Fujimoto, and S. Tsukita. 1998b. A single gene product, claudin-1 or -2, reconstitutes tight junction strands and recruits occludin in fibroblasts. *The Journal of cell biology*. 143:391-401.

Furuse, M., H. Sasaki, and S. Tsukita. 1999. Manner of interaction of heterogeneous claudin species within and between tight junction strands. *The Journal of cell biology*. 147:891-903.

Gan, H., G. Wang, Q. Hao, Q.J. Wang, and H. Tang. 2013. Protein kinase D promotes airway epithelial barrier dysfunction and permeability through down-regulation of claudin-1. *The Journal of biological chemistry*. 288:37343-37354.

Gavard, J., and J.S. Gutkind. 2008. VE-cadherin and claudin-5: it takes two to tango. *Nature cell biology*. 10:883-885.

Geer, L.Y., A. Marchler-Bauer, R.C. Geer, L. Han, J. He, S. He, C. Liu, W. Shi, and S.H. Bryant. 2010. The NCBI BioSystems database. *Nucleic acids research*. 38:D492-496.

Gonzalez-Mariscal, L., A. Betanzos, P. Nava, and B.E. Jaramillo. 2003. Tight junction proteins. *Progress in biophysics and molecular biology*. 81:1-44.

Gow, A., C.M. Southwood, J.S. Li, M. Pariali, G.P. Riordan, S.E. Brodie, J. Danias, J.M. Bronstein, B. Kachar, and R.A. Lazzarini. 1999. CNS myelin and sertoli cell tight junction strands are absent in Osp/claudin-11 null mice. *Cell*. 99:649-659.

Gunzel, D., S. Amasheh, S. Pfaffenbach, J.F. Richter, P.J. Kausalya, W. Hunziker, and M. Fromm. 2009. Claudin-16 affects transcellular Cl- secretion in MDCK cells. *The Journal of physiology*. 587:3777-3793.

Gunzel, D., and A.S. Yu. 2013. Claudins and the modulation of tight junction permeability. *Physiological reviews*. 93:525-569.

Hanahan, D. 1985. Techniques for transformation of E. Coli. In DNA cloning: A Practical Approach *IRL Press*. 1:109-135.

Hanisch, F.G., and I. Breloy. 2009. Protein-specific glycosylation: signal patches and cis-controlling peptidic elements. *Biological chemistry*. 390:619-626.

Haskins, J., L. Gu, E.S. Wittchen, J. Hibbard, and B.R. Stevenson. 1998. ZO-3, a novel member of the MAGUK protein family found at the tight junction, interacts with ZO-1 and occludin. *The Journal of cell biology*. 141:199-208.

Hawkins, B.T., and T.P. Davis. 2005. The blood-brain barrier/neurovascular unit in health and disease. *Pharmacological reviews*. 57:173-185.

Hawkins, B.T., S. Grego, and K.L. Sellgren. 2015. Three-dimensional culture conditions differentially affect astrocyte modulation of brain endothelial barrier function in response to transforming growth factor beta1. *Brain research*. 1608:167-176.

Heo, J.H., S.W. Han, and S.K. Lee. 2005. Free radicals as triggers of brain edema formation after stroke. *Free radical biology & medicine*. 39:51-70.

Heye, A.K., R.D. Culling, C. Valdes Hernandez Mdel, M.J. Thrippleton, and J.M. Wardlaw. 2014. Assessment of blood-brain barrier disruption using dynamic contrast-enhanced MRI. A systematic review. *NeuroImage. Clinical*. 6:262-274.

Hoshi, Y., Y. Uchida, M. Tachikawa, T. Inoue, S. Ohtsuki, and T. Terasaki. 2013. Quantitative atlas of blood-brain barrier transporters, receptors, and tight junction proteins in rats and common marmoset. *Journal of pharmaceutical sciences*. 102:3343-3355.

Hou, J., A.S. Gomes, D.L. Paul, and D.A. Goodenough. 2006. Study of claudin function by RNA interference. *J Biol Chem*. 281:36117-36123.

Hou, J., A. Renigunta, M. Konrad, A.S. Gomes, E.E. Schneeberger, D.L. Paul, S. Waldegger, and D.A. Goodenough. 2008. Claudin-16 and claudin-19 interact and form a cation-selective tight junction complex. *The Journal of clinical investigation*. 118:619-628.

Hou, J., A. Renigunta, J. Yang, and S. Waldegger. 2010. Claudin-4 forms paracellular chloride channel in the kidney and requires claudin-8 for tight junction localization. *Proceedings of the National Academy of Sciences of the United States of America*. 107:18010-18015.

Huang, J., U.M. Upadhyay, and R.J. Tamargo. 2006. Inflammation in stroke and focal cerebral ischemia. *Surgical neurology*. 66:232-245.

Ikenouchi, J., M. Furuse, K. Furuse, H. Sasaki, S. Tsukita, and S. Tsukita. 2005. Tricellulin constitutes a novel barrier at tricellular contacts of epithelial cells. *The Journal of cell biology*. 171:939-945.

Inai, T., J. Kobayashi, and Y. Shibata. 1999. Claudin-1 contributes to the epithelial barrier function in MDCK cells. *European journal of cell biology*. 78:849-855.

Ito, K., Y. Uchida, S. Ohtsuki, S. Aizawa, H. Kawakami, Y. Katsukura, J. Kamiie, and T. Terasaki. 2011. Quantitative membrane protein expression at the blood-brain barrier of adult and younger cynomolgus monkeys. *Journal of pharmaceutical sciences*. 100:3939-3950.

Itoh, M., M. Furuse, K. Morita, K. Kubota, M. Saitou, and S. Tsukita. 1999. Direct binding of three tight junction-associated MAGUKs, ZO-1, ZO-2, and ZO-3, with the COOH termini of claudins. *The Journal of cell biology*. 147:1351-1363.

Iwamoto, N., T. Higashi, and M. Furuse. 2014. Localization of angulin-1/LSR and tricellulin at tricellular contacts of brain and retinal endothelial cells in vivo. *Cell structure and function*. 39:1-8.

Jerabek-Willemsen, M., T. André, R. Wanner, H.M. Roth, S. Duhr, P. Baaske, and D. Breitsprecher. 2014. MicroScale Thermophoresis: Interaction analysis and beyond. *Journal of Molecular Structure*. 1077:101-113.

Jovov, B., C.M. Van Itallie, N.J. Shaheen, J.L. Carson, T.M. Gambling, J.M. Anderson, and R.C. Orlando. 2007. Claudin-18: a dominant tight junction protein in Barrett's esophagus and likely contributor to its acid resistance. *American journal of physiology. Gastrointestinal and liver physiology*. 293:G1106-1113.

Kaempf, N., G. Kochlamazashvili, D. Puchkov, T. Maritzen, S.M. Bajjalieh, N.L. Kononenko, and V. Haucke. 2015. Overlapping functions of stonin 2 and SV2 in sorting of the calcium sensor synaptotagmin 1 to synaptic vesicles.

*Proceedings of the National Academy of Sciences of the United States of America*. 112:7297-7302.

Kaplan, H.A., J.K. Welply, and W.J. Lennarz. 1987. Oligosaccharyl transferase: the central enzyme in the pathway of glycoprotein assembly. *Biochimica et biophysica acta*. 906:161-173.

Katsuno, T., K. Umeda, T. Matsui, M. Hata, A. Tamura, M. Itoh, K. Takeuchi, T. Fujimori, Y. Nabeshima, T. Noda, S. Tsukita, and S. Tsukita. 2008. Deficiency of zonula occludens-1 causes embryonic lethal phenotype associated with defected yolk sac angiogenesis and apoptosis of embryonic cells. *Molecular biology of the cell*. 19:2465-2475.

Kausalya, P.J., S. Amasheh, D. Gunzel, H. Wurps, D. Muller, M. Fromm, and W. Hunziker. 2006. Disease-associated mutations affect intracellular traffic and paracellular Mg2+ transport function of Claudin-16. *The Journal of clinical investigation*. 116:878-891.

Kim, E., M. Niethammer, A. Rothschild, Y.N. Jan, and M. Sheng. 1995. Clustering of Shaker-type K+ channels by interaction with a family of membrane-associated guanylate kinases. *Nature*. 378:85-88.

Kim, M.J., C.H. Moon, M.Y. Kim, M.H. Kim, S.H. Lee, E.J. Baik, and Y.S. Jung. 2004. Role of PKC-delta during hypoxia in heart-derived H9c2 cells. *The Japanese journal of physiology*. 54:405-414.

Kooij, G., K. Kopplin, R. Blasig, M. Stuiver, N. Koning, G. Goverse, S.M. van der Pol, B. van Het Hof, M. Gollasch, J.A. Drexhage, A. Reijerkerk, I.C. Meij, R. Mebius, T.E. Willnow, D. Muller, I.E. Blasig, and H.E. de Vries. 2014. Disturbed function of the blood-cerebrospinal fluid barrier aggravates neuro-inflammation. *Acta neuropathologica*. 128:267-277.

Koto, T., K. Takubo, S. Ishida, H. Shinoda, M. Inoue, K. Tsubota, Y. Okada, and E. Ikeda. 2007. Hypoxia disrupts the barrier function of neural blood vessels through changes in the expression of claudin-5 in endothelial cells. *The American journal of pathology*. 170:1389-1397.

Kratzer, I., A. Vasiljevic, C. Rey, M. Fevre-Montange, N. Saunders, N. Strazielle, and J.F. Ghersi-Egea. 2012. Complexity and developmental changes in the expression pattern of claudins at the blood-CSF barrier. *Histochemistry and cell biology*. 138:861-879.

Krause, G., L. Winkler, S.L. Mueller, R.F. Haseloff, J. Piontek, and I.E. Blasig. 2008. Structure and function of claudins. *Biochimica et biophysica acta*. 1778:631-645.

Krause, G., L. Winkler, C. Piehl, I. Blasig, J. Piontek, and S.L. Muller. 2009. Structure and function of extracellular claudin domains. *Annals of the New York Academy of Sciences*. 1165:34-43.

Krug, S.M., S. Amasheh, J.F. Richter, S. Milatz, D. Gunzel, J.K. Westphal, O. Huber, J.D. Schulzke, and M. Fromm. 2009. Tricellulin forms a barrier to macromolecules in tricellular tight junctions without affecting ion permeability. *Molecular biology of the cell*. 20:3713-3724.

Krug, S.M., D. Gunzel, M.P. Conrad, R. Rosenthal, A. Fromm, S. Amasheh, J.D. Schulzke, and M. Fromm. 2012. Claudin-17 forms tight junction channels with distinct anion selectivity. *Cellular and molecular life sciences : CMLS*. 69:2765-2778.

Kuroiwa, T., P. Ting, H. Martinez, and I. Klatzo. 1985. The biphasic opening of the blood-brain barrier to proteins following temporary middle cerebral artery occlusion. *Acta neuropathologica*. 68:122-129.

Lewandowsky, M. 1900. Zur Lehre der Cerebrospinalflüssigkeit. *Z. Klin. Med.* 40:480-494.

Li, L., D.W. McBride, D. Doycheva, B.J. Dixon, P.R. Krafft, J.H. Zhang, and J. Tang. 2015. G-CSF attenuates neuroinflammation and stabilizes the blood-brain barrier via the PI3K/Akt/GSK-3beta signaling pathway following neonatal hypoxia-ischemia in rats. *Experimental neurology*. 272:135-144.

Li, Y., A.S. Fanning, J.M. Anderson, and A. Lavie. 2005. Structure of the conserved cytoplasmic C-terminal domain of occludin: identification of the ZO-1 binding surface. *Journal of molecular biology*. 352:151-164.

Liu, F., M. Koval, S. Ranganathan, S. Fanayan, W.S. Hancock, E.K. Lundberg, R.C. Beavis, L. Lane, P. Duek, L. McQuade, N.L. Kelleher, and M.S. Baker. 2016. Systems Proteomics View of the Endogenous Human Claudin Protein Family. *Journal of proteome research*. 15:339-359.

Liu, J., X. Jin, K.J. Liu, and W. Liu. 2012. Matrix metalloproteinase-2-mediated occludin degradation and caveolin-1-mediated claudin-5 redistribution contribute to blood-brain barrier damage in early ischemic stroke stage. *The*

*Journal of neuroscience : the official journal of the Society for Neuroscience*. 32:3044-3057.

Liu, W., J. Hendren, X.J. Qin, J. Shen, and K.J. Liu. 2009. Normobaric hyperoxia attenuates early blood-brain barrier disruption by inhibiting MMP-9-mediated occludin degradation in focal cerebral ischemia. *Journal of neurochemistry*. 108:811-820.

Mandel, I., T. Paperna, A. Volkowich, M. Merhav, L. Glass-Marmor, and A. Miller. 2012. The ubiquitin-proteasome pathway regulates claudin 5 degradation. *Journal of cellular biochemistry*. 113:2415-2423.

Mandell, K.J., I.C. McCall, and C.A. Parkos. 2004. Involvement of the junctional adhesion molecule-1 (JAM1) homodimer interface in regulation of epithelial barrier function. *The Journal of biological chemistry*. 279:16254-16262.

Mao, X., L. Xie, R.B. Greenberg, J.B. Greenberg, B. Peng, I. Mieling, K. Jin, and D.A. Greenberg. 2014. Flow-induced regulation of brain endothelial cells in vitro. *Vascular pharmacology*. 62:82-87.

Mariano, C., I. Palmela, P. Pereira, A. Fernandes, A.S. Falcao, F.L. Cardoso, A.R. Vaz, A.R. Campos, A. Goncalves-Ferreira, K.S. Kim, D. Brites, and M.A. Brito. 2013. Tricellulin expression in brain endothelial and neural cells. *Cell and tissue research*. 351:397-407.

Marshall, R.D. 1972. Glycoproteins. *Annual review of biochemistry*. 41:673-702.

Martin, T.A., J. Lane, H. Ozupek, and W.G. Jiang. 2013. Claudin-20 promotes an aggressive phenotype in human breast cancer cells. *Tissue barriers*. 1:e26518.

McCabe, M.J., C.F. Foo, M.E. Dinger, P.M. Smooker, and P.G. Stanton. 2016. Claudin-11 and occludin are major contributors to Sertoli cell tight junction function, in vitro. *Asian journal of andrology*. 18:620-626.

McCarthy, K.M., I.B. Skare, M.C. Stankewich, M. Furuse, S. Tsukita, R.A. Rogers, R.D. Lynch, and E.E. Schneeberger. 1996. Occludin is a functional component of the tight junction. *Journal of cell science*. 109 ( Pt 9):2287-2298.

Milatz, S., S.M. Krug, R. Rosenthal, D. Gunzel, D. Muller, J.D. Schulzke, S. Amasheh, and M. Fromm. 2010. Claudin-3 acts as a sealing component of the tight junction for ions of either charge and uncharged solutes. *Biochimica et biophysica acta*. 1798:2048-2057.

Mineta, K., Y. Yamamoto, Y. Yamazaki, H. Tanaka, Y. Tada, K. Saito, A. Tamura, M. Igarashi, T. Endo, K. Takeuchi, and S. Tsukita. 2011. Predicted expansion of the claudin multigene family. *FEBS letters*. 585:606-612.

Mitic, L.L., C.M. Van Itallie, and J.M. Anderson. 2000. Molecular physiology and pathophysiology of tight junctions I. Tight junction structure and function: lessons from mutant animals and proteins. *American journal of physiology. Gastrointestinal and liver physiology*. 279:G250-254.

Mojsilovic-Petrovic, J., M. Nesic, A. Pen, W. Zhang, and D. Stanimirovic. 2004. Development of rapid staining protocols for laser-capture microdissection of brain vessels from human and rat coupled to gene expression analyses. *Journal of neuroscience methods*. 133:39-48.

Moremen, K.W., M. Tiemeyer, and A.V. Nairn. 2012. Vertebrate protein glycosylation: diversity, synthesis and function. *Nature reviews. Molecular cell biology*. 13:448-462.

Morgan, J.P., P.F. Delnero, Y. Zheng, S.S. Verbridge, J. Chen, M. Craven, N.W. Choi, A. Diaz-Santana, P. Kermani, B. Hempstead, J.A. Lopez, T.N. Corso, C. Fischbach, and A.D. Stroock. 2013. Formation of microvascular networks in vitro. *Nature protocols*. 8:1820-1836.

Morita, K., M. Furuse, K. Fujimoto, and S. Tsukita. 1999a. Claudin multigene family encoding four-transmembrane domain protein components of tight junction strands. *Proceedings of the National Academy of Sciences of the United States of America*. 96:511-516.

Morita, K., H. Sasaki, K. Fujimoto, M. Furuse, and S. Tsukita. 1999b. Claudin-11/OSP-based tight junctions of myelin sheaths in brain and Sertoli cells in testis. *The Journal of cell biology*. 145:579-588.

Morita, K., H. Sasaki, M. Furuse, and S. Tsukita. 1999c. Endothelial claudin: claudin-5/TMVCF constitutes tight junction strands in endothelial cells. *The Journal of cell biology*. 147:185-194.

Muller, D., P.J. Kausalya, F. Claverie-Martin, I.C. Meij, P. Eggert, V. Garcia-Nieto, and W. Hunziker. 2003. A novel claudin 16 mutation associated with childhood hypercalciuria abolishes binding to ZO-1 and results in lysosomal mistargeting. *American journal of human genetics*. 73:1293-1301.

Muller, S.L., M. Portwich, A. Schmidt, D.I. Utepbergenov, O. Huber, I.E. Blasig, and G. Krause. 2005. The tight junction protein occludin and the adherens

junction protein alpha-catenin share a common interaction mechanism with ZO-1. *The Journal of biological chemistry*. 280:3747-3756.

Ni, C., C. Wang, J. Zhang, L. Qu, X. Liu, Y. Lu, W. Yang, J. Deng, D. Lorenz, P. Gao, Q. Meng, X. Yan, I.E. Blasig, and Z. Qin. 2014. Interferon-gamma safeguards blood-brain barrier during experimental autoimmune encephalomyelitis. *The American journal of pathology*. 184:3308-3320.

Nitta, T., M. Hata, S. Gotoh, Y. Seo, H. Sasaki, N. Hashimoto, M. Furuse, and S. Tsukita. 2003. Size-selective loosening of the blood-brain barrier in claudin-5-deficient mice. *The Journal of cell biology*. 161:653-660.

Nomme, J., A. Antanasijevic, M. Caffrey, C.M. Van Itallie, J.M. Anderson, A.S. Fanning, and A. Lavie. 2015. Structural Basis of a Key Factor Regulating the Affinity between the Zonula Occludens First PDZ Domain and Claudins. *The Journal of biological chemistry*. 290:16595-16606.

Oby, E., and D. Janigro. 2006. The blood-brain barrier and epilepsy. *Epilepsia*. 47:1761-1774.

Ohtsuki, S., S. Sato, H. Yamaguchi, M. Kamoi, T. Asashima, and T. Terasaki. 2007. Exogenous expression of claudin-5 induces barrier properties in cultured rat brain capillary endothelial cells. *Journal of cellular physiology*. 210:81-86.

Ohtsuki, S., H. Yamaguchi, Y. Katsukura, T. Asashima, and T. Terasaki. 2008. mRNA expression levels of tight junction protein genes in mouse brain capillary endothelial cells highly purified by magnetic cell sorting. *Journal of neurochemistry*. 104:147-154.

Overgaard, C.E., L.A. Mitchell, and M. Koval. 2012. Roles for claudins in alveolar epithelial barrier function. *Annals of the New York Academy of Sciences*. 1257:167-174.

Oyagi, A., N. Morimoto, J. Hamanaka, M. Ishiguro, K. Tsuruma, M. Shimazawa, and H. Hara. 2011. Forebrain specific heparin-binding epidermal growth factor-like growth factor knockout mice show exacerbated ischemia and reperfusion injury. *Neuroscience*. 185:116-124.

Pardridge, W.M. 2003. Blood-brain barrier drug targeting: the future of brain drug development. *Molecular interventions*. 3:90-105, 151.

Pardridge, W.M. 2007. Blood-brain barrier delivery. *Drug discovery today*. 12:54-61.

Patton, W.F., M.R. Dhanak, and B.S. Jacobson. 1989. Differential partitioning of plasma membrane proteins into the triton X-100-insoluble cytoskeleton fraction during concanavalin A-induced receptor redistribution. *Journal of cell science*. 92 ( Pt 1):85-91.

Piehl, C., J. Piontek, J. Cording, H. Wolburg, and I.E. Blasig. 2010. Participation of the second extracellular loop of claudin-5 in paracellular tightening against ions, small and large molecules. *Cellular and molecular life sciences : CMLS*. 67:2131-2140.

Piontek, J., S. Fritzsche, J. Cording, S. Richter, J. Hartwig, M. Walter, D. Yu, J.R. Turner, C. Gehring, H.P. Rahn, H. Wolburg, and I.E. Blasig. 2011. Elucidating the principles of the molecular organization of heteropolymeric tight junction strands. *Cellular and molecular life sciences : CMLS*. 68:3903-3918.

Piontek, J., L. Winkler, H. Wolburg, S.L. Muller, N. Zuleger, C. Piehl, B. Wiesner, G. Krause, and I.E. Blasig. 2008. Formation of tight junction: determinants of homophilic interaction between classic claudins. *FASEB journal : official publication of the Federation of American Societies for Experimental Biology*. 22:146-158.

Podjaski, C., J.I. Alvarez, L. Bourbonniere, S. Larouche, S. Terouz, J.M. Bin, M.A. Lecuyer, O. Saint-Laurent, C. Larochelle, P.J. Darlington, N. Arbour, J.P. Antel, T.E. Kennedy, and A. Prat. 2015. Netrin 1 regulates blood-brain barrier function and neuroinflammation. *Brain : a journal of neurology*. 138:1598-1612.

Price, M.G., C.F. Davis, F. Deng, and D.L. Burgess. 2005. The alpha-amino-3-hydroxyl-5-methyl-4-isoxazolepropionate receptor trafficking regulator "stargazin" is related to the claudin family of proteins by Its ability to mediate cell-cell adhesion. *The Journal of biological chemistry*. 280:19711-19720.

Raleigh, D.R., A.M. Marchiando, Y. Zhang, L. Shen, H. Sasaki, Y. Wang, M. Long, and J.R. Turner. 2010. Tight junction-associated MARVEL proteins marveld3, tricellulin, and occludin have distinct but overlapping functions. *Molecular biology of the cell*. 21:1200-1213.

Ruffer, C., and V. Gerke. 2004. The C-terminal cytoplasmic tail of claudins 1 and 5 but not its PDZ-binding motif is required for apical localization at epithelial and endothelial tight junctions. *European journal of cell biology*. 83:135-144.

S. Rozen, and H. Skaletsky. 2000. Primer3 on the WWW for general users and for biologist programmers. *Bioinformatics Methods and Protocols: Methods in Molecular Biology*:365-386.

Sandoval, K.E., and K.A. Witt. 2008. Blood-brain barrier tight junction permeability and ischemic stroke. *Neurobiology of disease*. 32:200-219.

Sas, D., M. Hu, O.W. Moe, and M. Baum. 2008. Effect of claudins 6 and 9 on paracellular permeability in MDCK II cells. *American journal of physiology. Regulatory, integrative and comparative physiology*. 295:R1713-1719.

Seidel, S.A., P.M. Dijkman, W.A. Lea, G. van den Bogaart, M. Jerabek-Willemsen, A. Lazic, J.S. Joseph, P. Srinivasan, P. Baaske, A. Simeonov, I. Katritch, F.A. Melo, J.E. Ladbury, G. Schreiber, A. Watts, D. Braun, and S. Duhr. 2013. Microscale thermophoresis quantifies biomolecular interactions under previously challenging conditions. *Methods (San Diego, Calif.)*. 59:301-315.

Shawahna, R., Y. Uchida, X. Decleves, S. Ohtsuki, S. Yousif, S. Dauchy, A. Jacob, F. Chassoux, C. Daumas-Duport, P.O. Couraud, T. Terasaki, and J.M. Scherrmann. 2011. Transcriptomic and quantitative proteomic analysis of transporters and drug metabolizing enzymes in freshly isolated human brain microvessels. *Molecular pharmaceutics*. 8:1332-1341.

Shi, Y., L. Zhang, H. Pu, L. Mao, X. Hu, X. Jiang, N. Xu, R.A. Stetler, F. Zhang, X. Liu, R.K. Leak, R.F. Keep, X. Ji, and J. Chen. 2016. Rapid endothelial cytoskeletal reorganization enables early blood-brain barrier disruption and long-term ischaemic reperfusion brain injury. *Nature communications*. 7:10523.

Sonenberg, N., and A.G. Hinnebusch. 2009. Regulation of translation initiation in eukaryotes: mechanisms and biological targets. *Cell*. 136:731-745.

Spiro, R.G. 2002. Protein glycosylation: nature, distribution, enzymatic formation, and disease implications of glycopeptide bonds. *Glycobiology*. 12:43R-56R.

Staat, C., C. Coisne, S. Dabrowski, S.M. Stamatovic, A.V. Andjelkovic, H. Wolburg, B. Engelhardt, and I.E. Blasig. 2015. Mode of action of claudin peptidomimetics in the transient opening of cellular tight junction barriers. *Biomaterials*. 54:9-20.

Staehelin, L.A. 1974. Structure and function of intercellular junctions. *International review of cytology*. 39:191-283.

Stowell, S.R., T. Ju, and R.D. Cummings. 2015. Protein glycosylation in cancer. *Annual review of pathology*. 10:473-510.

Studier, F.W., A.H. Rosenberg, J.J. Dunn, and J.W. Dubendorff. 1990. Use of T7 RNA polymerase to direct expression of cloned genes. *Methods in enzymology*. 185:60-89.

Szulcek, R., H.J. Bogaard, and G.P. van Nieuw Amerongen. 2014. Electric cell-substrate impedance sensing for the quantification of endothelial proliferation, barrier function, and motility. *Journal of visualized experiments : JoVE*.

Tamura, A., Y. Kitano, M. Hata, T. Katsuno, K. Moriwaki, H. Sasaki, H. Hayashi, Y. Suzuki, T. Noda, M. Furuse, S. Tsukita, and S. Tsukita. 2008. Megaintestine in claudin-15-deficient mice. *Gastroenterology*. 134:523-534.

Tanaka, H., Y. Yamamoto, H. Kashihara, Y. Yamazaki, K. Tani, Y. Fujiyoshi, K. Mineta, K. Takeuchi, A. Tamura, and S. Tsukita. 2016. Claudin-21 Has a Paracellular Channel Role at Tight Junctions. *Mol Cell Biol*. 36:954-964.

Tanaka, M., R. Kamata, and R. Sakai. 2005. EphA2 phosphorylates the cytoplasmic tail of Claudin-4 and mediates paracellular permeability. *The Journal of biological chemistry*. 280:42375-42382.

Teng, F., V. Beray-Berthat, B. Coqueran, C. Lesbats, M. Kuntz, B. Palmier, M. Garraud, C. Bedfert, N. Slane, V. Berezowski, F. Szeremeta, J. Hachani, D. Scherman, M. Plotkine, B.T. Doan, C. Marchand-Leroux, and I. Margaill. 2013. Prevention of rt-PA induced blood-brain barrier component degradation by the poly(ADP-ribose)polymerase inhibitor PJ34 after ischemic stroke in mice. *Experimental neurology*. 248:416-428.

Tokumasu, R., K. Yamaga, Y. Yamazaki, H. Murota, K. Suzuki, A. Tamura, K. Bando, Y. Furuta, I. Katayama, and S. Tsukita. 2016. Dose-dependent role of claudin-1 in vivo in orchestrating features of atopic dermatitis. *Proc Natl Acad Sci U S A*. 113:E4061-4068.

Tominaga, N., N. Kosaka, M. Ono, T. Katsuda, Y. Yoshioka, K. Tamura, J. Lotvall, H. Nakagama, and T. Ochiya. 2015. Brain metastatic cancer cells release microRNA-181c-containing extracellular vesicles capable of destructing blood-brain barrier. *Nature communications*. 6:6716.

Uchida, Y., S. Ohtsuki, Y. Katsukura, C. Ikeda, T. Suzuki, J. Kamiie, and T. Terasaki. 2011. Quantitative targeted absolute proteomics of human blood-brain barrier transporters and receptors. *Journal of neurochemistry*. 117:333-345.

Umeda, K., J. Ikenouchi, S. Katahira-Tayama, K. Furuse, H. Sasaki, M. Nakayama, T. Matsui, S. Tsukita, M. Furuse, and S. Tsukita. 2006. ZO-1 and ZO-2 independently determine where claudins are polymerized in tight-junction strand formation. *Cell*. 126:741-754.

Urich, E., S.E. Lazic, J. Molnos, I. Wells, and P.O. Freskgard. 2012. Transcriptional profiling of human brain endothelial cells reveals key properties crucial for predictive in vitro blood-brain barrier models. *PloS one*. 7:e38149.

Van Itallie, C., C. Rahner, and J.M. Anderson. 2001. Regulated expression of claudin-4 decreases paracellular conductance through a selective decrease in sodium permeability. *The Journal of clinical investigation*. 107:1319-1327.

Van Itallie, C.M., and J.M. Anderson. 2014. Architecture of tight junctions and principles of molecular composition. *Seminars in cell & developmental biology*. 36:157-165.

Van Itallie, C.M., A.S. Fanning, A. Bridges, and J.M. Anderson. 2009. ZO-1 stabilizes the tight junction solute barrier through coupling to the perijunctional cytoskeleton. *Molecular biology of the cell*. 20:3930-3940.

Van Itallie, C.M., T.M. Gambling, J.L. Carson, and J.M. Anderson. 2005. Palmitoylation of claudins is required for efficient tight-junction localization. *Journal of cell science*. 118:1427-1436.

Van Itallie, C.M., S. Rogan, A. Yu, L.S. Vidal, J. Holmes, and J.M. Anderson. 2006. Two splice variants of claudin-10 in the kidney create paracellular pores with different ion selectivities. *American journal of physiology. Renal physiology*. 291:F1288-1299.

Wang, C.X., and A. Shuaib. 2007. Critical role of microvasculature basal lamina in ischemic brain injury. *Progress in neurobiology*. 83:140-148.

Wang, L., X. Zhang, L. Liu, L. Cui, R. Yang, M. Li, and W. Du. 2010. Tanshinone II A down-regulates HMGB1, RAGE, TLR4, NF-kappaB expression, ameliorates BBB permeability and endothelial cell function, and protects rat brains against focal ischemia. *Brain research*. 1321:143-151.

Watanabe, T., S. Dohgu, F. Takata, T. Nishioku, A. Nakashima, K. Futagami, A. Yamauchi, and Y. Kataoka. 2013. Paracellular barrier and tight junction protein expression in the immortalized brain endothelial cell lines bEND.3, bEND.5 and mouse brain endothelial cell 4. *Biological & pharmaceutical bulletin*. 36:492-495.

Wen, H., D.D. Watry, M.C. Marcondes, and H.S. Fox. 2004. Selective decrease in paracellular conductance of tight junctions: role of the first extracellular domain of claudin-5. *Molecular and cellular biology*. 24:8408-8417.

Wittchen, E.S., J. Haskins, and B.R. Stevenson. 1999. Protein interactions at the tight junction. Actin has multiple binding partners, and ZO-1 forms independent complexes with ZO-2 and ZO-3. *The Journal of biological chemistry*. 274:35179-35185.

Wolburg, H., K. Wolburg-Buchholz, J. Kraus, G. Rascher-Eggstein, S. Liebner, S. Hamm, F. Duffner, E.H. Grote, W. Risau, and B. Engelhardt. 2003. Localization of claudin-3 in tight junctions of the blood-brain barrier is selectively lost during experimental autoimmune encephalomyelitis and human glioblastoma multiforme. *Acta neuropathologica*. 105:586-592.

Wollscheid, B., D. Bausch-Fluck, C. Henderson, R. O'Brien, M. Bibel, R. Schiess, R. Aebersold, and J.D. Watts. 2009. Mass-spectrometric identification and relative quantification of N-linked cell surface glycoproteins. *Nature biotechnology*. 27:378-386.

Wu, J., D. Peng, Y. Zhang, Z. Lu, M. Voehler, C.R. Sanders, and J. Li. 2015. Biophysical characterization of interactions between the C-termini of peripheral nerve claudins and the PDZ(1) domain of zonula occludens. *Biochemical and biophysical research communications*. 459:87-93.

Yang, Y., E.Y. Estrada, J.F. Thompson, W. Liu, and G.A. Rosenberg. 2007. Matrix metalloproteinase-mediated disruption of tight junction proteins in cerebral vessels is reversed by synthetic matrix metalloproteinase inhibitor in focal ischemia in rat. *Journal of cerebral blood flow and metabolism : official journal of the International Society of Cerebral Blood Flow and Metabolism*. 27:697-709.

Yang, Y., and G.A. Rosenberg. 2011. MMP-mediated disruption of claudin-5 in the blood-brain barrier of rat brain after cerebral ischemia. *Methods in molecular biology*. 762:333-345.

Yu, A.S., K.M. McCarthy, S.A. Francis, J.M. McCormack, J. Lai, R.A. Rogers, R.D. Lynch, and E.E. Schneeberger. 2005. Knockdown of occludin expression leads to diverse phenotypic alterations in epithelial cells. *American journal of physiology. Cell physiology*. 288:C1231-1241.

Yu, J.G., R.R. Zhou, and G.J. Cai. 2011. From hypertension to stroke: mechanisms and potential prevention strategies. *CNS neuroscience & therapeutics*. 17:577-584.

Zhang, Y., S. Yeh, B.A. Appleton, H.A. Held, P.J. Kausalya, D.C. Phua, W.L. Wong, L.A. Lasky, C. Wiesmann, W. Hunziker, and S.S. Sidhu. 2006. Convergent and divergent ligand specificity among PDZ domains of the LAP and zonula occludens (ZO) families. *The Journal of biological chemistry*. 281:22299-22311.

Zlokovic, B.V. 2008. The blood-brain barrier in health and chronic neurodegenerative disorders. *Neuron*. 57:178-201.

# List of publications

## Oral presentations at scientific conferences

Berndt P, Cording J, Rausch V, Breitkreuz-Korff V, Rex A, Zhang J, Wolburg H, Haseloff RF, Blasig R, Blasig IE, Winkler L. Quantification of claudins and TAMPs in the human and mouse brain endothelium, International conference tight junctions and their proteins, Berlin, 2016**.**

## Poster presentations at scientific conferences

Berndt P, Cording J, Rausch V, Breitkreuz-Korff V, Rex A, Zhang J, Wolburg H, Haseloff RF, Blasig R, Blasig IE, Winkler L. Quantification of claudins and TAMPs in the human and mouse brain endothelium, International conference tight junctions and their proteins, Berlin, 2016.

Berndt P, Blasig R, Meyer H, Blasig IE, Winkler L. Quantification of tight junction forming claudins in the brain endothelium, International Conference on Cerebral Vascular Biology, Paris, 2015.

Berndt P, Winkler L, Blasig IE. Claudin expression in tight junctions of the blood-brain barrier, Berlin Neuroscience Forum, Berlin, 2014.

## Curriculum vitae

For reasons of data protection, the curriculum vitae is not published in the electronic version.

# Supplemental data

**Table S 1 mRNA levels in the human and mouse brain endothelium determined via qRT-PCR (mRNA expression [$2^{\Delta Ct}$]).** Expression in laser-dissected human and mouse brain capillaries, purified mouse brain capillaries, primary mouse brain capillary endothelial cells (primary bEND) and bEND.3, an endothelial cell line of the mouse cerebral cortex. mRNA normalized to β-actin (*Actb*) ($\Delta Ct = Ct_{target} - Ct_{Actb}$). Mean ± SD; n ≥ 4; # not found in human; ## no primer for mCldn21 (Table 11); „n.d.“, not detectable. *Cldn*, claudin; *Tric*, tricellulin; *Ocln*, occludin; *Zo1*, *zonula occludens* protein 1; *Cdh5*, cadherin-5 (VE-cadherin). Grayscale indicates the order of magnitude relative to *Ocln* expression in laser-dissected brain capillaries within the same species.

| | **human** laser dissected brain capillaries | | **mouse** laser dissected brain capillaries | | purified brain capillaries | | primary bEND | | bEND.3 | |
|---|---|---|---|---|---|---|---|---|---|---|
| ***Ocln*** | 1.64E-03 | ±2.04E-03 | 1.08E-02 | ±4.02E-03 | 5.76E-03 | ±1.00E-03 | 1.26E-02 | ±1.63E-02 | 1.12E-03 | ±9.08E-04 |
| ***Cldn1*** | 3.00E-03 | ±4.20E-03 | 4.43E-03 | ±4.55E-03 | 3.59E-03 | ±1.60E-03 | 4.69E-04 | ±2.60E-04 | 2.13E-06 | ±8.57E-07 |
| ***Cldn2*** | 1.26E-04 | ±1.58E-04 | 1.48E-04 | ±1.58E-04 | 1.73E-03 | ±9.37E-04 | 7.02E-05 | ±7.20E-05 | 9.45E-07 | ±3.93E-07 |
| ***Cldn3*** | 6.08E-04 | ±7.60E-04 | 4.73E-04 | ±3.14E-04 | 1.40E-04 | ±6.23E-05 | 3.89E-05 | ±1.33E-05 | 3.85E-06 | ±1.51E-06 |
| ***Cldn4*** | 4.43E-04 | ±3.51E-04 | 4.23E-04 | ±5.21E-04 | 4.88E-04 | ±6.95E-04 | 7.24E-04 | ±5.70E-04 | 7.65E-06 | ±5.70E-06 |
| ***Cldn5*** | 2.05E-02 | ±1.81E-02 | 7.26E-02 | ±1.88E-02 | 1.02E-01 | ±2.69E-02 | 5.75E-02 | ±6.06E-02 | 1.33E-01 | ±3.83E-02 |
| ***Cldn6*** | 7.51E-04 | ±5.53E-04 | 1.31E-04 | ±1.21E-04 | 8.17E-05 | ±7.65E-05 | 1.69E-04 | ±1.76E-04 | 2.33E-05 | ±1.40E-05 |
| ***Cldn7*** | n.d. | | n.d. | | n.d. | | n.d. | | n.d. | |
| ***Cldn8*** | n.d. | | n.d. | | 5.36E-05 | ±9.63E-06 | n.d. | | 2.67E-06 | ±1.26E-06 |
| ***Cldn9*** | 1.34E-03 | ±2.18E-03 | 3.99E-04 | ±1.12E-04 | 1.14E-04 | ±5.48E-05 | 4.05E-06 | ±3.67E-06 | 3.55E-06 | ±1.71E-06 |
| ***Cldn10*** | n.d. | | n.d. | | n.d. | | n.d. | | n.d. | |
| ***Cldn11*** | 1.62E-02 | ±8.40E-03 | 5.72E-02 | ±3.42E-02 | 3.14E-04 | ±3.08E-04 | 2.23E-06 | ±2.33E-06 | 8.83E-07 | ±3.63E-07 |
| ***Cldn12*** | 1.14E-02 | ±5.05E-03 | 1.63E-02 | ±1.23E-02 | 1.30E-03 | ±4.44E-04 | 1.29E-03 | ±3.73E-04 | 1.04E-03 | ±1.64E-04 |
| ***Cldn13*** | # | | n.d. | | 5.52E-05 | ±1.46E-05 | 5.58E-06 | ±4.44E-06 | 1.42E-06 | ±7.31E-07 |
| ***Cldn14*** | n.d. | | 1.77E-03 | ±1.72E-03 | 5.06E-05 | ±2.34E-05 | 5.75E-07 | ±2.50E-07 | 1.07E-06 | ±6.67E-07 |
| ***Cldn15*** | 6.13E-04 | ±3.38E-04 | 8.06E-05 | ±7.91E-05 | 2.03E-05 | ±1.53E-05 | 6.20E-05 | ±3.25E-05 | 2.14E-03 | ±1.00E-03 |
| ***Cldn16*** | n.d. | | n.d. | | n.d. | | n.d. | | n.d. | |
| ***Cldn17*** | 5.85E-04 | ±1.06E-03 | 8.22E-04 | ±4.85E-04 | 1.24E-04 | ±3.08E-05 | 3.10E-06 | ±1.88E-06 | 1.31E-05 | ±5.31E-06 |
| ***Cldn18*** | n.d. | | n.d. | | n.d. | | n.d. | | 1.96E-06 | ±1.00E-06 |
| ***Cldn19*** | n.d. | | n.d. | | n.d. | | n.d. | | n.d. | |
| ***Cldn20*** | 3.35E-04 | ±9.46E-05 | 8.47E-03 | ±5.22E-03 | 1.70E-04 | ±1.86E-04 | 1.95E-05 | ±1.60E-05 | 2.19E-05 | ±7.63E-06 |
| ***Cldn21*** | n.d. | | ## | | n.d. | | n.d. | | n.d. | |
| ***Cldn22*** | 3.95E-04 | ±2.46E-04 | 1.24E-03 | ±6.73E-04 | 9.55E-05 | ±1.57E-05 | 7.13E-05 | ±2.06E-05 | 5.06E-05 | ±1.73E-05 |
| ***Cldn23*** | 1.59E-04 | ±1.33E-04 | n.d. | | 2.02E-05 | ±5.67E-06 | 2.78E-06 | ±1.74E-06 | 1.08E-05 | ±4.10E-06 |
| ***Cldn24*** | n.d. | | 1.70E-03 | ±2.03E-03 | 6.39E-04 | ±4.58E-04 | 9.11E-05 | ±6.24E-05 | 3.28E-05 | ±1.20E-05 |
| ***Cldn25*** | 6.36E-02 | ±2.44E-02 | 1.72E-02 | ±1.17E-02 | 4.37E-03 | ±1.98E-03 | 2.95E-03 | ±9.21E-04 | 2.35E-03 | ±1.86E-04 |
| ***Cldn26*** | n.d. | | 1.48E-03 | ±1.01E-03 | n.d. | | n.d. | | n.d. | |
| ***Cldn27*** | 7.75E-03 | ±1.14E-02 | n.d. | | n.d. | | n.d. | | n.d. | |
| ***Tric*** | 2.80E-04 | ±2.86E-04 | 3.02E-04 | ±2.93E-04 | 3.85E-04 | ±1.78E-04 | 4.11E-05 | ±1.23E-05 | 3.42E-06 | ±8.59E-07 |
| ***Marveld3*** | n.d. | | n.d. | | n.d. | | n.d. | | n.d. | |
| ***Zo1*** | 7.93E-03 | ±1.60E-03 | 1.79E-02 | ±1.31E-02 | 4.85E-03 | ±1.86E-03 | 2.18E-02 | ±2.06E-02 | 1.77E-02 | ±5.28E-03 |
| ***Cdh5*** | 1.45E-03 | ±1.02E-03 | 1.27E-02 | ±5.28E-03 | 1.56E-01 | ±4.73E-02 | 2.71E-01 | ±1.69E-01 | 2.52E-01 | ±5.32E-02 |

| $\geq 10^{1} \cdot [2^{\Delta Ct}]_{Ocln}$ | $> 10^{0} \cdot [2^{\Delta Ct}]_{Ocln}$ | $\leq 10^{0} \cdot [2^{\Delta Ct}]_{Ocln}$ | $\leq 10^{-1} \cdot [2^{\Delta Ct}]_{Ocln}$ | $\leq 10^{-2} \cdot [2^{\Delta Ct}]_{Ocln}$ | $\leq 10^{-3} \cdot [2^{\Delta Ct}]_{Ocln}$ | $\leq 10^{-4} \cdot [2^{\Delta Ct}]_{Ocln}$ |
|---|---|---|---|---|---|---|

**Table S 2 Molalities of claudins and occludin in purified mouse brain capillaries.** CLDN, claudin; OCLN, occludin; sol, Triton X-100 soluble lysate fraction; insol, Triton X-100 insoluble lysate fraction; m, slope; s, degree of purity; BLU, biochemical light units; mass, [ng]; mass concentration, [ng/µl]; molar concentration, [mol/µl]; molality, [fmol/µg]. Superscripted numbers indicate the respective equation used to determine the values (Chapter 3.5.9).

| | m | [kDa] MBP-epitope | s MBP-epitope | [µg/µl] lysate | [µl]lysate | [BLU] | [1][ng] | [2][ng/µl] | [3][mol/µl] | [4][fmol/µg] |
|---|---|---|---|---|---|---|---|---|---|---|
| CLDN1 $A_{insol}$ | 1220.7 | 45.83 | 0.47 | 0.80 | 15 | 7308 | 2.79 | 0.19 | 4.05E-15 | 5.06 |
| CLDN1 $A_{sol}$ | 1220.7 | 45.83 | 0.47 | 0.80 | 15 | 24675 | 9.41 | 0.63 | 1.37E-14 | 17.08 |
| CLDN1 $B_{insol}$ | 2011.8 | 45.83 | 0.47 | 2.68 | 10 | 50853 | 11.76 | 1.18 | 2.57E-14 | 9.56 |
| CLDN1 $B_{sol}$ | 2011.8 | 45.83 | 0.47 | 2.68 | 10 | 7705 | 1.78 | 0.18 | 3.89E-15 | 1.45 |
| CLDN1 $C_{insol}$ | 1492.6 | 45.83 | 0.47 | 0.81 | 15 | 34724 | 10.82 | 0.72 | 1.57E-14 | 19.54 |
| CLDN1 $C_{sol}$ | 1492.6 | 45.83 | 0.47 | 0.81 | 15 | 1187 | 0.37 | 0.02 | 5.38E-16 | 0.67 |
| CLDN1 $D_{insol}$ | 857.9 | 45.83 | 0.47 | 0.71 | 15 | 4151 | 2.25 | 0.15 | 3.28E-15 | 4.64 |
| CLDN1 $D_{sol}$ | 857.9 | 45.83 | 0.47 | 0.71 | 15 | 153 | 0.08 | 0.01 | 1.21E-16 | 0.17 |
| CLDN4 $A_{insol}$ | 10132.0 | 45.74 | 0.79 | 0.81 | 20 | 16696 | 1.31 | 0.07 | 1.43E-15 | 1.77 |
| CLDN4 $A_{sol}$ | 10132.0 | 45.74 | 0.79 | 0.81 | 20 | 47380 | 3.71 | 0.19 | 4.06E-15 | 5.03 |
| CLDN4 $B_{insol}$ | 13010.0 | 45.74 | 0.79 | 0.71 | 20 | 4489 | 0.27 | 0.01 | 2.99E-16 | 0.42 |
| CLDN4 $B_{sol}$ | 13010.0 | 45.74 | 0.79 | 0.71 | 20 | 41914 | 2.56 | 0.13 | 2.79E-15 | 3.96 |
| CLDN4 $C_{insol}$ | 22772.0 | 45.74 | 0.79 | 2.68 | 10 | 50269 | 1.75 | 0.18 | 3.83E-15 | 1.43 |
| CLDN4 $C_{sol}$ | 22772.0 | 45.74 | 0.79 | 2.68 | 10 | 144250 | 5.03 | 0.50 | 1.10E-14 | 4.09 |
| CLDN4 $D_{insol}$ | 6097.9 | 45.74 | 0.79 | 0.80 | 20 | 39402 | 5.13 | 0.26 | 5.60E-15 | 7.00 |
| CLDN4 $D_{sol}$ | 6097.9 | 45.74 | 0.79 | 0.80 | 20 | 132807 | 17.28 | 0.86 | 1.89E-14 | 23.59 |
| CLDN5 $A_{insol}$ | 586.9 | 46.99 | 0.38 | 0.80 | 5 | 24832 | 16.00 | 3.20 | 6.81E-14 | 85.01 |
| CLDN5 $A_{sol}$ | 128.0 | 46.99 | 0.38 | 0.80 | 5 | 37346 | 110.29 | 22.06 | 4.69E-13 | 586.08 |
| CLDN5 $B_{insol}$ | 586.9 | 46.99 | 0.38 | 0.71 | 5 | 32828 | 21.15 | 4.23 | 9.00E-14 | 127.42 |
| CLDN5 $B_{sol}$ | 128.0 | 46.99 | 0.38 | 0.71 | 5 | 38761 | 114.47 | 22.89 | 4.87E-13 | 689.65 |
| CLDN5 $C_{insol}$ | 487.3 | 46.99 | 0.38 | 2.68 | 5 | 27153 | 21.07 | 4.21 | 8.97E-14 | 33.40 |
| CLDN5 $C_{sol}$ | 121.3 | 46.99 | 0.38 | 2.68 | 5 | 13496 | 42.06 | 8.41 | 1.79E-13 | 66.67 |
| CLDN5 $D_{insol}$ | 487.3 | 46.99 | 0.38 | 0.81 | 5 | 50864 | 39.47 | 7.89 | 1.68E-13 | 208.50 |
| CLDN5 $D_{sol}$ | 121.3 | 46.99 | 0.38 | 0.81 | 5 | 14505 | 45.20 | 9.04 | 1.92E-13 | 238.80 |
| CLDN11 $A_{insol}$ | 1090.9 | 46.07 | 1.00 | 1.90 | 30 | 750 | 0.69 | 0.02 | 4.97E-16 | 0.26 |
| CLDN11 $A_{sol}$ | 1090.9 | 46.07 | 1.00 | 1.90 | 30 | 1601 | 1.47 | 0.05 | 1.06E-15 | 0.56 |
| CLDN11 $B_{insol}$ | 2052.3 | 46.07 | 1.00 | 2.68 | 18 | 46502 | 22.66 | 1.26 | 2.73E-14 | 10.18 |
| CLDN11 $B_{sol}$ | 2052.3 | 46.07 | 1.00 | 2.68 | 25 | 21326 | 10.39 | 0.42 | 9.02E-15 | 3.36 |
| CLDN11 $C_{insol}$ | 1810.2 | 46.07 | 1.00 | 0.71 | 15 | 7220 | 3.99 | 0.27 | 5.77E-15 | 8.17 |
| CLDN11 $C_{sol}$ | 1810.2 | 46.07 | 1.00 | 0.71 | 15 | 1239 | 0.68 | 0.05 | 9.90E-16 | 1.40 |
| CLDN11 $D_{insol}$ | 4556.8 | 46.07 | 1.00 | 0.80 | 10 | 10765 | 2.36 | 0.24 | 5.13E-15 | 6.40 |
| CLDN11 $D_{sol}$ | 4556.8 | 46.07 | 1.00 | 0.80 | 7 | 1763 | 0.39 | 0.06 | 1.20E-15 | 1.50 |
| CLDN12 $A_{insol}$ | 934.7 | 48.06 | 0.13 | 2.68 | 10 | 0 | 0.00 | 0.00 | 0.00E+00 | 0.00 |
| CLDN12 $A_{sol}$ | 934.7 | 48.06 | 0.13 | 2.68 | 10 | 27118 | 3.89 | 0.39 | 8.09E-15 | 3.01 |
| CLDN12 $B_{insol}$ | 161.9 | 48.06 | 0.13 | 0.95 | 20 | 0 | 0.00 | 0.00 | 0.00E+00 | 0.00 |
| CLDN12 $B_{sol}$ | 161.9 | 48.06 | 0.13 | 0.95 | 20 | 4108 | 3.40 | 0.17 | 3.54E-15 | 3.72 |
| CLDN12 $C_{insol}$ | 161.9 | 48.06 | 0.13 | 0.84 | 20 | 0 | 0.00 | 0.00 | 0.00E+00 | 0.00 |
| CLDN12 $C_{sol}$ | 161.9 | 48.06 | 0.13 | 0.84 | 20 | 9014 | 7.46 | 0.37 | 7.76E-15 | 9.28 |
| CLDN12 $D_{insol}$ | 882.8 | 48.06 | 0.13 | 0.81 | 20 | 0 | 0.00 | 0.00 | 0.00E+00 | 0.00 |
| CLDN12 $D_{sol}$ | 882.8 | 48.06 | 0.13 | 0.81 | 20 | 5993 | 0.91 | 0.05 | 9.46E-16 | 1.17 |
| CLDN25 $A_{insol}$ | 415.1 | 58.10 | 1.00 | 2.68 | 10 | 27319 | 65.82 | 6.58 | 1.13E-13 | 42.20 |
| CLDN25 $A_{sol}$ | 415.1 | 58.10 | 1.00 | 2.68 | 10 | 0 | 0.00 | 0.00 | 0.00E+00 | 0.00 |
| CLDN25 $B_{insol}$ | 619.6 | 58.10 | 1.00 | 0.81 | 10 | 14465 | 23.35 | 2.33 | 4.02E-14 | 49.88 |

| | | | | | | | | | | |
|---|---|---|---|---|---|---|---|---|---|---|
| CLDN25 $B_{sol}$ | 619.6 | 58.10 | 1.00 | 0.81 | 10 | 0 | 0.00 | 0.00 | 0.00E+00 | 0.00 |
| CLDN25 $C_{insol}$ | 16.2 | 58.10 | 1.00 | 1.11 | 20 | 5590 | 344.53 | 17.23 | 2.97E-13 | 266.46 |
| CLDN25 $C_{sol}$ | 16.2 | 58.10 | 1.00 | 1.11 | 20 | 0 | 0.00 | 0.00 | 0.00E+00 | 0.00 |
| CLDN25 $D_{insol}$ | 50.9 | 58.10 | 1.00 | 1.90 | 18 | 3291 | 64.65 | 3.59 | 6.18E-14 | 32.46 |
| CLDN25 $D_{sol}$ | 50.9 | 58.10 | 1.00 | 1.90 | 20 | 0 | 0.00 | 0.00 | 0.00E+00 | 0.00 |
| OCLN $A_{insol}$ | 454.2 | 56.98 | 0.99 | 0.84 | 10 | 7482 | 16.32 | 1.63 | 2.86E-14 | 34.22 |
| OCLN $A_{sol}$ | 454.2 | 56.98 | 0.99 | 0.84 | 10 | 2179 | 4.75 | 0.48 | 8.34E-15 | 9.97 |
| OCLN $B_{insol}$ | 647.1 | 56.98 | 0.99 | 0.95 | 10 | 11154 | 17.08 | 1.71 | 3.00E-14 | 31.52 |
| OCLN $B_{sol}$ | 647.1 | 56.98 | 0.99 | 0.95 | 10 | 4402 | 6.74 | 0.67 | 1.18E-14 | 12.44 |
| OCLN $C_{insol}$ | 500.7 | 56.98 | 0.99 | 2.68 | 10 | 19739 | 39.06 | 3.91 | 6.85E-14 | 25.53 |
| OCLN $C_{sol}$ | 500.7 | 56.98 | 0.99 | 2.68 | 10 | 9638 | 19.07 | 1.91 | 3.35E-14 | 12.47 |
| OCLN $D_{insol}$ | 798.5 | 56.98 | 0.99 | 0.81 | 10 | 5468 | 6.78 | 0.68 | 1.19E-14 | 14.78 |
| OCLN $D_{sol}$ | 798.5 | 56.98 | 0.99 | 0.81 | 10 | 1242 | 1.54 | 0.15 | 2.70E-15 | 3.36 |

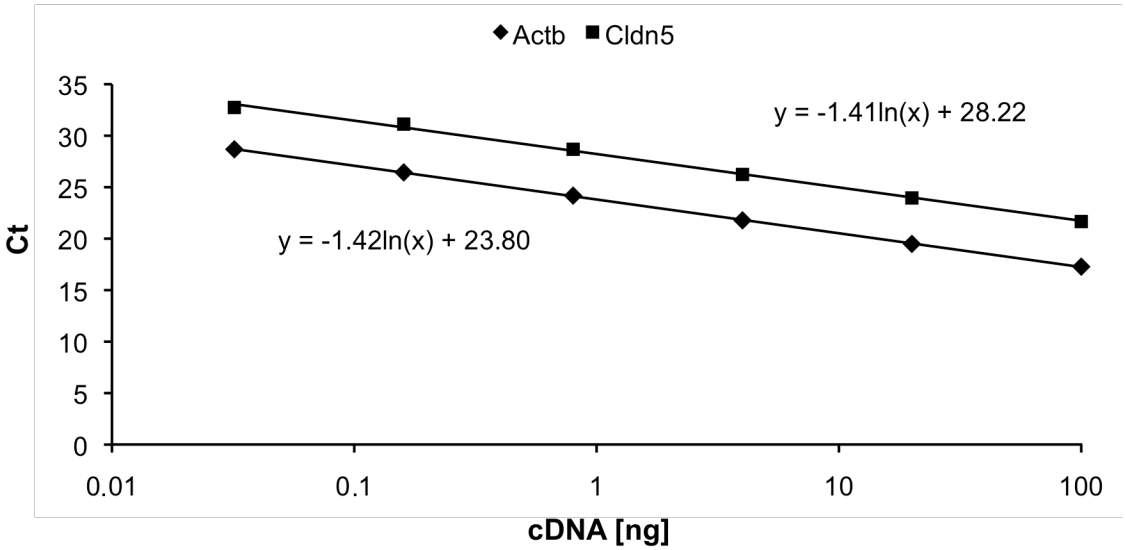


**Figure S 1 Primer efficiency test.** Primer efficiency (P) = $10^{(-1 \cdot \log10(e) / m)}$; m, slope; Ct, cycle threshold; Actb, ß-actin; Cldn, claudin. $P_{ActB}$ = 2.02; $P_{Cldn5}$ = 2.03 (P = 2, amplification efficiency 100%). Further tested primer efficiencies: $P_{Cldn10}$ = 2.04; $P_{Cldn12}$ = 1.95. cDNA, mouse kidney.

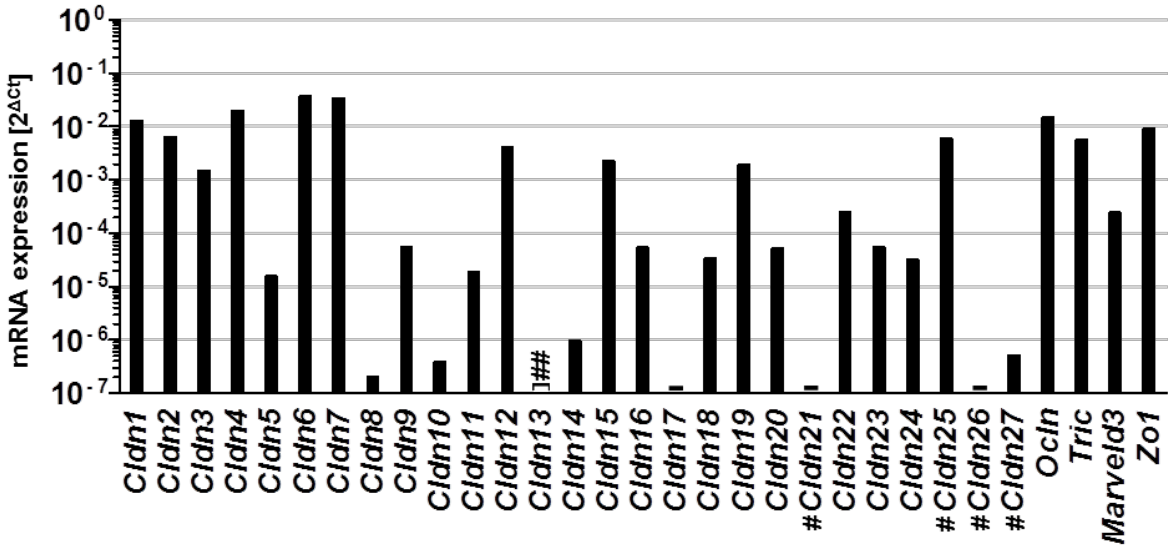


**Figure S 2 In Caco-2 (human colon epithelial cells), a higher level of pore forming claudins is detected compared to the brain endothelium.** mRNA normalized to β-actin (*Actb*), ($\Delta Ct = Ct_{target} - Ct_{Actb}$), (Ct, cycle threshold). „-“, not detectable. Mean, n = 2. # synonyms: *Cldn21*, putative *Cldn25*; *Cldn25*, *Cldnd1*; *Cldn26*, *Tmem114*; *Cldn27*, *Tmem235*; ## not coded in human. *Cldn*, claudin; *Tric*, tricellulin; *Ocln*, occludin; Zo1, *zonula occludens* protein 1 (cell-cell contact marker).

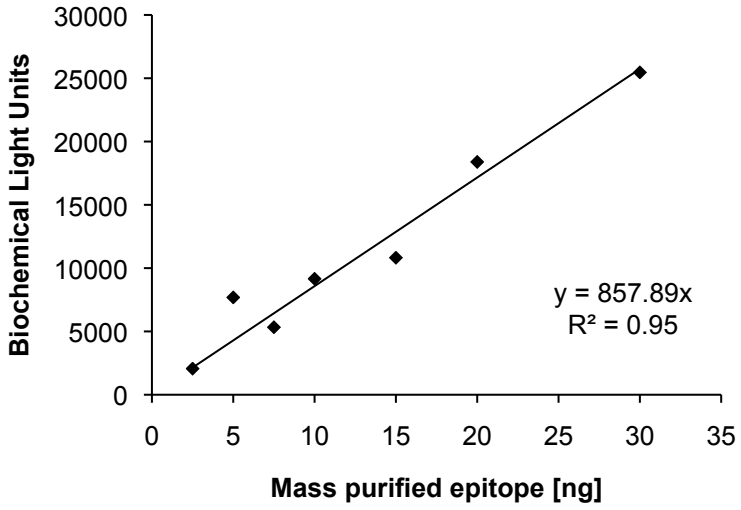


**Figure S 3 Calibration curve of epitope masses and densitometrically determined biochemical light units.** Example shown for the dilution series of MBP-mCldn1$_{188-211}$. Line, linear regression; $R^2$, coefficient of determination; slope (m), 857.89.

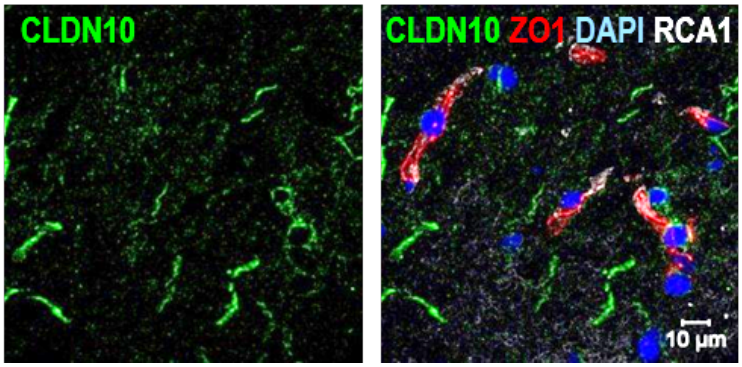


**Figure S 4 Claudin (CLDN)-10 is not localized in brain capillaries.** Immunofluorescence staining of human brain sections for Cldn10 (green). Microvessels stained by RCA1 (white) with zonula occludens protein 1 (Zo1) (red), localized in the TJ area. The nuclei were stained by DAPI (blue).

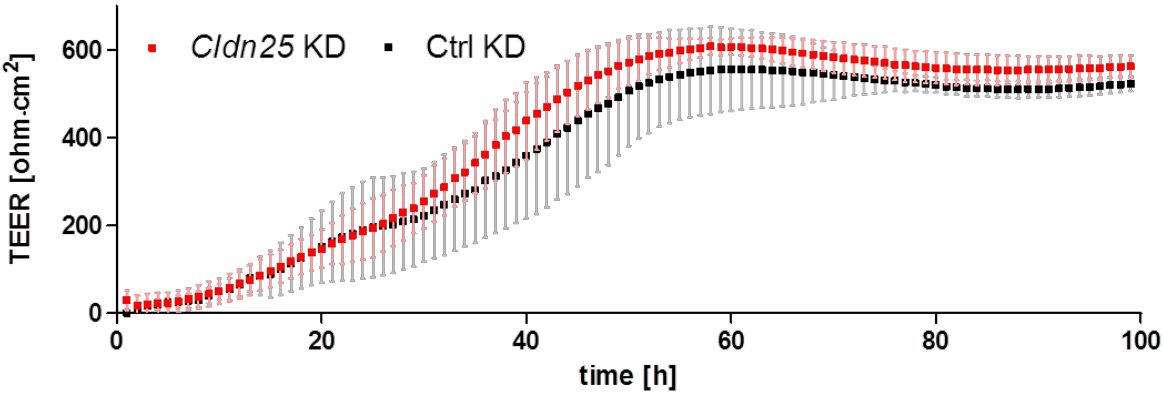


**Figure S 5 No delay in proliferation of bEND.3 cells upon knockdown (KD) of claudin-25 (*Cldn25*).** TEER recorded at 40000 Hz represents the endothelial proliferation (Szulcek et al., 2014). Monolayer of control (Ctrl) and *Cldn25* KD cells were fully developed ~60 h after seeding. Means ± SD; n ≥ 11.

```
MDNRFATAFVIACVLSLISTIYMAASIGTDFWYEYRSPIQENSSDSNKIAWEDFLGDEADEKTYNDVLFRYNGSLGLWRR      80
CITIPKNTHWYAPPERTESFDVVTKCMSFTLNEQFMEKYVDPGNHNSGIDLLRTYLWRCQFLLPFVSLGLMCFGALIGLC     160
ACICRSLYPTLATGILHLLAGLCTLGSVSCYVAGIELLHQKVELPKDVSGEFGWSFCLACVSAPLQFMAAALFIWAAHTN     240
RKEYTLMKAYRVA
.....................................N.............................N........      80
.....................................................................................     160
.....................................................................................     240
.............                                                                         320

(Threshold=0.5)
---------------------------------------------------------------------
SeqName      Position  Potential    Jury    N-Glyc
                                  agreement result
---------------------------------------------------------------------
Sequence       42 NSSD   0.6513     (9/9)   ++
Sequence       72 NGSL   0.7664     (9/9)   +++
---------------------------------------------------------------------
```

**Figure S 6 The asparagines at position 42 and 72 in the first extracellular loop (ECL1) of claudin (CLDN)-25 are the only predicted glycosylation sites as identified by mass spectrometry (Wollscheid et al., 2009).** N (highlighted in red), predicted as N-glycosylated. Consensus tripeptide: N-X-S/T (X, any amino acid except proline) (Kaplan et al., 1987; Marshall, 1972). N-Glyc result: + Potential > 0.5; ++ Potential > 0.5 and Jury agreement (9/9) or Potential > 0.75; +++ Potential > 0.75 and Jury agreement; ++++ Potential > 0.90 and Jury agreement. Potential, averaged output of nine neural networks. Jury agreement, number of nine networks supporting the prediction. (NetNGlyc 1.0 Server, Center for biological sequence analyses, Technical University of Denmark)

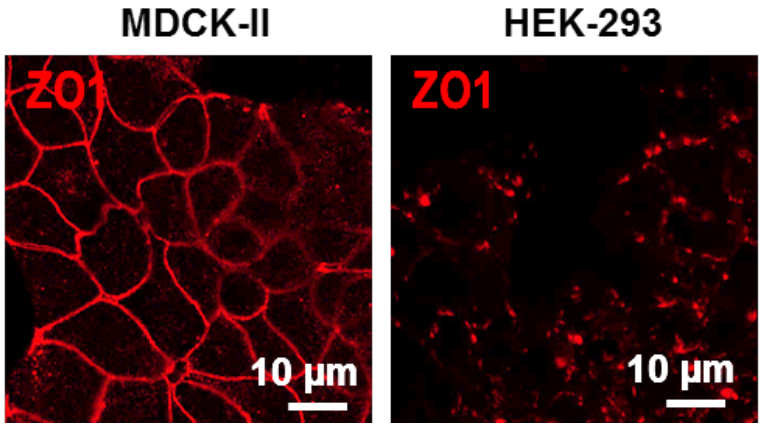


**Figure S 7 Subcellular localization of Zo1 in MDCK-II and HEK-293 cells.** In MDCK-II cells, Zo1 was evenly distributed at cell-cell-contacts. In HEK-293 cells, incapable to form TJs (Krause et al., 2008), Zo1 displayed a fragmented localization. The cells were stained by use of an antibody against Zo1 and imaged by confocal microscopy.

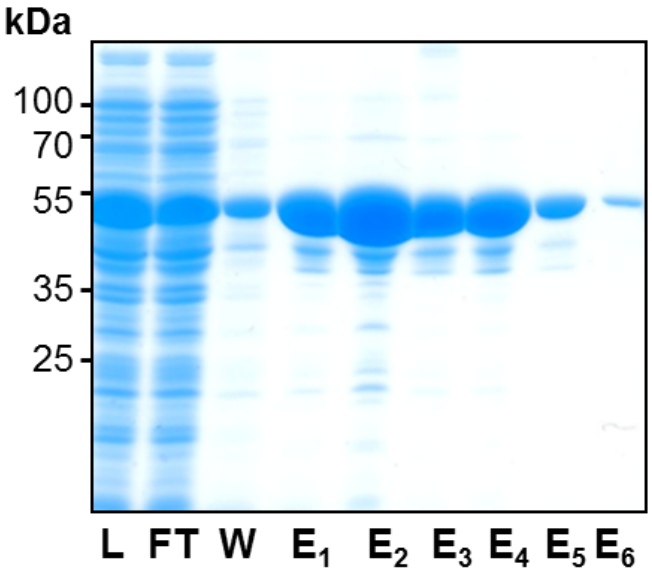


**Figure S 8 Coomassie stained SDS-PAGE for quality and quantity check of purified MBP tagged protein domains.** Example shown for PDZ1 of *zonula occludens* protein 1. L, lysate; FT, flow-through; W, wash fraction; E, elution fraction.

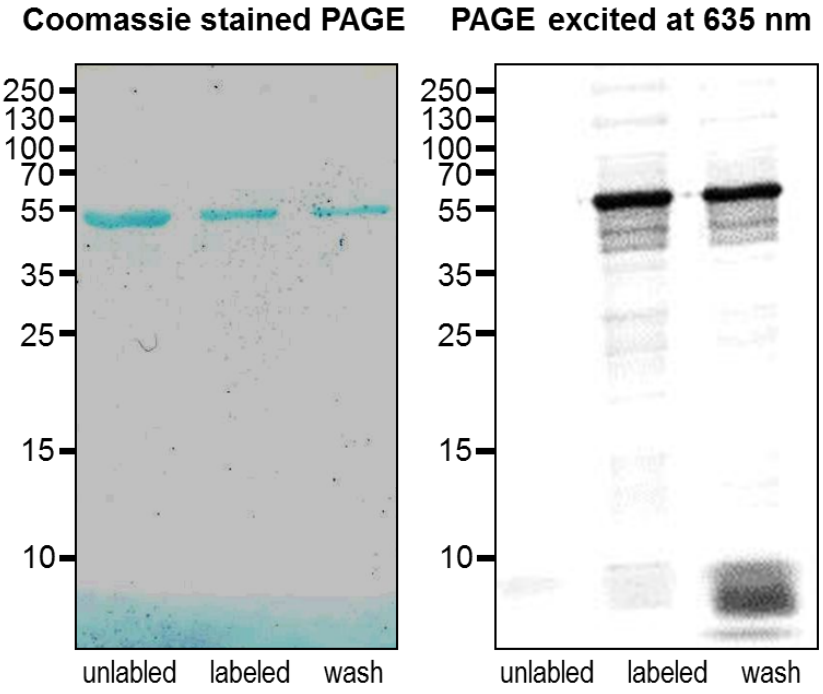


**Figure S 9 Labeling of MBP tagged protein domains**. Example shown for Zo1-PDZ1. Left: Coomassie stained SDS-PAGE of MBP tagged Zo1-PDZ1 (unlabeled, labeled and wash fraction) Right: Zo1-PDZ1 was fluorescently labeled (excited at 635 nm) and unbound dye was enriched in the wash fraction.

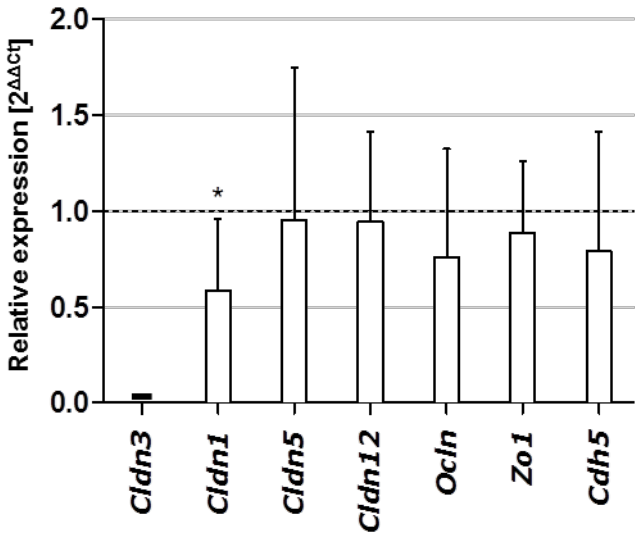


**Figure S 10 Claudin (*Cldn)*-1 mRNA expression is reduced upon knockout of *Cldn3* in mice.** The expression levels in laser-dissected brain capillaries were normalized with respect to the wild type. $\Delta\Delta Ct = (Ct_{target} - Ct_{Rn28s})_{Cldn3KO} - (Ct_{target} - Ct_{Rn28s})_{wild\ type}$. Mean ± SD; n ≥ 4; Mann–Whitney U test; * $p < 0.05$; „-“, not detectable. *Ocln*, occludin; *Zo1*, *zonula occludens* protein 1; *Cdh5*, cadherin-5.

## Declaration of Authorship

I hereby certify that this thesis first submitted has been composed by me and is based on my own work, unless stated otherwise. No other person's work has been used without acknowledgement in this thesis. All references and verbatim extracts have been quoted, and all sources of information, including graphs and data sets, have been specifically acknowledged.

Berlin, 18 June 2017

Philipp Berndt